ARBS

T NAGATA

Shinshu University, JAPAN

Aging Changes of Macromolecular Synthesis in the Digestive Organs of Mice as Revealed by Microscopic Radioautography and X-Ray Microanalysis

Contents

Correspondence

Tetsuji Nagata
Department of Anatomy and Cell Biology, Shinshu University School of Medicine, Matsumoto 390-8621, Japan Phone: +81-263-35-4600 FAX: +81-263-37-3086
E-mail: nagatas@po.cnet.ne.jp

F ;)(Grants-in-Aids for Scientific Research from the Ministry of Education, Science, Sports and Culture of Japan Government (No. 001054, 801066, 801031, 501010, 501533, 56870001, 58015046, 02454564); and Grants for Promotion of Characteristic Research and Education from the Japan Foundation for Promotion of Private Schools (1997, 1998, 1999, 2000).

Abstract

For the purpose of elucidating the aging changes of macromolecular synthesis such as DNA, RNA, proteins, glycoproteins, glucides and lipids in various organ systems of experimental animals, we have studied the digestive organs of aging mice and rats as a series of systematic studies using light and electron microscopic radioautography after incorporations with macromolecular precursors. The experimental animals mainly used were ddY strain mice at various aging groups from embryo to postnatal days 1 and 3, weeks 1 and 2, months 1, 2, 6, 12 up to 2 year senescent stages as well as several groups of adult Wistar rats. The animals were injected with such macromolecular precursors as ^{3}H-thymidine for DNA, ^{3}H-uridine for RNA, ^{3}H-leucine and ^{3}H-proline for proteins, $^{35}SO_4$ for glycoproteins, ^{3}H-glucosamine for glucides and ^{3}H-glycerol for lipids. The results demonstrated that these precursors were incorporated into various cell types in the oral cavity, the salivary glands, the esophagus, the stomach, the small and large intestines, the liver and the pancreas at various ages from perinatal to juvenile, mature and senescent stages, showing specific patterns of macromolecular synthesis. It is concluded that these specific patterns of macromolecular synthesis in respective cell types demonstrated the organ specificity of aging of animals.

Key words: radioautography, DNA, RNA, proteins, glucides, digestive organs, aging mice.

Review Article Received on Dec/03/02 Accepted on Jan/24/03

Introduction

For the purpose of estimating the aging changes of various organs of experimental animals, we have developed novel techniques for both light and electron microscopic radioautography to localize intracellular sites of metabolism at cell organelle level by fixing tissues with chemical fixatives followed by conventional wet-mounting radioautography as well as to demonstrate soluble compounds by fixing tissues with cryo-fixation followed by dry-mounting radioautography to demonstrate the sites of incorporations, syntheses and discharge and to estimate the quantities of synthesized molecules of various substances in animals during these 45 years in our laboratory (Nagata, 1992, 1994[a,b,c], 1996[a,b], 1997[a], 1998[a], 2001[c], 2002). The localization of silver grains developed by means of conventional radioautography demonstrates only the insoluble radioactive substances bound to the macromolecules fixed in the cell with the chemical fixatives used (Nagata, 1992, 1996[a,b], 1997[a], 1998[a]) , while the radioisotopes bound to the small molecules which are not fixed with conventional fixatives can be demonstrated by only cryo-fixation (Nagata, 1994[a]). Conventional radioautographic procedures can be designated as wet-mounting radioautography, since the tissues are processed through both conventional wet treatments fixing in such chemical fixatives as formaldehyde or gultaraldehyde and applying wet radioautographic emulsions to the specimens (Nagata, 1992, 1996[a,b], 1997[a], 1998[a]). In order to demonstrate any soluble radioactive compounds, special techniques are required in accordance with the characteristics of the radioisotopes used for radioautography (Nagata, 1994[a]; Nagata & Murata, 1977). We have applied these methodologies to various organ systems of experimental animals during aging, from embryo to postnatal juvenile, mature and senescent stages, using radiolabeled precursors for macromolecular synthesis and reported the aging changes of macromolecular synthesis in some organ systems of mice by means of light microscopic (LM) and electron microscopic (EM) radioautography (RAG). The aging changes of DNA synthesis in the locomotive system (Hayashi *et al.*, 1993; Nagata, 1998[c]), in the digestive system (Duan *et al.*, 1993;

Jin, 1996; Jin & Nagata, 1995[a,b]; Ma & Nagata, 1988[a,b], 1990[a]; Morita *et al.*, 1994[a]; Nagata & Usuda, 1986; Nagata *et al.*, 2000[a]), in the endocrine system (Gao *et al.*, 1995[a,b]; Ito, 1996; Ito & Nagata, 1996; Nagata *et al.*, 2000[b]), in the urinary system (Hanai, 1993; Hanai & Nagata, 1994[a,b]; Hanai *et al.*, 1993), in the respiratory system (Matsumura *et al.*, 1994; Sun *et al.*, 1994,1995[a,b,] 1997[a]), in the reproductive system (Gao, 1993; Gao *et al.*, 1994; Li, 1994; Li & Nagata, 1995; Yamada & Nagata, 1992[a,b]), in the circulatory system (Murata *et al.*, 1977[a,b], 1978; Olea & Nagata, 1992[a]), in the nervous system (Nagata, 1965; Cui, 1995), and in the sensory system (Gao *et al.*, 1992[a,b]; Gunarso *et al.*, 1997; Kong, 1993; Kong & Nagata, 1994; Kong *et al.*, 1992[a]; Nagata *et al.*, 1994; Nagata, 1998[c]), or RNA synthesis in the digestive system (Ma & Nagata, 1990[b]; Nagata & Usuda, 1986, 1993[b]; Nagata *et al.*, 1984), the respiratory system (Sun, 1995), the endocrine system (Liang, 1998; Liang *et al.*, 1999), the urinary system (Hanai & Nagata, 1994[a,b]), the reproductive system (Gao, 1993; Li & Nagata, 1995; Yamada & Nagata, 1992[a], 1993), the circulatory system (Olea & Nagata, 1992[b]), the nervous system (Nagata, 1965; Nagata *et al.*, 1999[b]) and the sensory system (Kong *et al.*, 1992[b]; Gunarso *et al.*, 1996; Nagata & Kong, 1998), and the protein synthesis in the locomotive system (Terauchi *et al.*, 1988; Terauchi & Nagata, 1993, 1994), in the digestive system (Ma & Nagata, 2000; Ma *et al.*, 1991; Nagata & Usuda, 1993[a]; Nagata, 2000[c]), the respiratory system (Sun *et al.*, 1997[b]), the reproductive system (Gao, 1993; Yamada, 1993), the circulatory system (Nagata & Olea, 1999) and the sensory system (Toriyama, 1995; Nagata, 1997[c]; Cui *et al.*, 2000), glucide and glycoprotein synthesis in the circulatory system (Murata *et al.*, 1979[a]), the digestive system (Morita, 1993; Nagata & Kawahara, 1999; Nagata *et al.*, 1992; Nagata *et al.*, 1988[a], 1999), the respiratory system (Nagata, 2000[d]), the urinary system (Johkura, 1996; Johkura *et al.*, 1996) the reproductive system (Oliveira *et al.*, 1991, 1995; Li *et al.*, 1992) and the sensory system (Nagata *et al.*, 1995; Nagata, 1999[d]), and the lipid synthesis in the digestive system (Nagata *et al.*, 1988[b], 1990) were already reported. We have reviewed those results on several organ systems (Nagata, 1993[b], 1997[a]; 1998[b], 1999[c]) or single organ system such as the digestive system (Nagata, 1995[a]), the endocrine system (Nagata *et al.*, 2000[b]), the respiratory system (Nagata, 2001[a,b,d]) and the sensory system (Nagata, 2000[f]).

This paper reviews the results obtained from the digestive system, especially the digestive tracts and the digestive glands of mice and rats in our laboratory, as a series of systematic studies on the aging changes during these 20 years (Nagata *et al.*, 1986; Nagata, 1993[b], 1997[a], 1998[b], 1999[c], 2001[c]).

Methods for the Demonstration of Macromolecular Synthesis

Formerly, we developed useful techniques for both light and electron microscopic radioautography to localize intracellular sites of metabolism at cell organelle level by fixing tissues with chemical fixatives followed by conventional wet-mounting radioautography as well as to demonstrate soluble compounds by fixing tissues with cryo-fixation followed by dry-mounting radioautography after administration of precursors for macromolecular compounds such as ^{3}H-thymidine for DNA, ^{3}H-uridine for RNA, ^{3}H-amino acids for proteins, ^{3}H-glucosamine for glucides, radiosulfate $^{35}SO_4$ for glycoproteins, ^{3}H-glycerol and ^{3}H-fatty acids for lipids (Nagata, 1992, 1997[a], 1998[a]). The methods were applied to study the macromolecular synthesis of the digestive organs in several groups of aging mice from fetal o postnatal stages from development to senescence. The digestive system consists of both the digestive tract and the digestive glands. The former consist of the oral cavity, the pharynx, the esophagus, the stomach, the small and large intestines and the anus, while the latter consists of the salivary glands, the liver and the pancreas.

We have studied the macromolecular synthesis of various organs in the digestive system of experimental animals, such as ddY strain mice or Wistar rats, at various ages by means of light microscopic and electron microscopic radioautography as well as X-ray microanalysis.

Experimental Animals

The experimental animals mainly used in these experiments were ddY strain mice, which were maintained and bred in our laboratory. We used around 180 ddY strain mice of both sexes in 6 experimental groups in 10 aging groups, each consisting of 3 litter animals of both sexes respectively, from fetal day 19 to postnatal newborns at days 1 and 3, juvenile at weeks 1 and 2, adults at months 1, 2, 6, 12 and 24, for microscopic radioautography. We also used some more 30 adult ddY mice and Wistar rats for X-ray microanalysis. They were bred in our laboratory and were housed under conventional conditions, fed with normal mice-rat chow (Clea CE2, Clea Co., Tokyo, Japan) with access to water *ad libitum*. The embryonic age was based on observations of the vaginal plugs of the female mice or rats (vaginal plug = day 0). They were sacrificed at given time with pentobarbital sodium (Nembutal, Abbott Laboratories, Chicago, IL, USA) anesthesia and perfusing via the left ventricles of the hearts with 2.5% glutaraldehyde in 0.1 M cacodylate buffer (pH 7.2) 1 hour after injections with radiolabeled compounds for demonstrating macromolecular compounds by wet-mounting radioautography (Nagata, 1982, 1985, 1996[a,b], 1997[a], 1998[a]). Some other animals were used for demonstration of soluble compounds by cryo-fixation and dry-mounting radioautography (Nagata, 1994, 1998[a]). In addition to the aging mice at various aging stages, we used other 5 groups of ddY strain mice and Wistar rats at adult stage, postnatal month 1, for time course after injections of RI-labeled precursors.

Administration of Radioactive Compounds

In order to localize the sites of incorporation of radioactive compounds in animal bodies, the compounds that were labeled with specific RIs were usually administered by injections given subcutaneously, intramuscularly, intravenously or intraperitonially. In these experiments, we injected the animals intraperitonially with radioactive precursors for macromolecular syntheses at varying concentrations such as 37-1850 KBq (1-50 μCi)/ gram body weight for both LMRAG and EMRAG or 370-3700 KBq (10-100 μCi)/ g.b.w. depending on the characteristics of the compounds and RIs used. The RI-labeled precursors used in these experiments were ^{3}H-thymidine (Amersham, England, UK, specific activity 877 GBq/mM) for DNA synthesis, ^{3}H-uridine (Amersham, England, 1.11 TBq/mM) for RNA synthesis, d-4,5-^{3}H-leucine (Amersham, England, UK, specific activity 1.04 TBq/ mM) or d-^{3}H-proline (Amersham, England, UK, specific activity 877 GBq/mM) for proteins, ^{35}S-sulfuric acid (Amersham, England, UK, specific activity 1.11 TBq/mM) for mucosubstances, d-1,6-^{3}H-glucosamine (New England Nuclear Corporation, Boston, MA, USA, specific activity 185 MBq/mM) for glucides, and ^{3}H-glycerol (New England Nuclear Corporation, Boston, MA, USA, specific activity 740 MBq/mM) for lipids.

On the other hand, we sometimes carried out *in vitro* labelings for tissue blocks or isolated cultured cells in media such as Eagle's MEM (Nissui, Tokyo, Japan) containing various radioactive compounds at concentrations of 37-3700 KBq per ml medium, using CO_2 incubator under normal conditions at 37 °C with 5% CO_2 in air for varying time intervals from several minutes up to several hours.

Animal Treatment and Tissue Processing

All the experimental animals used in these experiments such as mice or rats were anesthetized by intraperitonially injections with pentobarbital sodium (Nembutal, Abbott Laboratories, Chicago, Ill., USA), after administrations of radioactive compounds by intraperitoneal injections, and are sacrificed at given time, usually 1 h after the RI administration by perfusing via the left ventricles of the hearts with 2.5% glutaraldehyde in 0.1M cacodylate buffer at pH 7.2, depending on whether insoluble or soluble radioautography would be carried out. For conventional insoluble radioautography the perfusion fixation was used and the tissues from various organs were taken out, cut into small pieces (1 x 1 x 1 mm), soaked in the same glutaraldehyde fixative at 4°C for 1 h and postfixed in 1% osmium tetroxide in the same buffer for 1 h, dehydrated with graded ethanol and embedded in epoxy resin (Epok 812, Oken Co., Tokyo, Japan). When in vitro labelings of cultured cells and tissue blocks obtained from either animals or human biopsy materials were used, the cells and tissues were incubated in media containing radioactive compounds under normal conditions at 37°C for given time. They were then rinsed in Hanks' solution (Nissui, Tokyo, Japan), fixed in the same buffered glutaraldehyde and osmium tetroxide solutions, dehydrated and embedded in epoxy resin as above. For the soluble radioautography, however, perfusion fixation cannot be used. The whole bodies of the small animals or organs and tissues taken out after decapitation without using any solution, should be immediately cryo-fixed by either metal contact method or immersion method cooled with liquid nitrogen and be processed by cryo-sectioning (Nagata & Murata, 1977) or freeze-drying or freeze-substitution (Nagata, 1994[a]).

For both LMRAG and EMRAG, embedded tissues in epoxy resin can be used. For LMRAG, thick sections at 2 μm were cut on an ultramicrotome and picked up onto clean glass slides and warmed for extension and drying. For electron microscopy, ultrathin sections of 100 nm thickness were cut for using a conventional transmission electron microscope with the accelerating voltage at 100 kV. It is generally accepted that the thinner the section is the better the resolution, but the less the radioactivity it contains and the longer the exposure time is required for radioautography. If any intermediate high voltage electron microscope is available at such accelerating voltages as 200, 300 or 400 kV, thicker sections at 200 or 400 nm thicknesses can be used. We prefer to use semithin sections at 200 nm thickness to be observed in a high voltage EM at 400 kV in order to shorten the exposure time (Nagata, 1997[b]). Semithin sections were cut on a Porter-Blum MT-2B ultramicrotome (Dupon t-Sorvall, Newtown, CONN, USA). Ultramicrotomes of mechanical feeding type are preferable than thermal feeding type because of the accuracy of the section thickness, which effect on the number of silver grains by radioautography. Ultrathin or semithin sections were picked up onto either platinum or gold meshes in order to prevent the copper meshes from rusting through the histological and radioautographic treatment especially by the development. Alternatively, collodion coated copper grid meshes can be used. For collodion coating, copper grid meshes (100-200 meshes) were soaked into 2% collodion solution for a few min, spread on a filter paper in a Petri dish and dried at 37°C for a few hours in an incubator.

In order to process many specimens at once, we have developed simple routine standard techniques to demonstrate insoluble compounds in various cells and tissues of experimental animals and to quantify the contents of synthesized macromolecules in each cell and cell organelle by both light and electron microscopy. The localization of silver grains developed by means of ordinary radioautography, however, demonstrates only the insoluble radioactive substances bound to the macromolecules fixed in the cell with the

chemical fixatives used (Nagata, 1992, 1996, 1997[a], 1998[a]). On the other hand, radioisotopes bound to the small molecules, which are not fixed with ordinary chemical fixatives, are washed away through conventional routine procedures such as fixation, dehydration, embedding, sectioning, and radioautographic procedures, so that these compounds cannot be demonstrated. Ordinary radioautographic procedures can be designated as wet-mounting radioautography, since the tissues are processed through both conventional wet treatments and applying wet radioautographic emulsions to the specimens. In order to demonstrate any soluble radioactive compounds, special techniques are required in accordance with the characteristics of the radioisotopes used for radioautography. By the cryo-fixation for dry-mounting radioautography, the labeled tissues are quickly frozen in a cooled liquid such as isopentane or propane cooled to its melting point with liquid nitrogen. Then the tissues can be cut by cryo-microtomy. At the light microscopic level, the frozen tissues can be cut in a cryostat at a thickness around 20-30 μm and the frozen sections are placed in contact with radioautographic emulsions by various techniques. Many papers have been published on this problem. We first used a large-wire loop to produce dry films, which were air-dried and applied to cryostat sections placed on glass slides (Nagata & Nawa, 1966[a]). This procedure is very convenient and often used for demonstrating soluble compounds. At the electron microscopic level, however, only a few papers have been published on this principle, cryo-ultramicrotomy. We reported the results for the first time (Nagata *et al.*, 1969). To demonstrate soluble small molecular compounds, we employed cryo-fixation and dry-mounting radioautography for both LMRAG and EMRAG (Nagata, 1994[a,b,c], 1997[a], 1998[a]).

Application of Radioautographic Emulsions to Specimens

We used the nuclear emulsions, Konica NR-M2 and NR-H2, produced by Konica Co. (Formerly Sakura), Tokyo, Japan, for both light microscopic (LM) and electron microscopic (EM) radioautography (RAG), which were sensitive for radiation and consisted of gelatin matrix and silver bromide crystals. Several kinds of emulsions are commercially available in several countries. They are classified into four types, *i.e.*, gel form or bulk liquid emulsions for light and electron microscopy, stripping films for LMRAG, coated plates or films for macro-RAG and LMRAG, and coated films for macro-RAG, produced by several photo-industry makers in the world such as Konica (Japan), Eastman-Kodak (USA), Ilford (UK). The silver bromide crystals are uniform in size ranging from 70 to 400 nm in diameter depending on their brands produced by the makers. We prefer to use bulk liquid emulsions produced by Konica Co. Tokyo, Japan, Konica NR-M2 for LMRAG and Konica NR-H2 for EMRAG, because of their fine grains and high sensitivity. Other types of emulsions such as Kodak NTB-2, 3, 5, or Ilford K-2 and L-4 can alternatively be used in other laboratory.

There are various techniques published for applying radioautographic emulsions to the specimens, depending on the kinds of specimens and radioactive compounds to examine. After the specimens are made contact with the emulsions, they are kept in a cold (4°C) dark room, usually in a light tight slide box kept in a refrigerator, for exposure for several weeks and finally developed. The development is a chemical reaction to reduce the silver bromide crystals in a developer and to convert them to metallic silver grains. When the emulsion is soaked in a developer, the developer reduces the silver bromide crystals, which contain specks of latent images building more and more metallic silver around the latent image. The size of silver grains depends on the constituents of the developer as well as the time and temperature of development. The standard developers

such as Kodak D-19 or Konica SD-X1 consist of some reducing reagents such as methol and hydroquinone, which are abbreviated as MQ developers. When MQ developers are used for both LM and EMRAG, large spiral silver grains as long as a few μm are grown, which can be observed by light microscopy without problems but are too large for electron microscopy. On the contrary, when a fine grain developer such as gold latensification and phenidone developer at a low temperature and a shorter time is used, small dot-like silver grains less than 1 μm in diameter are produced. We prefer to use this development for electron microscopy (Nagata, 1992, 1996[a,b], 1997[a], 1998[a], 2002).

Wet-mounting radioautography

For conventional light microscopic wet-mounting radioautography, the same tissue blocks for electron microscopy, which were fixed in buffered glutaraldehyde and osmium tetroxide solutions then embedded in epoxy resin can be used. We cut semithin sections on a Porter-Blum MT-2B ultramicrotome at 2 μm thickness, picked up onto clean glass slides and warmed for extension and drying. Otherwise, conventional formalin fixed, paraffin embedded tissues can alternatively be used. In order to produce many radioautograms at once and also to compare each other quantitatively, we carried out the following procedures, which were developed in our laboratory (Nagata, 1992, 1997[a], 1998[a]). A bottle of bulk emulsion (we used Konica NR-M2 emulsion, Konica Co., Tokyo, Japan), was melted in a water bath at 45°C for about 10 min, to which an equal amount of distilled water was added and mixed for 5-10 min with a glass slide to remove all air bubbles. Then, a slide holder, made of stainless steal, holding 15 glass slides that carried several thick sections, was dipped into the melted emulsion for several seconds, then they were pulled up vertically for about 3 seconds to assure equal thickness coating (3-4 μm) over the sections. The faster the speed was, the thinner became the emulsion coating. The bottom of the slide holder was wiped with a paper towel to remove excess emulsion and the slide holder was placed in an electric incubator at 28°C with a humidity about 80%, containing a wet sponge at the bottom, and dried for 1 h. When the slides were dry, they were stored in a light tight slide box containing a desiccant (silica gel). After the edge of the box was sealed with black tape, it was kept in a refrigerator at 4°C for exposure. After an appropriate exposure time, all the slides were developed at once by pouring the developer into the slide box. We used Konica KD-X1 (formerly SD-X1) developer for Konica NR-M2 emulsion. Kodak D-19 may be used for any types of emulsions. After the development, the slides were rinsed in stop bath (2% aqueous acetic acid solution), fixed in a fixer (30% aqueous sodium thiosulphate solution) for 5 min twice, washed gently in running tap water for 10 min, and finally they were stained in 1% toluidine blue solution for light microscopy.

For EMRAG, we used the same embedded tissues in epoxy resin as for LMRAG. Ultrathin sections at 0.1 μm (100 nm) or semithin sections at 0.2 μm (200 nm) were cut on an ultramicrotome and picked up on collodion coated grid meshes. The semithin sections should be observed by high voltage electron microscopy (Nagata, 1995[b], 1997[b], 2001[b]). As for the radioautographic emulsions, several types of emulsions are commercially available. We used Konica NR-H2 emulsion (Konica Co., Tokyo, Japan) because of the small sized silver bromide crystals and better sensitivity. To obtain thin monolayer of silver bromide crystals, two techniques, dipping and wire-loop methods, are now in general use. The choice lies between mounting the sections on a flat microscopic glass slide or on a grid mesh during the exposure. By the former method, glass slides are covered with thin collodion films on which sections are placed and they are coated with radioautographic

the unregulated D_2 receptors can account for the previously reported changes in apomorphine-induced behaviors after PSD. An increase in DA release in PS deprived group will exhibit greater dopaminergic-mediated effects due to up-regulation of DA receptors in the striatum of PS deprived rats compared to control group (Farooqui *et al.*, 1996), giving further support to the early studies on behavioral effects of dopaminergic stimulants in PS deprived animals (Tufik *et al.*, 1978; Clark *et al.*, 1987; Asakura *et al.*, 1992).

Since activity of both neurotransmitter systems is also altered by stress (De Kloet, 1991), animals were chronically exposed to different stress modalities and the evaluation of yawning induced by dopaminergic and cholinergic drugs show that immobilization caused suppression of this behavior, whereas forced swimming and footshock increased the number of yawns suggesting that yawning is differently altered by constant and intermittent stressors (Tufik *et al.*, 1995).

As these stressful manipulations altered drug-induced yawning, Hipólide *et al.* (1999) investigated the effects of single and repeated treatments with a synthetic glucocorticoid, dexamethasone (DEXA) on apomorphine- and pilocarpine-induced yawning in rats. Neither single nor repeated treatment with DEXA altered apomorphine-induced yawning. On the other hand, single injection of DEXA caused in an increased number of yawns induced by pilocarpine. Repeated treatment with DEXA led to a decreased number of yawns induced by pilocarpine. The authors concluded that dopaminergic and cholinergic are distinctly altered by DEXA, in terms of yawning behavior. Furthermore, yawning behavior was evaluated to examine whether concomitant treatment of PSD with DA agonists could reverses PSD effects (Lobo *et al.*, 1995) as observed with stereotypy and aggressiveness (Troncone *et al.*, 1988). Atropine increased yawning of PS deprived rats induced by pilocarpine, but not by apomorphine. Treatments with methamphetamine and haloperidol did not change PSD effect on pilocarpine- and apomorphine-induced yawning, revealed that reversal of PSD-induced yawning inhibition is mediated distinctly by both acetylcholine and DA systems (Lobo *et al.*, 1995).

Based upon the PSD effects on both systems (cholinergic and dopaminergic) and that the septal-hippocampal cholinergic neurons are necessary to elicit the stretching-yawning syndrome following ACTH or α-MSH (Wood *et al.*, 1978, 1979), Lobo *et al.* (1990) proposed to study the effects of PSD on ACTH-induced yawning by injecting the peptide immediately after the PSD period or after 24 h of recovery. PSD for 96 h impaired ACTH-induced yawning, but a 24-h recovery period restores the system responsible for the displaying of yawning after the central administration of ACTH, suggesting an involvement of the acetylcholine receptor after ACTH treatment (Lobo *et al.*, 1990).

In spite of several papers reporting PSD alters drug-induced behaviors, very little is known about the relationship between PSD and the effect of theses drugs in female rats. In this context, Hipólide and Tufik (1995) reported that, as in males, PSD in females resulted in increased apomorphine-induced stereotypy; however unlike males, no apomorphine-induced aggressiveness or apomorphine- and pilocarpine-induced yawning were observed in PS deprived females.

More recently, the effects of Δ^8- and Δ^9-tetrahydrocannabinol (Δ^8 and Δ^9-THC) were examined both acute and chronically on yawning induced by pilocarpine or apomorphine. The data suggest that cannabinoid agonists inhibited yawning induced by cholinergic or dopaminergic agonists. In addition, the increased frequency of spontaneous yawning following cessation of chronic administration of a cannabinoid agonist may be of importance as a withdrawal sign for these drugs (Nakamura-Palacios *et al.*, 2002).

many authors recommended this technique at the light microscopic level. However, those procedures are very much complicated to treat both specimens and emulsions. We first used dry-films produced with a large wire-loop, which were air-dried and applied to cryostat sections placed on glass slides (Nagata & Nawa, 1966). We believe that this method is the most convenient one. Radioautographic emulsion is diluted equal part with distilled water at 45 °C. We used Konica NR-M2 emulsion from Konica (formerly Sakura) Ltd., Tokyo, Japan. Any other emulsions such as Kodak can alternatively be used. In order to prevent the emulsion film from bursting, 10 ml of diluted emulsion were added with 0.2 ml at 2% aqueous solution of dioctyl sodium sulfosuccinate (a surfactant) (Nagata & Nawa, 1966). Thus, we obtained a thin film of emulsion by dipping a wire-loop, 2.5 cm in diameter, which was made of platinum wire or vinyl coated iron wire and set with a piece of Scotch tape on a glass slide as a handle. The handle was set horizontally on a flat desk for air-drying. After air-drying for 1-2 min, when the center of emulsion film was gelled and dried appearing transparent but the peripheral zone was still wet appearing opaque, we applied the film to the slide horizontally. We kept the glass slide in a Petri dish and warmed at 28 °C in an incubator for 1 hour for drying the emulsion. After an appropriate exposure time, the glass slides were processed for development, then stopped in stop bath, fixed in a fixer and stained with toluidine blue solution for staining. Control tissues should be fixed with chemical fixative, dehydrated, embedded, wet-sectioned and wet-mounted by conventional dipping procedure.

For electron microscopic dry-mounting procedure, the grids carrying dry sections (either freeze-dried or freeze-substituted Epon embedded sections or freeze-sectioned and freeze-dried) were coated with carbon at 5-10 nm thick before emulsion application. They were then put on a grid holder made of a glass slide (25 mm x 75 mm) and 3 glass rods (3 mm in diameter and 10 mm in length, respectively (Nagata *et al.*, 1969). Radioautographic emulsion was diluted 1 part in 10 with distilled water at 45 °C in the dark room. Ten mL of the diluted emulsion was added to 0.2 ml of 2% aqueous solution of dioctyl sodium sulfosuccinate and was maintained at 45°C in a thermobath for several minutes to complete mixing. Dioctyl sodium sulfosuccinate, a surface activating agent was used to prevent the emulsion films from bursting while they were being dried in the air. We used Konica NR-H2 emulsion, produced by Konica Co., Ltd., Tokyo, Japan. Other emulsions for electron microscopic radioautography such as Kodak NTB or Ilford L4 can be used in a similar way. A thin film of the emulsion thus prepared was obtained by dipping a platinum wire loop, about 1 cm in diameter, into the emulsion. Instead of a small platinum wire loop, we used a large vinyl coated iron wire loop, 2.5 cm in diameter (Nagata, 1996, 1998*). The handle of the wire loop was set on a flat surface for air-drying (for 1-2 minutes). The films were almost 100% air-dried without breaking by use of dioctyl sodium sulfosuccinate solution. The dried films were then applied to the grids on the holders like quoits. The grids were then transferred into Petri dishes and were warmed at 37 °C for 1 h to help the films adhere to the grids. They were exposed, developed, fixed and stained simultaneously similarly to the wet-mounting radioautography.

X-Ray Microanalysis

In order to analyze trace elements in macromolecules, X-ray microanalysis was carried out by means of analytical electron microscopes, which consisted of transmission electron microscopes and X-ray analyzers. By X-ray microanalysis, electron beams (with diameters 5-100 nm) were irradiated at a small spot (with diameters 5-100 nm) and the emitted X-rays were analyzed with either energy dispersive X-ray analyzer

(EDX) or wave-dispersive X-ray analyzer (WDX). To analyze the elements in biological specimens, EDX was usually preferred to WDX because all the elements can be detected by EDX (Chandler, 1976). We used 3 types of transmission analytical electron microscopes equipped with energy dispersive X-ray analyzers, *i.e.*, Hitachi H-700 with EMAX-1800E (Horiba, Kyoto, Japan), JEOL JEM 200CX with Kevex 7000-77 (Kevex, England, U.K.), and JEOL JEM-4000EX with TN-5400 (Tracor-Northern, Middleton, USA) at accelerating voltages from 100 kV to 400 kV. X-ray microanalysis is an excellent method to qualify and quantify basic elements in biological specimens. We first quantified the end products of cytochemical reactions such as Ag in radioautograms (Nagata, 1992, 1993[a]) or Ce in acid phosphatase reaction (Olea & Nagata, 1992[a]), then several endogenous trace elements contained in macromolecules such as Zn, Ca, S which originally exist in karyoplasm, cytoplasm or cell organelles of various cells and intracellular matrix after conventional chemical fixation or cryo-fixation. From our results, it was shown that X-ray microanalysis using intermediate high voltage transmission electron microscopy at 300 or 400 kV was very useful resulting in high P/B ratios for quantifying these trace elements in biological specimens (Nagata, 1991, 1993[a], 2000[b]).

We first started to use X-ray microanalysis in order to quantify the silver grains in electron microscopic radioautograms (Nagata 1991; Nagata & Usuda, 1985, 1986). In order to quantify the concentrations of radiolabeled compounds incorporated into cells and tissues, the number of silver grains was counted with the unaided eye (grain counting). However, it was very troublesome to count the number of silver grains on many photographs one by one. We tried to quantify the silver contents on EMRAG using X-ray microanalysis. Initially, we used the energy dispersive X-ray microanalyzers in the STEM mode, a Hitachi H-700 electron microscope equipped with Horiba EMAX-1800E or a JEOL JEM 200CX equipped with Kevex 7000-77, where the specimens were observed in the STEM mode (Nagata & Usuda, 1985, 1986). The peak counts of Ag-Kα lines were counted with a probe current of 500 pico ampere and a small probe diameter (2 μm) in the nucleolus for 100 seconds with a dead time of 30% as was shown previously (Nagata, 1993[a]). However, we lately changed to a JEOL JEM-4000EX high voltage electron microscope equipped with Tracor-Northern TN-5400 EDX in the TEM mode, which is better than the STEM mode, because we can observe the ultrastructure directly when measuring (Nagata, 1991). In order to quantify the silver content in silver grains in radioautograms, we first used the radioautograms prepared from mouse hepatocytes or pancreatic acinar cells labeled with either ^{3}H-thymidine or ^{3}H-uridine as the models. The diameter of microprobe ranged from 0.2 to 1.0 μm. The integrated detecting time was 100 s and the dead time was 30%. The beam currents were from 2 to 8 nano ampere and the accelerating voltages from 100, 200, 300, 350, and 400 kV. Figure 1A shows an example of electron microscopic radioautogram of mouse liver labeled with ^{3}H-tymidine, demonstrating DNA synthesis. Figure 1A shows four spectra obtained from a single silver grain observed at accelerating voltages of 100, 200, 300 and 400 kV, demonstrating Ag-Kα, respectively. The results showed the mean peak counts and background counts of silver grains measured at different accelerating voltages, 100, 200, 300, 350 and 400 kV. The peak to background ratios (P/B) at the different accelerating voltages were determined. The curve of the P/B ratios of silver grains calculated, as a function of the accelerating voltage from 100 to 400 kV is shown in Figure 1B. A maximum was found at 350 kV (Nagata, 1995[d]). We further tested to quantify several elements in biological specimens by 400 kV high voltage analytical electron microscopy and found it useful to increase the P/B ratio. On the other hand, it was also shown by Bando *et al.* (1985) and

1A. Spectra obtained from a specimen prepared from mouse hepatocytes labeled with ^{3}H-thymidine and observed in a JEOL JEM-4000EX high voltage electron microscope equipped with Tracor-Northern TN-5400 EDX in the TEM system. Thediameter of microprobe ranged from 0.2 to 1 μm. The integrated detecting time was 100 s and the dead time was 30%. The beam currents were from 2 to 8 nano ampere and the accelerating voltages from 100, 200, 300 and 400 kV, demonstrating Ag-Kα, respectively. From Nagata (2000[b], Figure 11, p. 23).

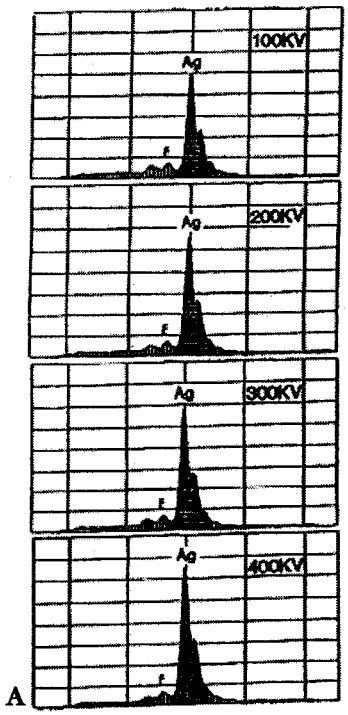

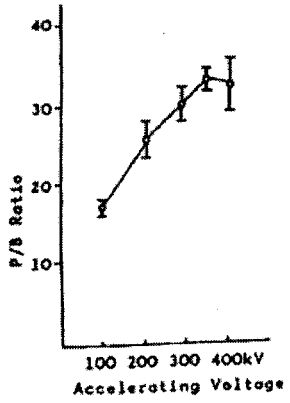

1B. Relation between P/B ratios and accelerating voltages. The peak to background ratios (P/B) at the different accelerating voltages from the spectra in Figure 1A were calculated. The curve of the P/B ratios of silver grains determined and plotted as a function of the accelerating voltage from 100 to 400 kV. A maximum was found at 350 kV. From Nagata (2000[b], Figure 12, p. 23).

Figure 1. X-ray microanalysis of silver grains in radioautograms.

Bando (1995) that the P/B ratios of Ag, Al and Ge in inorganic materials such as ceramics increased with increasing accelerating voltage from 100 to 400 kV similar to biological specimens.

The Macromolecular Synthesis of the Oral Cavity

The digestive system consists of the digestive tract and the digestive glands. The digestive tract can be divided into several portions, the oral cavity, the esophagus, the stomach, the small and large intestines and the anus, while the digestive glands consist of the salivary glands, the liver and the pancreas. We have published many papers from our laboratory dealing with the macromolecular synthesis of respective digestive organs from the oral cavity to the gastrointestinal tract and the digestive glands in both review papers (Nagata, 1992, 1993[b], 1995[a]) and the original articles. The outline of the results obtained should be described in the order of systematic anatomy and special histology starting from the oral cavity.

The oral cavity consists of the lips, the tongue, the teeth, the pharynx and the salivary glands. The DNA synthesis of mucosal epithelia of the lips and the tongues as well as the salivary glands of aging mice from fetal day 19 to postnatal 2 years were studied by LM and EMRAG labeled with ^{3}H-thymidine. The glucide syntheses with ^{3}H-glucosamine and the glycoprotein synthesis with radiosulfate ($^{35}SO_4$) incorporations of the large salivary glands, the parotid, the submandibular and the sublingual glands, of aging mice were also studied.

The DNA Synthesis of the Oral Mucosa

The DNA synthesis of the oral mucosal epithelia of the lips and the tongues of ddY mice at various ages from fetal day 19 to postnatal month 24, after injections of ^{3}H-thymidine, were studied by LM and EMRAG. It was found that the basal layers of the

stratified squamous epithelial cells were labeled at respective aging stages, from fetal day 19 to postnatal day 1, 3, week 1, 2, and month 1, 2, 6, 12 and 24. Thus, it was clarified that the epithelial cells synthesized DNA and proliferated at respective aging stages (Watanabe *et al.*, 1997).

The DNA Synthesis of the Salivary Gland

There are many salivary glands in the oral cavity. Many of them are small salivary glands in the mucosa or submucosa of the oral cavity and are named according to their localizations such as the labial, lingual, palatal and buccal glands. On the other hand, there are 3 kinds of pair of large glands independent from the oral mucosa, *i.e.*, the parotid, the submandibular and the sublingual glands. We studied the DNA synthesis of mouse submandibular glands at various ages from embryo to postnatal 2 years (Chen *et al.*, 1995; Nagata *et al.*, 2000*). The submandibular gland of male mouse embryonic day 19 consisted with the glandular acini and duct system. The duct system was composed of juxtaacinar cells (JA), intercalated duct cells ICD, and striated duct (SD) cells. Many labeled developing acinar cells (AC), JA and ICD cells were observed (Figure 2A). At postnatal day 1 to 3 (Figure 2B), there were more JA cells and secretary granules than those of former stage. JA cells were cuboidal cells, characterized by small darkly stained granules in the supranuclear cytoplasm and by basophilic mitochondria mostly at the basal half of the cells. JA cells were present at the acinar-intercalated duct junction of the mouse submandibular gland. Many labeled AC, JA, ICD and SD cells were also observed by electron microscopy (Figure 2C). At postnatal week 2 to month 3, developing immature acinar cells gradually matured to acinar cells, and JA cells increased and granular convoluted duct cells (GCT) appeared. At postnatal month 6 to year 2, the GCT cells were very well developed and were composed of the taller cells packed with many granules and became highly convoluted, and only a few labeled cells were found.

The aging changes of frequency of five main individual cell types in submandibular glands of male mouse from embryonic day 19 to postnatal 2 years of age are shown in Figure 3A. At embryonic day 19, the gland consisted of developing acinar cells (49%), intercalated duct cells (37%), juxta-acinar (JA) cells (3%), and striated duct (SD) cells (11%). Immediately after birth, JA cells increased rapidly to 32%, thereafter decreased gradually. At postnatal month 1, JA cells disappeared and granular convoluted tubule (GCT) cells appeared and increased rapidly in number with age. They reached a maximum at postnatal month 6. Then they decreased gradually from month 6 to 21. The quantity proportion of acini was relatively stable during these stages. The frequency of ICD cells was the highest (37%) at postnatal day 1 immediately after birth. Thereafter it gradually decreased month by month and reached 2.6% at month 21, while the ratio of SD cells persisted in 7-12% from embryonic day 19 to postnatal week 2 and it disappeared at month 3. The proliferative activity of the cell population can be expressed by the labeling index (LI) which is defined as the percentage of labeled nuclei with ^{3}H-thymidine in a given cell population. The aging change of the LI of the entire gland cells at respective aging stages was shown in Figure 3B. It increased from 13.6% at embryonic day 19 to 18.3% at postnatal neonate day 1, when it reached the first peak (Figure 3B). Then it declined to 2.2% at postnatal week 1. A second small peak (2.9%) occurred at week 2. Thereafter, the LI decreased progressively to less than 1% at week 4 and then remained low. The analysis of the LI of respective cell types revealed that the first peak at neonate was due to the increased LI of AC, ICD and JA cells, and the second peak at week 2 was due to the increase of ICD and SD cells (Figure 3B). Thereafter, the LI of ICD cells

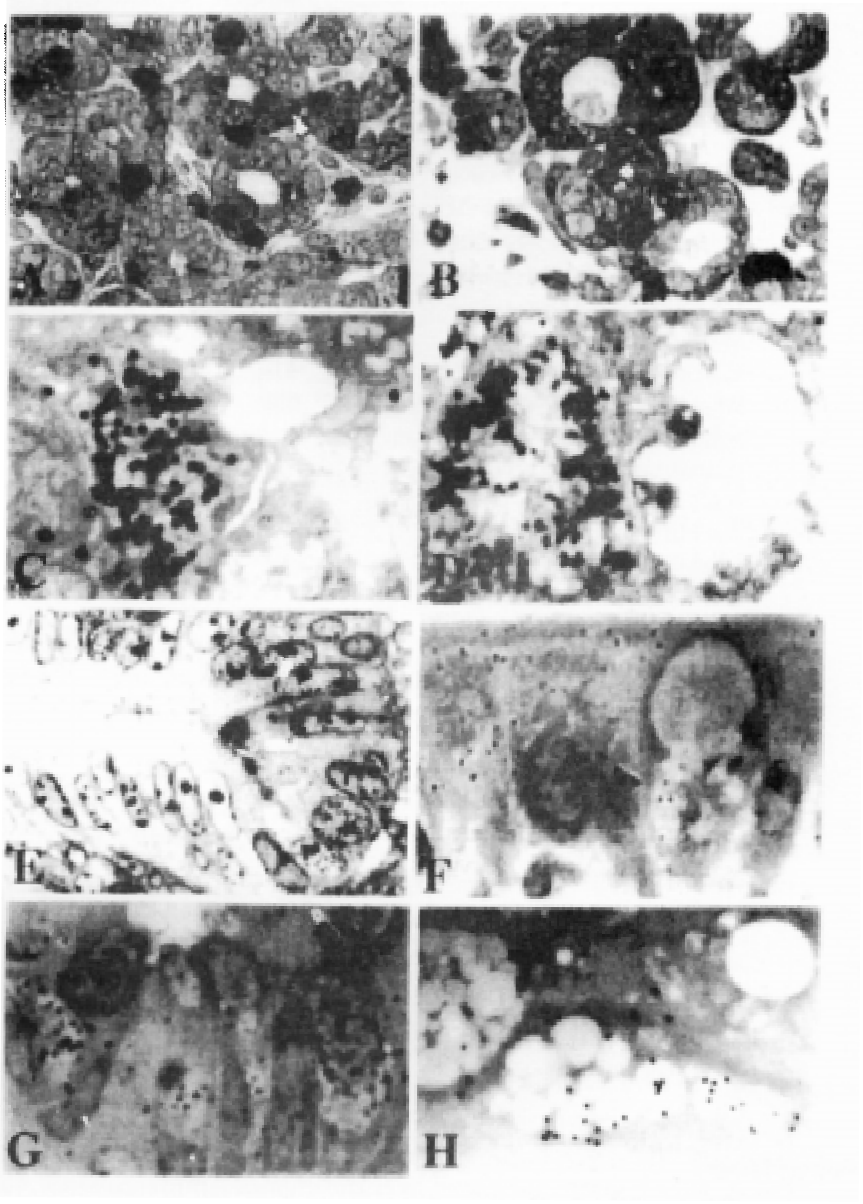

Figure 2. LM and EMRAG of the oral cavity, the esophagus and the intestines.

2A. LMRAG of the submandibular gland obtained from a mouse embryo at fetal day 19, labeled with ^{3}H-thymidine in vitro and radioautographed. Many nuclei of acinar cells and ductal cells are labeled with silver grains demonstrating DNA synthesis. x500. From Nagata (2002, Figure 13A, p. 118). 2B. LMRAG of the submandibular gland obtained from a newborn mouse at postnatal day 3, labeled with ^{3}H-thymidine in vitro and radioautographed. Only a few nuclei of acinar cells and ductal cells are labeled with silver grains. x500. From Nagata (2002, Figure 13B, p. 118). 2C. EMRAG of the submandibular gland obtained from a newborn mouse at postnatal day 1, labeled with ^{3}H-thymidine in vitro and radioautographed. Many silver grains are localized over the nucleus of an intercalated ductal cell. x10,000. From Nagata *et al.* (2000[a], Figure 9, p. 11). 2D. EMRAG of the esophageal epithelial cells of a newborn mouse at postnatal day 1, labeled with ^{3}H-thymidine in vivo and radioautographed. Many silver grains are localized over one of the nuclei of epithelial cells. x10,000. From Duan *et al.*(1993, Figure 4, p. 313). 2E. LMRAG of the colonic epithelial cells of a mouse embryo at fetal day 19, labeled with ^{3}H-thymidine in vivo and radioautographed. Many silver grains are localized over the nuclei of several epithelial cells in the bottom of the crypt (right). x800. From Jin (1996, Figure 1, p. 257). 2F. LMRAG of the ileum epithelial cells of a mouse at postnatal 6 months, labeled with ^{3}H-glucosamine in vivo and radioautographed. Many silver grains are seen over the brush border of the columnar epithelial cells and several silver grains are localized over the Golgi region of one of the goblet cell (arrow head). x1,200. From Morita (1993, Figure 2, p. 879). 2G. LMRAG of the colonic epithelial cells of a mouse at postnatal 1 month, labeled with 35SO4 in vivo and radioautographed. Several silver grains are localized over the Golgi region of 3 goblet cells as well as over the cytoplasm of several absorptive columnar cells. x1,000. From Nagata *et al.*(1999[a], Figure 4, p. 818). 2H. EMRAG of a goblet cell in the deeper crypt of the colonic epithelium of an adult mouse after injection with $^{35}SO_4$, fixed at 30 min, and radioautographed. Many electron dense silver grains are localized over the Golgi zone and mucous droplets in the goblet, demonstrating incorporation of radiosulfate into sulfomucins. x 4,800. From Nagata (2001[c], Figure 2, p. 40).

decreased steadily but remained higher than those of any other cell types (Chen *et al.*, 1995; Nagata *et al.*, 2000[b]). Since the LI of ICD cells was more than the other cell types and persisted for a long time, it was suggested from these results that ICD cells concerned with the generation of other cell types (Nagata *et al.*, 2000[b]).

The Glucide Synthesis of the Salivary Glands

Among the glucide synthesis, we studied the incorporations of ^{3}H-glucosamine into submandibular glands of 10 groups of litter mates at various ages from embryonic day 19 to postnatal day 1, 3, 7, 14, and month 1, 3, 6 to 1 and 2 years by LM and EMRAG (Watanabe *et al.*, 1997; Watanabe & Nagata, 2001). The results showed that the silver

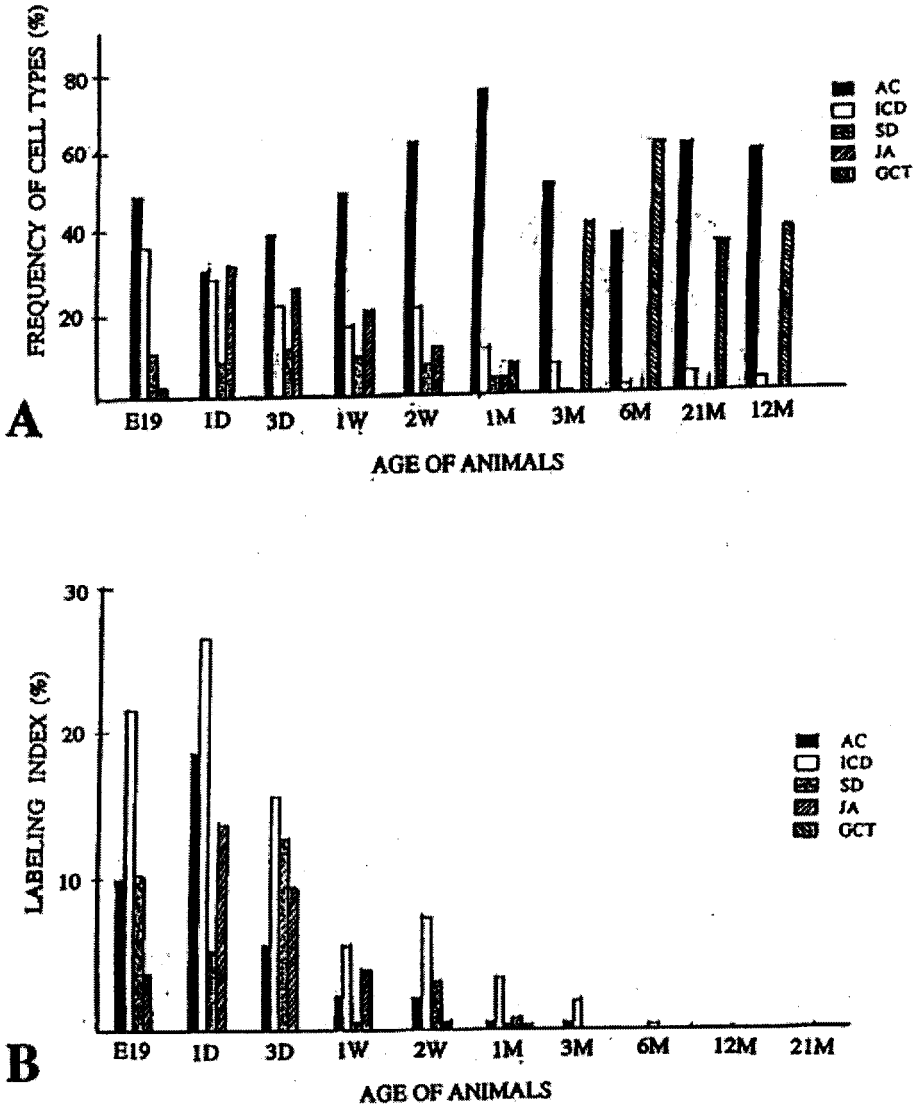

Figure 3. Histogram showing the frequencies of appearance of the five individual cell types and their labeling indices in the submandibular glands of male ddY mice at respective ages. 3A. Histogram showing the frequencies of appearance of the 5 individual cell types at respective ages. Abbreviations to the figure. AC: acinar cells, ICD: intercalated duct cells, SD: striated duct cells, JA: juxta-acinar cells, GCT: granular convoluted cells. From Nagata *et al.*(2000[a], Figure 11, p. 12). 3B. Histogram showing the labeling indices of the five individual cell types in the submandibular glands of male ddY mice at respective ages. Abbreviations are the same as in Figure 3B. From Nagata *et al.* (2000[a], Figure 12, p. 12).

grains appeared over the endoplasmic reticulum, Golgi apparatus and the secretory granules of the acinar cells, demonstrating the glycoprotein synthesis in these cells. Grain counting revealed that the counts increased from the fetal stage to postnatal day 1, 3, 7, reaching the peak at day 14 and decreased from month 1 to 24, showing the aging changes. These changes could impact on the composition of the saliva with age.

The Glycoprotein Synthesis of the Salivary Glands

The glycoprotein synthesis of the large salivary glands of adult ddY mice was studied by the incorporation of radiosulfate $Na_2{}^{35}SO_4$ by LMRAG (Nagata *et al.*, 1999[a]). We used two litters of normal adult ddY mice 30 days after birth, each consisting of 3 litter mates. One litter of animals was sacrificed at 30 min after the intraperitoneal injections with phosphate buffered $Na_2{}^{35}SO_4$, and the other litter animals were sacrificed at 12 h after the injections. Then the parotid glands, the submandibular glands and the sublingual glands were taken out. The tissues were fixed, processed for RAG. Many silver grains were observed on serous cells of the salivary glands at 30 min and 12 h after the injection. The numbers of silver grains at 30 min were less than those at 12 h. From the results, it was concluded that glycoprotein synthesis was demonstrated in the 3 large salivary glands, the parotid, the submandibular and the sublingual glands by radiosulfate incorporation.

The number of silver grains in the parotid gland cells, the serous cells, was more than the other 2 glands. In the submandibular and the sublingual glands, silver grains were more observed in serous cells than mucous cells at 30 min, while in mucous cells more at 12 h than 30 min after the injection. These results showed the time difference of glycoprotein synthesis and the difference between the serous and the mucous cells in these 3 salivary glands (Nagata *et al.*, 1999[a]).

The Macromolecular Synthesis of the Esophagus

The esophagus of mammals consists of epithelial cells, connective tissue cells and skeletal or smooth muscle cells. Among the macromolecular synthesis of the esophagus, we have studied only the DNA synthesis, which attracted the interests in the turnover of the epithelial cells. Other macromolecular synthesis such as RNA, proteins or glycoproteins has not yet been elucidated.

The DNA Synthesis of the Esophagus

We studied the DNA synthesis of the esophagus of several groups of aging ddY mice aged at postnatal day 1, 3, 7, 14, month 1, 2, 6, 12, 24, each consisting of 3 litter mates, labeled with ^{3}H-thymidine by LM and EM RAG (Duan *et al.* 1992, 1993). The labeled cells were mainly found in the basal layer of the esophageal epithelium (Figure 2D). The nuclei and nucleoli of labeled cells were larger than those of unlabeled cells, but contained fewer cell organelles. The LI in respective aging groups showed a peak at postnatal day 1 (12%) and decreased with aging to a few percents at 2 years (Figure 4). The results indicated that the esophageal epithelial cells proliferated in the basal layer at early neonatal stages to adult stage at month 1 and 2, then continued to substitute the lost cells from the epithelial surface into the esophageal lumen.

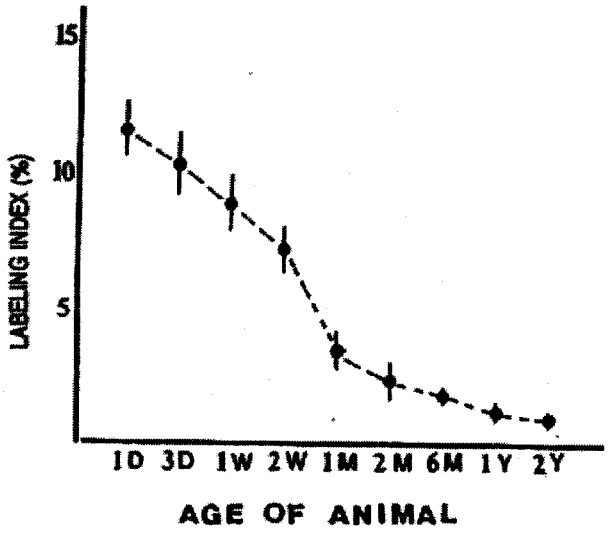

Figure 4. Transitional curve of the labeling indices of the esophageal epithelial cells labeled with ^{3}H-thymidine obtained from respective aging groups at postnatal day 1 to 2 years. Mean ± standard deviation. From Duan *et al.* (1993, Figure 3, p. 312).

The Macromolecular Synthesis of the Stomach

The stomach consists of 4 layers, the mucosa, the submucosa, the muscular layer and the serosa. These layers are composed of the epithelial cells, the connective tissues and the smooth muscle cells. Among the macromolecular synthesis of these cells,

we mainly studied the protein and glycoprotein synthesis in several groups of ddY strain mice at various aging stages.

The DNA Synthesis of the Stomach

The turnover of the gastric glandular cells by ^{3}H-thymidine radioautography was already extensively investigated by Leblond and his co-workers (Leblond, 1981). They demonstrated cell kinetics of the antral epithelial cells including fundic glandular cells of mice (Lee, 1985[ab]; Lee & Leblond, 1985[ab]). Therefore, we have not studied the DNA synthesis of the stomach so much.

The Protein Synthesis of the Stomach

We studied the protein synthesis and the secretion process in G-cells by EMRAG using ^{3}H-amino acid incorporation (Sato *et al.*, 1977; Sato, 1978). We labeled the stomach tissues of adult Wistar rats in a medium containing either ^{3}H-glutamic acid or ^{3}H-glycine in vitro for varying time intervals, from 3 min to 12 hr, fixed and processed for EMRAG. As the results, silver grains in the EMRAG appeared first over the Golgi zones within 5 min, then migrated to secretory granules and were stored in the cytoplasm while few grains remained on the nuclei at 30 min. No alteration in the intracellular distribution pattern of the silver grains was observed at 60 min. These results suggested the incorporation of both the amino acids into the cell organelles and into the secretory granules, which were discharged into the gastric lumen revealing the secretory kinetics of the stomach (Sato *et al.*, 1977; Sato, 1978).

The Glycoprotein Synthesis of the Stomach

We studied the incorporation of radiosulfate into sulfated complex carbohydrate in the stomachs of adult ddY mice by LM and EM RAG after labeling with $^{35}SO_4$ in vivo (Nagata *et al.*, 1988[a]). Three litters of normal mice, each consisting of 3 individuals, were injected intraperitoneally with radiosulfate solution. At 30 min, 60 min and 180 min after the injections, the 3 groups of animals were sacrificed and the stomachs were fixed, embedded, sectioned and processed for LM and EM RAG. On radioautograms silver grains appeared over the glandular epithelial cells of the pyloric glands but not over those of the fundic gland cells, demonstrating the mucous synthesis in the pyloric glands (Nagata *et al.*, 1988[a]; Nagata & Kawahara, 1999). The radiosulfate uptake and accumulation in the stomach of ddY mouse were also studied by LMRAG (Nagata *et al.*, 1999[a]). Two litters of normal adult ddY mice, 30 days after birth, each consisting of 3 animals, were studied. One litter of animals was sacrificed at 30 min after the intraperitonially injections with phosphate buffered $Na_2{}^{35}SO_4$, and the other litter animals were sacrificed at 12 h after the injections. Then the antrums and funduses of the stomachs were taken out. The tissues were fixed, dehydrated, embedded in epoxy resin, sectioned, processed for radioautography, stained with toluidine blue and analyzed by light microscopy. As the results, many silver grains were observed on the mucosa and submucosa of the stomach at 30 min after the injection. Then at 12 h after the injection silver grains were observed over the gastric glands showing glycoprotein synthesis. The numbers of silver grains observed in the stomach at 30 min were less than those at 12 h. The results revealed the time difference of glycoprotein synthesis in the stomach (Nagata *et al.*, 1999[a]).

We also studied the mechanism of serum albumin passing through the gastric epithelial cells by EMRAG (Komiyama *et al.*, 1978). When Wistar rat stomach tissues were labeled in a medium containing 132I-albumin in vitro for varying time intervals

from 3 min to 30 min, silver grains in the radioautograms appeared over rough endoplasmic reticulum of the gastric mucosal epithelial cells within 3 min, then moved to the Golgi apparatus from 3 min to 10 min, and on to secretory granules as well as into the lumen in 30 min, suggesting the pathway of serum albumin from the blood vessels through the gastric mucous epithelial cells and finally into the gastric lumen. It was supposed that albumin which was absorbed from the blood into the epithelial cells was incorporated into glycoprotein in the endoplasmic reticulum of the gastric mucosal epithelial cells and passed through the Golgi apparatus, moved into the secretory granules and was finally discharged as the components of the mucous into the gastric lumen (Komiyama *et al.*, 1978).

The Macromolecular Synthesis of the Intestines

The intestines of mammals are divided into 2 portions, small and large intestines, which can be further divided into several portions. The small intestines are divided into the duodenum, the jejunum, and the ileum, while the large intestines into the cecum, the colon and the rectum. The intestinal wall in any portions consists of 4 layers, the mucosa, the submucosa, the muscular layer and the serosa. These layers are composed

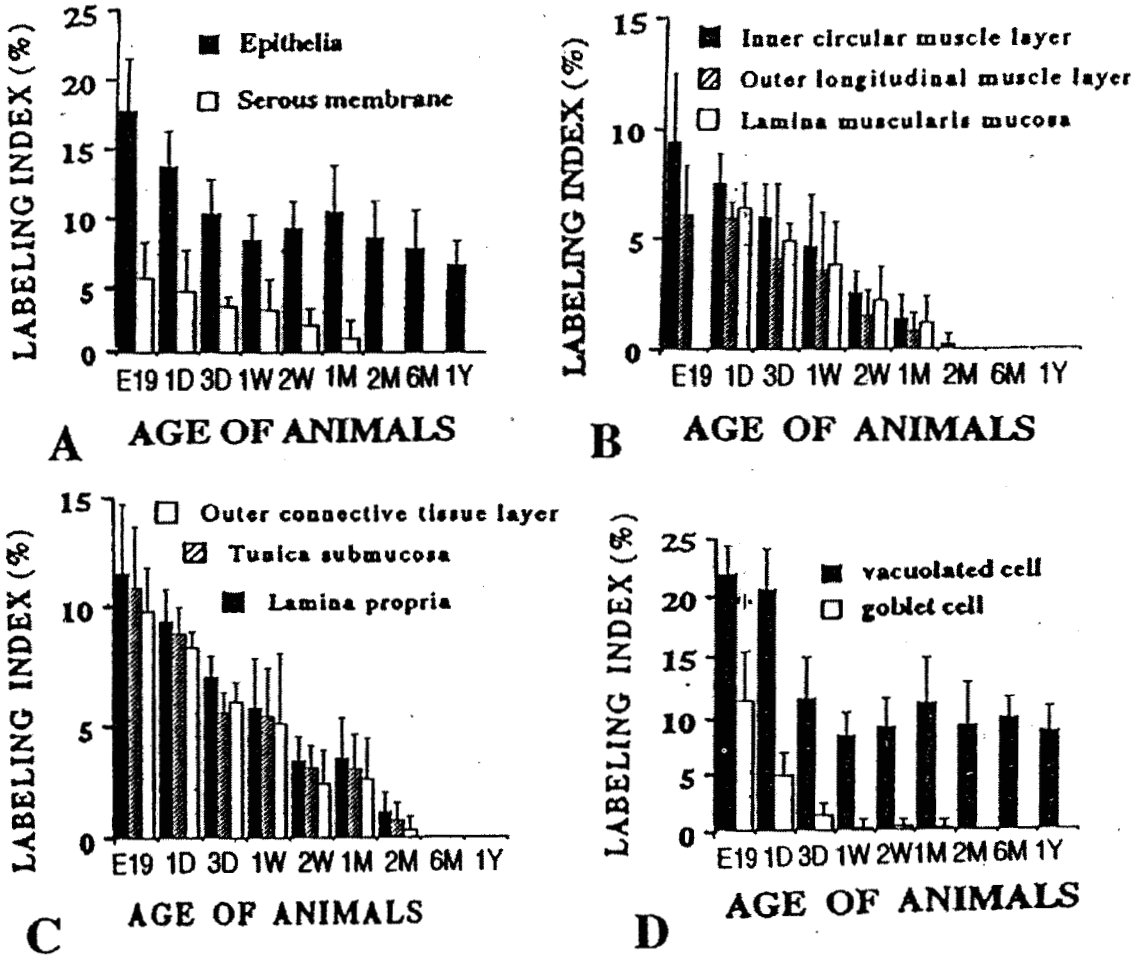

Figure 5. Histograms showing aging changes of average labeling indices in respective tissue layers and cells of mouse colon at various ages from embryo to postnatal 1 year labeled with ^{3}H-thymidine. 5A. Labeling indices of the epithelia and the serous membranes. 5B. Labeling indices of the inner circular muscle layer, the outer longitudinal muscle layer and the lamina muscularis mucosae. 5C. Labeling indices of the lamina propria, the tunica submucosa and the outer connective tissue layer. 5D. Labeling indices of the vacuolated cells and the goblet cell. From Jin (1996, Figures 30, 31, 32, 33, p. 263).

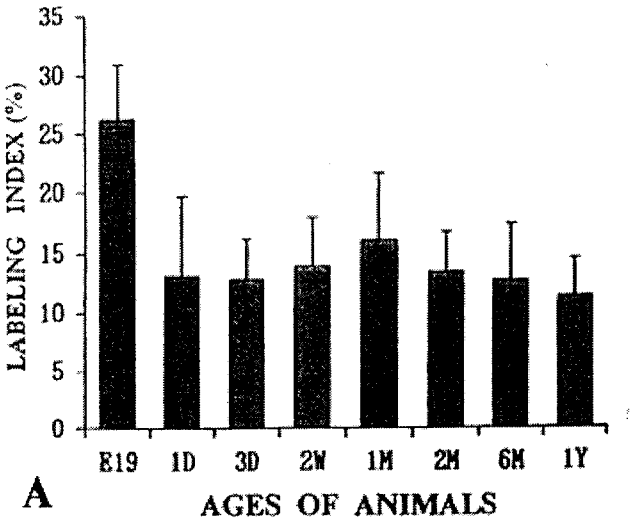

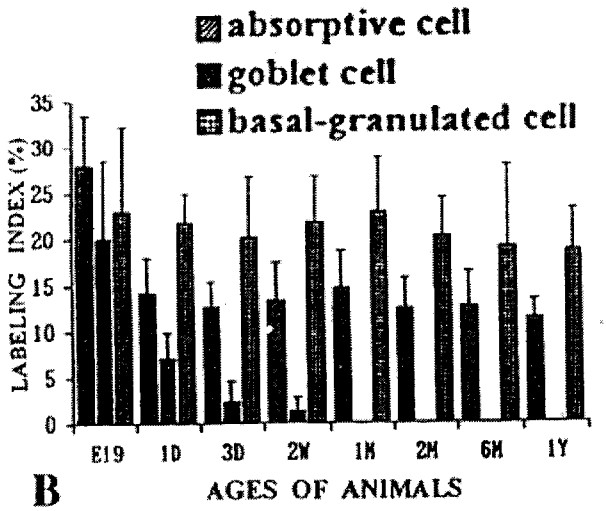

Figure 6. Histograms showing aging changes of average labeling indices in the epithelial cells (6A) and vacuolated cells, goblet cells and basal granulated cells (6B) of mouse cecum from prenatal day 19 to postnatal 1 year labeled with ^{3}H-thymidine. From Jin (1996, Figure 29, p. 262).

of the columnar epithelial cells including absorptive and secretory cells, mucosal and submucosal connective tissue cells, smooth muscle cells in the muscular layer and the serosal epithelial cells. We studied the macromolecular synthesis, mainly DNA, glycoproteins and glucides, in these cells by LM and EM RAG as well as by histochemical stainings.

The DNA Synthesis of the Intestines

As for the DNA synthesis, incorporating ^{3}H-thymidine, Leblond and his co-workers (Leblond & Messier, 1958; Cheng, 1974[a,b]; Cheng & Leblond, 1974[a,b]) had already studied the cell kinetics of the 4 main epithelial cell types in the small intestines of adult mice. We studied not only the epithelial cells but also all the cell types in the 4 layers of both the small and the large intestines of ddY strain mice at various ages from embryos to senescence at postnatal 2 years (Nagata, 1995[a], 1999[c]). The epithelial cells of mice labeled with ^{3}H-thymidine were localized in the crypts of both the small and the large intestines at various ages from fetal day 19 to postnatal day 1, 3, 7, 14, month 1, 2, 6 and 12 (Figure 2E). This region was formerly defined by Cheng and Leblond (1974[a,b]) as the proliferative zone. In the colon of aging mice from fetal to postnatal 2 years, the labeled cells in the columnar epithelia were frequently found in the perinatal groups from embryo to postnatal day 1. However, the labeling indices (LI) of the columnar epithelial cells of mouse colon as demonstrated by ^{3}H-thymidine RAG as well as PCNA/cyclin immunostaining became constant from the suckling period until senescence (Morita *et al.*, 1994[a]). We also examined the LI of respective cell types in each layer of mouse colon such as columnar absorptive epithelial cells, vacuolated cells and goblet cells in the mucosa, the connective tissue cells in the lamina propria mucosae, tunica submucosae and outer connective tissue layer, the smooth muscle cells in the lamina muscularis mucosae, the inner circular muscle layer, the outer longitudinal muscle layer, and the epithelial cells in the serous membrane of the colons and the cecums changed due to aging at various ages (Jin, 1996; Jin & Nagata, 1996). It was found that most LI decreased after birth (10%) to 2 month (a few percent) except the epithelial cells,

which kept constant value (10-15%) to senescence (Figure 6). Similar results were also obtained from the cecum of ddY mouse at various ages (Figure 7) by LM and EMRAG (Jin & Nagata, 1995[a,b]).

On the other hand, we also studied immunostaining for PCNA/cyclin and compared the results with RAG (Morita *et al.*, 1994[a]). We fixed the colonic tissues of litter mice of 6 aging groups from the embryonic day 19, to newborn postnatal day 1, 5, 21, adult month 2 and senescent month 11 in methacarn fixative, embedded in paraffin, sectioned and immunostained for the cyclin proliferating nuclear antigen (PCNA/cyclin), which appear from G1 to S phase of the cell cycle, with the monoclonal antibody and the avidin-biotin peroxidase complex technique (Morita *et al.*, 1994[a]). The immunostaining positive cells were localized in the crypts of colons similar to the labeled cells with ^{3}H-thymidine by RAG, a region defined as the proliferative zone (Cheng & Leblond, 1974[a,b]). The PCNA/cyclin positive cells in the columnar epithelia were frequently found in the perinatal groups from embryo to postnatal day 1, and became constant from postnatal day

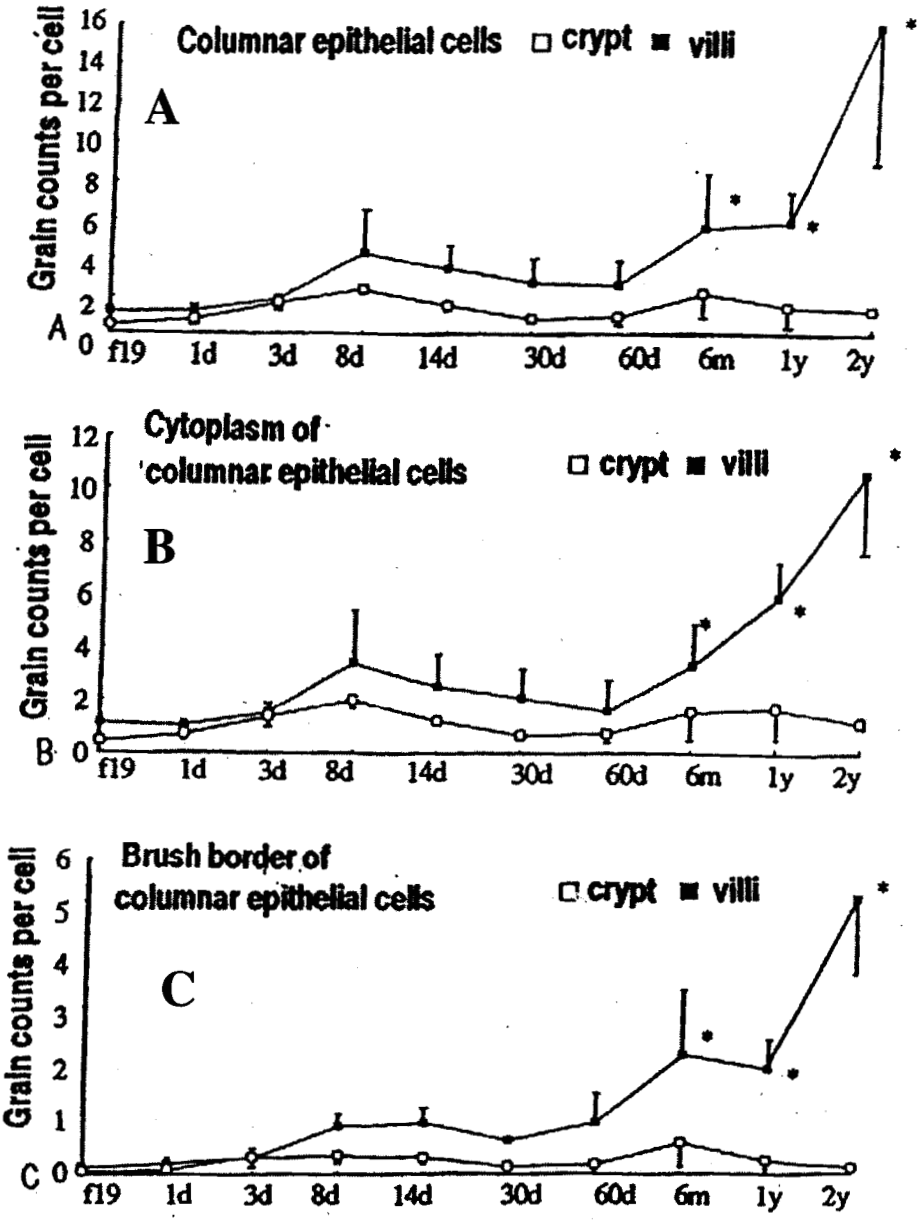

Figure 7. Transitional curves of the grain counts in columnar epithelial cells in mouse ileum at various ages labeled with ^{3}H-glucosamine. Closed squares express the grain counts on the intestinal villi while the open squares on the crypts.

7A. Total grain counts.

7B. The grain counts on the cell bodies of the epithelial cells, including Golgi regions and nuclei.

7C. The grain counts on the brush borders. From Morita (1993, Figure 3, p. 881).

5 until senescence (Morita *et al.*, 1994[a]).

Comparing the results by immunostaining with the labeling index by RAG, it was found that the former was higher in each aging group than the latter. The reason for the difference should be due to that PCNA/cyclin positive cells included not only S-phase cells but also the late G1 cells (Morita *et al.*, 1994[a]).

The Glucide Synthesis of the Intestines

We also studied the aging changes of ^{3}H-glucosamine uptake in the mouse ileum (Morita, 1993), and found that the silver grains in the columnar epithelial cells were mainly localized over brush borders and the Golgi region, whereas in the goblet cells they were over the Golgi region and mucous granules (Figure 2F). The grain counting revealed that the total number of silver grains (Figure 7A) as well as grains over the cytoplasm (Figure 7B) and the brush borders (Figure 7C) of the columnar epithelial cells increased in the villi than in the crypts from postnatal month 6 up to year 2 due to aging. The grain counting of other cell types also showed that the number of silver grains in goblet cells (Figure 8A), basal granulated cells (Figure 8B) and Paneth cells (Figure 8C) increased by aging but did not in undifferentiated cells (Figure 8D).

On the other hand, in order to analyze the sugar residues of the glycoproteins in the goblet cells, the colonic tissues of mice from several aging groups were fixed in buffered paraformaldehyde/ glutaraldehyde and stained with two lectins, Triticum vulgaris (WGA, wheat germ agglutinin) and Datura stramonium (DSA, Datura stramonium agglutinin). The former is specific for GlcNAc (N-acetyl-D-glucosamine), while the latter for chito-oligosaccharide (Nagata, 2001[c]). From the results, it was shown that the staining pattern of the goblet cell granules in the colonic epithelia in various aging groups changed from the perinatal to postnatal development to the senescence (Morita *et al.*, 1994[b]).

The Glycoprotein Synthesis of the Intestines

As for the glycoprotein in the intestines, we first studied the synthesis of mucosubstances in goblet cells as well as in absorptive epithelial cells demonstrating $^{35}SO_4$ incorporations in the duodenum, the jejunum and the colon at varying time intervals from 30, 60, to 180 min after the RI administration (Nagata *et al.*, 1988[a]). The results from LMRAG (Figure 2G) showed that many silver grains were localized over the columnar absorptive cells and the goblet cells, especially over the Golgi regions and mucous granules of the goblet cells. The intracellular localization of silver grains in goblet cells, especially over the Golgi apparatus, was clearly shown by EMRAG. By EMRAG silver grains first appeared over the Golgi zone at 30 min after the administration (Figure 2H) and then moved to the secretory granules at 60 and 180 min. Grain counting of these radioautograms revealed that the average grain counts were different in the upper and deeper regions of the crypts in the 4 portions of the intestines of mice, the duodenum, the jejunum, the cecum and the distal colon (Figure 9A), and it was shown that silver grains over goblet cells in the lower region of the colonic crypt transferred rapidly from 30 min to 180 min, while they transferred slowly in goblet cells in the upper region of the colonic crypt (Figure 9B), leading to the conclusion that the rates of transport and secretion of mucous products of the goblet cells at these two levels in the crypts were different.

On the other hand, we also studied the incorporations of $Na_2{}^{35}SO_4$ into sulfated complex carbohydrate in the small and large intestines of adult ddY mice at postnatal month 1 by both LM and EM RAG (Nagata & Kawahara, 1999). We injected $Na_2{}^{35}SO_4$ in saline into the peritoneal cavities of 9 male litter mice at postnatal month 1, and they

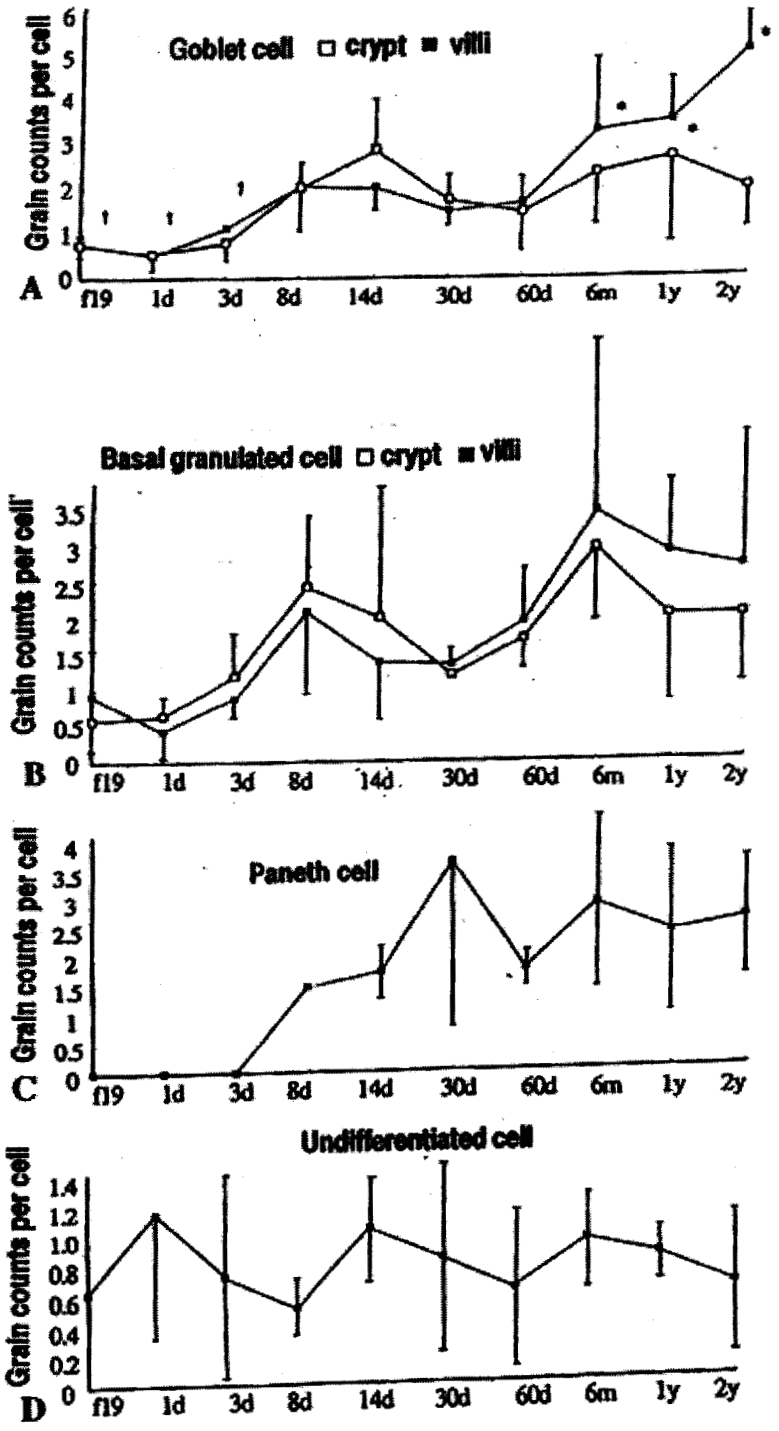

Figure 8. Transitional curves of the grain counts in respective epithelial cells in mouse ileum at various ages labeled with ^{3}H-glucosamine. Closed squares express the grain counts on the intestinal villi while the open squares on the crypts. 8A. The grain counts of the goblet cells. 8B. The grain counts of the basement granular cells. 8C. The grain counts of the Paneth cells. 8D. The grain counts of the undifferentiated stem cells. From Morita (1993, Figure 4, p. 882).

were successively sacrificed at 30, 60 and 180 min after the injection. We took the 6 portions of the small and large intestines of the animals, the duodenum, the jejunum, the ileum, the cecum, the proximal colon and the distal colon, respectively, and processed for RAG. By grain counting, quantitative differences were observed in the relative uptake of radiosulfate in the various labeled cells of each organ. Incorporation by the colon in goblet cells exceeded that elsewhere in the deep goblet cells of the colonic crypts migration of label progressed during the time tested from the supranuclear Golgi region to the deep

position of the goblet and then extended throughout the mucosubstance in the goblet in the superficial goblet cells of the colon. The radioautographic and cytochemical staining differences between secretory cells in the deeper region compared with the upper region of the colonic crypts were considered to reflect differences in the rate of transport of secretory products in the theca and the rate of secretion at the low levels in the crypt. These results showed the time differences of glycoprotein synthesis in respective organs. The sulfate uptake and accumulation in several mouse digestive organs were also studied by LMRAG (Nagata *et al.*, 1999[a]). Two litters of normal ddY mice at postnatal day 30, each consisting of 3 animals, were studied. One litter of animals was sacrificed at 30 min after the intraperitonially injections with phosphate buffered $Na_2{}^{35}SO_4$, and the other litter animals were sacrificed at 12 h after the injections. Then several digestive organs, the parotid gland, the submandibular gland, the sublingual gland, antrum and fundus of the stomach, the duodenum, the jejunum, the ileum, the cecum, the ascending colon and the descending colon were taken out and radioautographed. As the results, many silver grains were observed on villous cells and crypt cells of the small intestines and whole mucosa of the large intestines at 30 min after the injection. Then at 12 h after the injection silver grains were observed on mucigen granules of goblet cells in the small intestines and the large intestines. The numbers of silver grains observed in respective organs at 30 min were less than those at 12 h. From the results, it is concluded that glycoprotein synthesis was demonstrated in several digestive organs by radiosulfate incorporation. In order to compare the cytochemical staining with RAG, some portions of the small and large intestines, the duodenum, the jejunum, the proximal and the distal colon were stained

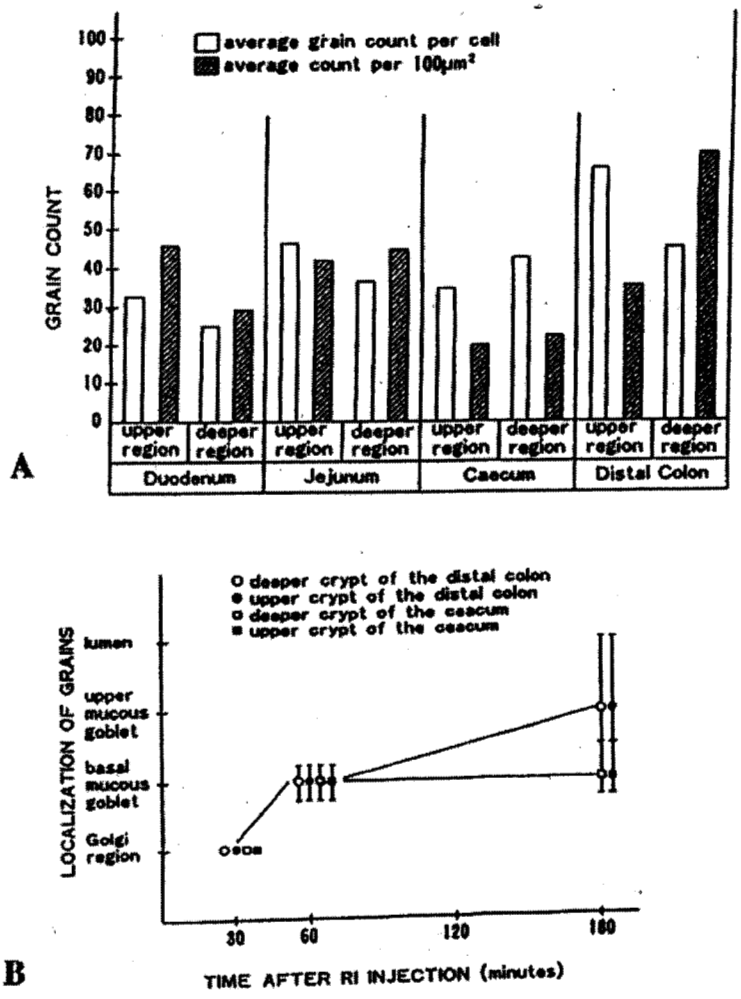

Figure 9. Analysis of radiosulfate incorporations into the goblet cells at respective digestive organs. 9A. Histogram showing the results of grain counting, both average grain counts per cell and average grain counts per unit area, in goblet cells of respective intestines. 9B. Transitional curves of grain localization in goblet cells in the large intestines, the cecum and the distal colon, from 30 min to 180 min after radiosulfate injection. From Nagata & Kawahara (1999, Figure 10, 11, p. 350).

with HID-AB (high iron diamin-alcian blue) sequence (Nagata & Kawahara, 1999). The surface absorptive cells in the small and large intestines did not show any staining with HID-AB sequence. However, goblet cells in small and large intestines stained either HID or AB, showing variations in respective regions.

Goblet cells deeper in the colonic crypt differed from those higher in the crypts in showing weaker staining for carbohydrate, lesser accumulation of secretion in the apical cytoplasm and distinct staining of a surpranuclear focus interpreted as being Golgi zone (Figure 10C). Goblet cells deeper in the colonic crypts differed from those higher in the crypts in showing weaker staining for carbohydrate, a lesser accumulation of secretion in the apical cytoplasm and distinct staining of a supranuclear focus interpreted as the Golgi zone. In general, the goblet cells in the upper region of the crypts stained black with HID, while the goblet cells in the deeper regions stained blue with AB (Figure 10C). The HID staining which was considered to be specific for demonstration of sulfated complex carbohydrate, correlated well with radioautographic evidence of radiosulfate incorporation (Nagata & Kawahara, 1999). When the colonic goblet cells of normal mice were stained with the PA-TCH-SP reactions for mucopolysacharides, the positive reaction with electron dense deposits appeared in the mucous granules in the Golgi area as well as the goblets in the apical cytoplasm of the goblet cells (Figures 10AB). The mucous granules in the Golgi area and the goblets can be observed 3-dimensionally as superimposed particles in stereo-pair pictures (Nagata, 1999[a], 2000[a], 2001[a,b]).

In order to determine the total content of sulfur (S) bound to glycoproteins in the Golgi regions of the goblet cells in different regions of the colon at different ages of animals, on the other hand, we carried out X-ray microanalysis using analytical electron microscopes (Maruyama & Nagata, 1987). Nine groups of aging ddY mice, aged from fetal day 19 to postnatal day 1, 3, 8, 14 and month 1, 2, 6 and 12, each consisting of 3 litter mates, were used. The proximal colon tissues were fixed in phosphate buffered 2.5% glutaraldehyde and 1% osmium tetroxide, embedded in Epon, sectioned at 0.2 or 0.4 μm thick. For X-ray microanalysis a high voltage JEOL JEM 4000EX TEM system equipped with a Tracor-Northern energy dispersive X-ray microanalyzer TN-5400 was used with a fixed beam current at 3.2 nA and 2 μm in diameter for 100 s with a dead time of 30%, changing the accelerating voltages at 100, 200, 300 and 400 kV for preliminary experiments. Figures 10GH are electron micrographs showing Golgi regions of colonic goblet cells in the lower crypts of aging mice from postnatal day 8 (Figure 10G) to month 1 (Figure 10H). The peak counts of S and background counts of goblet cell cytoplasm of the upper and lower crypt goblet cells at 0.2 or 0.4 μm thickness were observed at 100, 200, 300, 350 and 400 kV (Figure 11). From these results, peak to background ratios were calculated respectively and the transitional curves of the P/B ratios of goblet cell granules in the upper and lower crypts in respective ages as observed at varying accelerating voltages from 100 to 400 kV were shown in Figure 12A. The maximum was found at 300 kV (Nagata, 2000[b]). Therefore, we used 300 kV for further quantification. The P/B ratios of sulfur in mucigen granules in the goblet cells in the lower crypts of mice aged from fetal day 19 to postnatal day 3 were higher than in the upper crypts of the same ages. The spectrum at day 30 was the highest in both the upper and lower crypts. However, the P/B ratios at day 14 were the highest in both the upper and lower crypts. The curves obtained from P/B ratios in both upper and lower crypt cells in relation to aging are shown in Figure 12B. These results demonstrated that the P/B ratios of sulfur in the goblet cells of aging mice increased from perinatal stages to postnatal week 2 and decreased to senescence at 1 year and they were higher in the upper crypts than the lower (Nagata, 2000[b]).

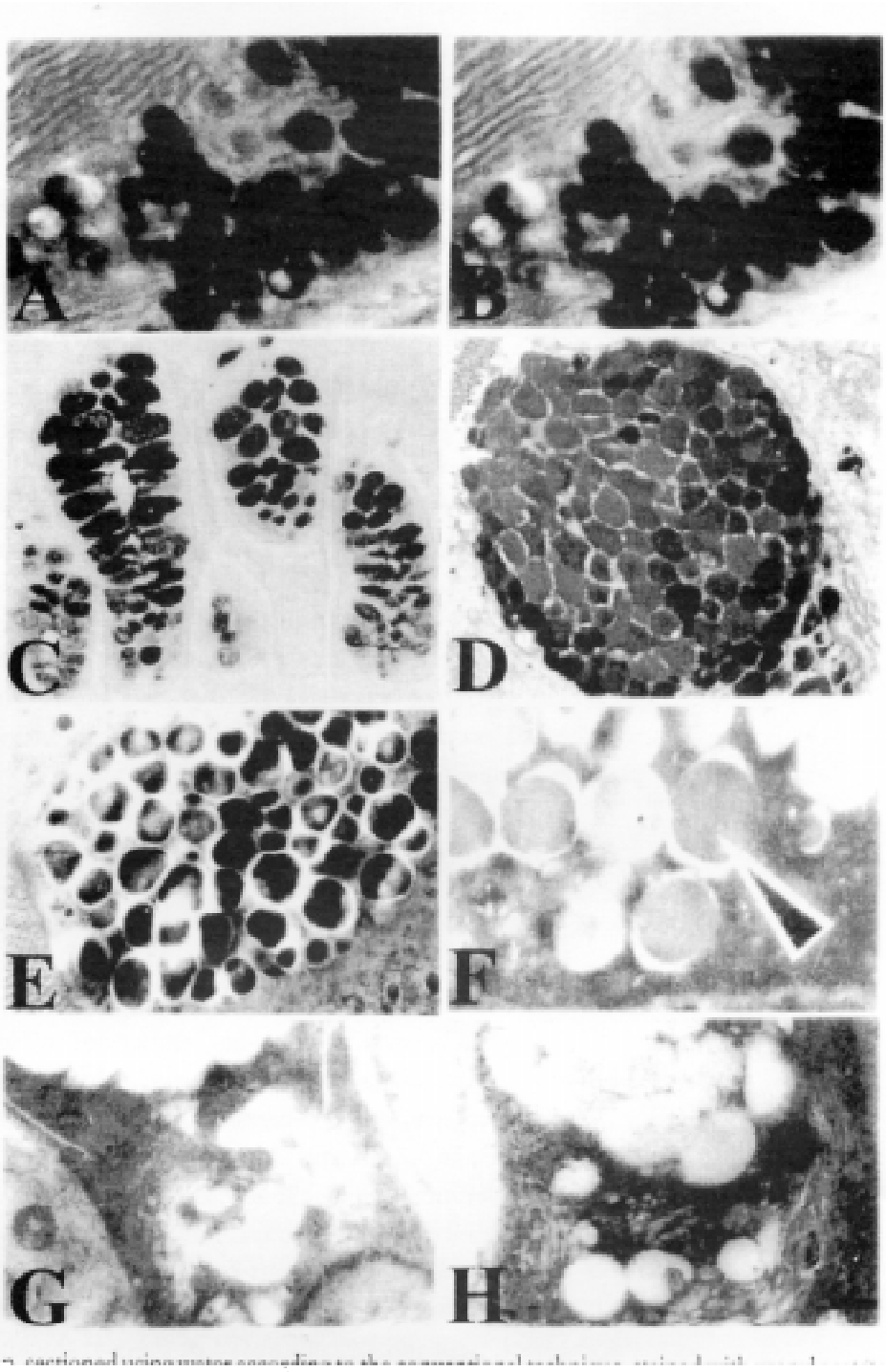

Figure 10. Histochemical staining of the intestinal cells. 10AB. Stereo-pair high voltage electron micrographs of a colonic goblet cell of a mouse colon, fixed, thick sectioned and stained with PA-TCH-SP, tilting +8°C (A) and -8°C (B), observed by high voltage electron microscopy at 1,000kV. The two pictures can be seen with a stereoscope or by stereoscopic imaging. Electron dense mucous granules piling up in the cytoplasm at center. x 10,000. Bar = 1μm. From Nagata T (2000[c]). 10C. Light micrograph of the colon of a mouse stained with HID-AB sequence. The goblet cells in the upper region (upper half of the picture) of the crypts stained black with HID (appearing dark in black and white picture), while the goblet cells in the deeper region (lower half) stained blue with AB (appearing light in black and white picture). The HID positivity is specific for sulfomucin in the goblet. x600. Bar=10μm. From Nagata T (2001[c], Figure 1A, color page p.2). 10D. Electron micrograph of a mouse proximal colon, fixed chemically with 2.5% glutaraldehyde in phosphate buffer at pH 7.4, dehydrated, embedded in Epon, sectioned using water according to the conventional technique, stained with uranyl acetate and lead citrate. Electron dense mucigen granules can be seen in the apical cytoplasm of the cell fusing together. x 8,000. Bar=1μm. From Nagata *et al.* (2000[c], Figure 1, p.4). 10E. Electron micrograph of a goblet cell of mouse proximal colon, cryofixed by metal contact method using a JFD-RFA freezing apparatus cooled with liquid nitrogen, freeze-substituted in absolute acetone containing osmium tetroxide, embedded in Epon and dry-sectioned. The apical cytoplasm of these goblet cells containing mucigen granules appears amorphous and dense surrounded with amorphous cytoplasm with cell organelles. x 9,000. Bar=1μm. From Nagata *et al.* (2000[c], Figure 3, p. 5). 10F. Electron micrograph of a Paneth cell in the duodenum of a 1 month old mouse, fixed in buffered glutaraldehyde, embedded in Epon, sectioned and stained with uranyl acetate and lead citrate. The granule indicated with an arrow was studied by X-ray microanalysis. x 8,000. Bar=1μm. From Nagata (2000[b], Figure 23, p. 29). 10GH. Electron micrographs of the goblet cells in the lower crypts of proximal colons of mice at different ages, showing Golgi regions. 10G. A goblet cell of a newborn mouse at postnatal day 8. x8,000. Bar=1μm. 10H. A goblet cell of an adult mouse at postnatal month 1. x8,000. Bar=1 μm. From Nagata (2000[b], Figure 31, p. 33).

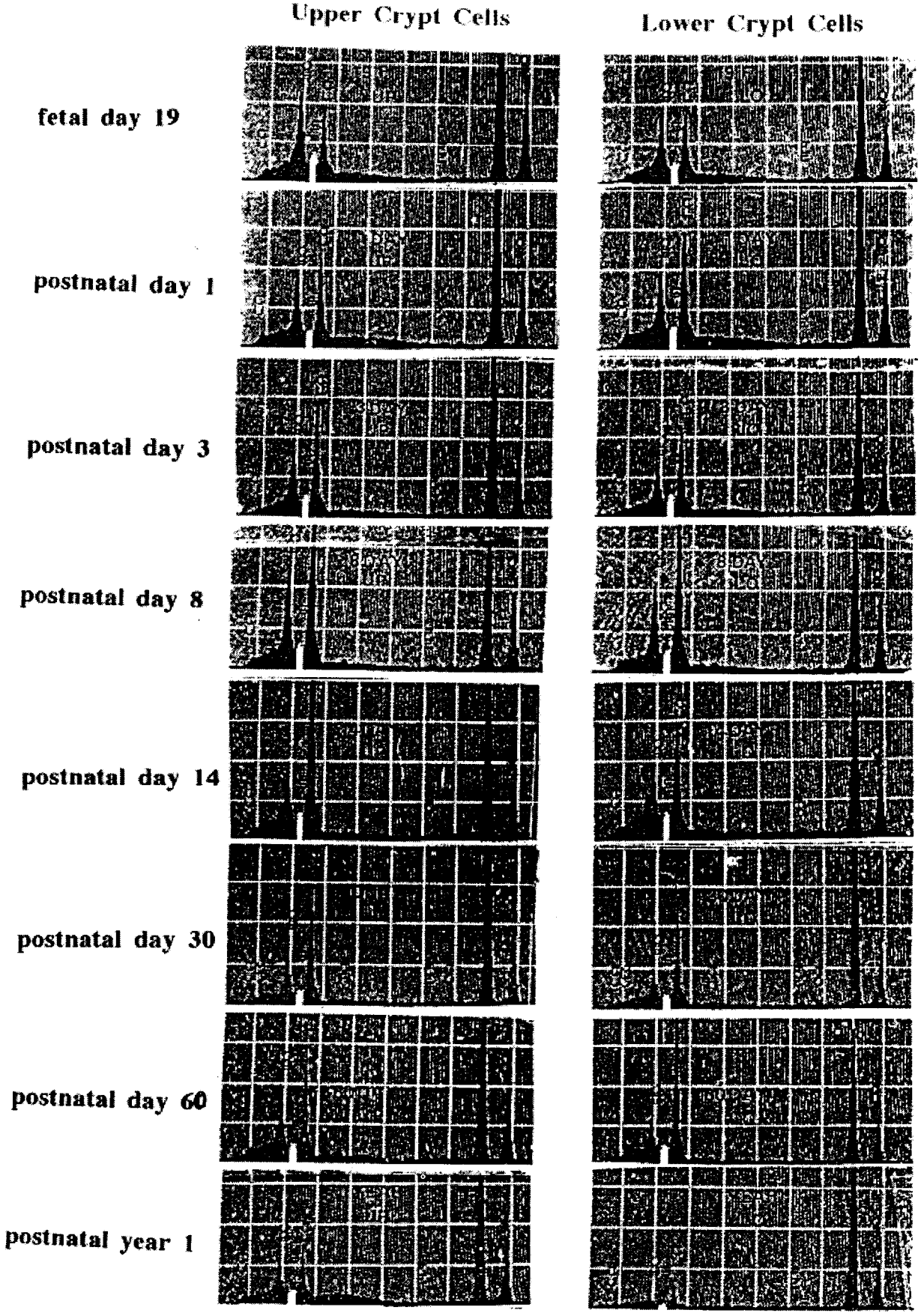

Figure 11. X-ray spectra of S-Kα obtained from the Golgi regions of goblet cells in the upper (left) and lower (right) crypts of mice aged from fetal day 19, newborn days 1, 3, 8, 14, 30, 60 and year 1 (from top to down). From Nagata (2000[b], Figure 32, p.33).

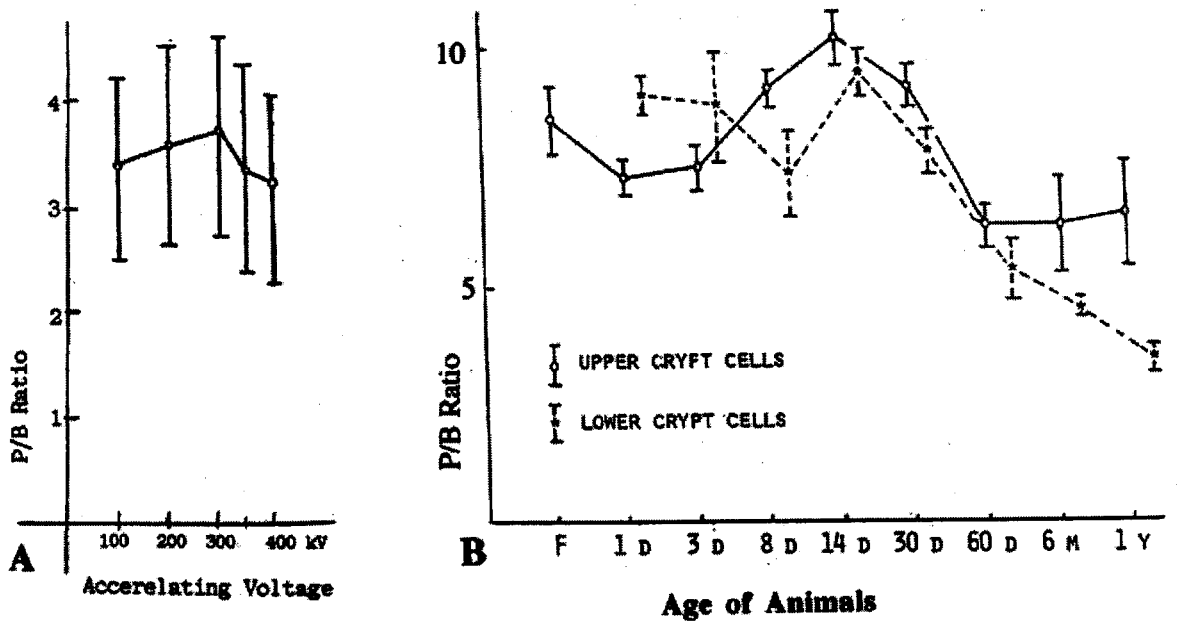

Figure 12. Relation of the P/B ratios of S in the mucigen granules in the colonic goblet cells of mice by X-ray microanalysis to the accelerating voltages and aging changes. 12A. Transitional curve of P/B ratios of S in mucigen granules in goblet cells observed at different accelerating voltages from 100 to 400 kV. From Nagata (2000[b], Figure 33, p. 34). 12B. Relation of the P/B ratios of S in mucigen granules in the goblet cells in the upper and the lower crypts of the colons to aging of mice. From Nagata (2000[b], Figure 34, p. 34).

The changes of elements in the goblet cell secretory granules in the three portions of the jejunum, proximal and distal colons aging from 14 days to 18 months after birth were studied by quantitative electron probe X-ray microanalysis on quick frozen and freeze-dried cryosections calculating P/B ratios of each element (Ichikawa *et al.*, 1994). As the results of the analysis of five elements, the peaks declined in turn S-Kα (sulfur), K-Kα (potassium), Cl-Kα (chlorine), P-Kα (phosphorus) and Ca-Kα (calcium) in the jejunum at postnatal month 1. In the proximal colon, the peaks declined in turn K-Kα, S-Kα, Cl-Kα, Ca-Kα and P-Kα at postnatal month 3. On the other hand, in the distal colon, the peaks declined in turn S-Kα, K-Kα, Ca-Kα, Cl-Kα and P-Kα at month 3. The highest average P/B ratio of S was obtained in the jejunum at month 1, and declined afterward with aging. In the proximal colon, the average P/B ratio of K was the highest at month 3, then declined afterward with aging. The highest average P/B ratio of S was at month 3. The highest average P/B ratio of K in the distal colon was at month 1. The ratio of peak counts to the background was calculated on each granule and significant differences in the P/B ratios of S and K between the proximal and distal colons were found out. As for S, the jejunum and the distal colon had the highest ratios and the proximal colon had the second. Concerning K, the proximal colon had the highest ratio and the jejunum and the distal colon had the second. The secretory granules of goblet cells in the three portions of intestinal tracts were shown to contain the different amount of each element. Especially, the amount of S appeared the most different from the proximal to the distal colon.

In order to quantify the elemental constituents of glycoproteins in mucigen granules of colonic goblet cells in mice under different fixations, mouse colonic tissues were treated either cryo-fixed, cryo-sectioned and freeze-dried (Figure 10E) or freeze-substituted, embedded and dry-sectioned (Nagata *et al.*, 2000[c]). The other tissues were also chemically fixed (Figure 10D), embedded and wet-sectioned. All the specimens were analyzed with a JEOL JEM-4000EX TEM system equipped with a Tracor-Northern energy

dispersive X-ray analyzer TN5400 at accelerating voltages of 300-400kV. The results showed that S and some other elements were better demonstrated in cryo-fixed sections than chemically fixed ones (Figure 13). Among the cryo-techniques tested, cryo-sections followed by freeze-drying were the best to preserve various elements in the granules (Figure 14). Then freeze-substituted plastic embedded absolutely dry-sections without any trough liquid followed. The freeze-substituted plastic embedded dry-sectioning on ethylene glycol induced some loss of K (Figure 14). Higher concentration of S in the mucigen granules of the goblet cells than in the cytoplasmic matrix suggests that S is the constituent of the glycoproteins in the granules in colonic goblet cells (Nagata *et al.*, 2000[c]).

To compare the difference between the intestines, quick-frozen and freeze-dried cryo-sections prepared from the 3 portions, *i.e.*, the duodenum, the proximal colon and the distal colon, obtained from 5 groups of aging mice from postnatal day 14, months 1, 3, 6 and 18, were studied (Kametani *et al.*, 1998). By quantitative X-ray microanalysis, the peaks of 5 elements decreased in the order of S, K, Cl, P and Ca in the duodenum at month 5, the peaks declined in the order of K, S, Cl, Ca and P at month 3 in the proximal colon, and the peaks declined as S, K, Ca, Cl and P at month 3 in the distal colon. The highest average ratio of S was obtained in the duodenum at month 1 and this value was declined with age. In the proximal colon, the average ratio of K was the highest at month 1, then declined afterwards with aging. In the distal colon, the highest average ratio of S was at month 3 and the highest average ratio of K was at month 1. Significant differences were found between these peaks (Kametani *et al.*, 1998).

On the other hand, we had previously demonstrated the presence of zinc (Zn) in the specific granules of Paneth cells of mouse duodenum (Figure 10F) and goblet cells of mouse colon by X-ray microanalysis, which was supposed to be one of the elemental constituents of the glycoproteins in the intestines (Ichikawa *et al.*, 1994; Nagata, 2000[b]). When the duodenum tissues were fixed by conventional double fixation in phosphate buffered 2.5% glutaraldehyde and 1% osmium tetroxide solutions, the X-ray spectrum showed a low Zn peak together with a high Os peak (Figure 15A). Therefore, we used single fixation in buffered 2.5% glutaraldehyde, thus obtaining a single Zn peak without Os peak in the spectrum (Figure 15B). In order to quantify the zinc content in these granules, we first studied the zinc concentrations in a model system. As a model experiment, we prepared Epon sections containing zinc sulfate at concentrations of either 0.05 or 0.1%. The two spectra obtained from the two Epon sections containing 0.05% and 0.1% zinc sulfate cut at 0.2 mm and observed at 100 kV by a JEOL JEM-4000EX TEM with a TN-5400 EDX system, with beam currents from 2 to 8 nano ampere and the microprobe at 1 μm in diameter and a detection time of 100 s appeared similar to Figure 13A. Comparing the two peaks of Zn obtained from 0.05% and 0.1% concentrations, the latter was higher than the former (Nagata, 2000[b]). The average peak counts and backgrounds in two kinds of sections containing 0.05 and 0.1% concentrations were calculated. From the results, P/B ratios at different concentrations were plotted. In such a figure, the linear relationship between the Zn concentration and the P/B ratio can be observed approximately like Beer's law in case of microspectrophotometry (Nagata, 1972[a]). When the sections containing 0.1% zinc sulfate were analyzed with the JEM-4000EX NT-5400 TEM system, with beam currents from 2 to 8 nano ampere and a microprobe at 1 μm in diameter and a detection time of 100 sec with a dead time of 30%, changing the accelerating voltage from 100 to 400 kV, spectra showing Zn peaks were obtained. The peak counts as well as the background changed from 100 to 400 kV. The results were plotted as the changes of P/B ratio related to accelerating voltage (Figure 16A). The maximum of these curves

Figure 13. X-ray microanalysis of several elements in mucigen granules in the goblet cells in the colons of mice.

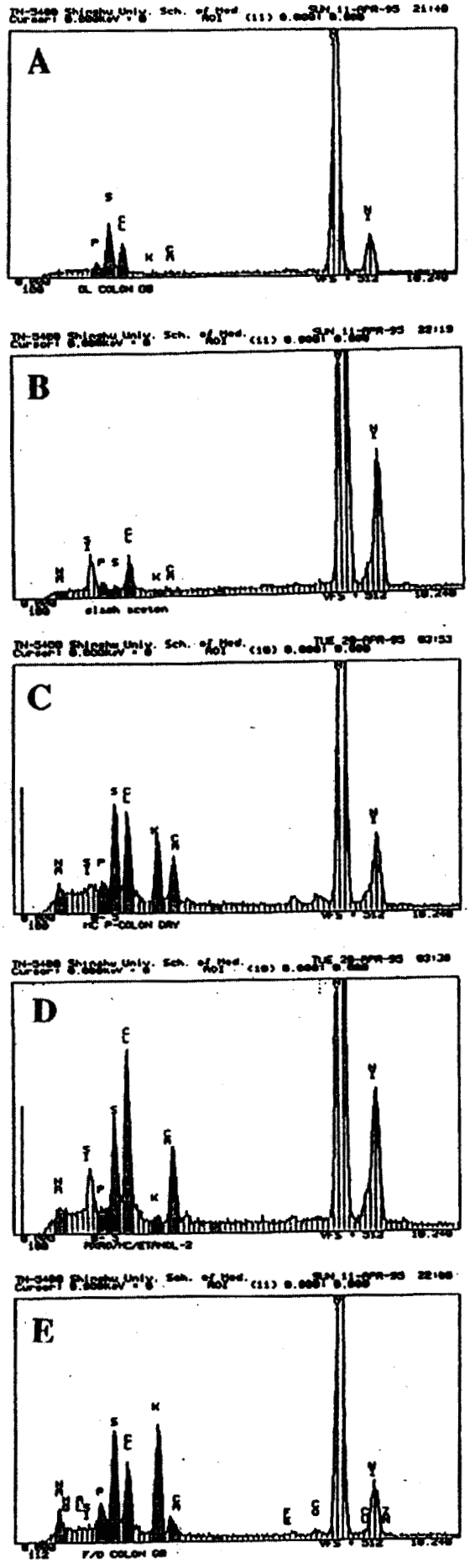

13A. X-ray spectrum obtained from one of the granules of the goblet cell fixed chemically in glutaraldehyde and processed through conventional procedures as shown in Figure 10D.

13B. X-ray spectrum obtained from one of the granules of the goblet cell, cryo-fixed, freeze-substituted and dry-sectioned.

13C. X-ray spectrum obtained from one of the granules of the goblet cell, cryo-fixed by metal contact method, freeze-substituted in absolute acetone without osmium tetroxide, embedded in Epok and dry-sectioned as shown in Figure 10E.

13D. X-ray spectrum obtained from one of the granules of the goblet cell, prefixed with acrolein gas and cryo-fixed by metal contact method, freeze-substituted in absolute acetone, embedded in Epok and dry sectioned.

13E. X-ray spectrum obtained from one of the granules of the goblet cell, cryo-fixed by metal contact method, cryo-sectioned and freeze-dried. Higher peaks of Na, P, S, Cl, K and Ca can be seen. From Nagata *et al.*(2000[c], Figures 2, 4, 9, 11, 13, pp. 3, 4, 5, 6).

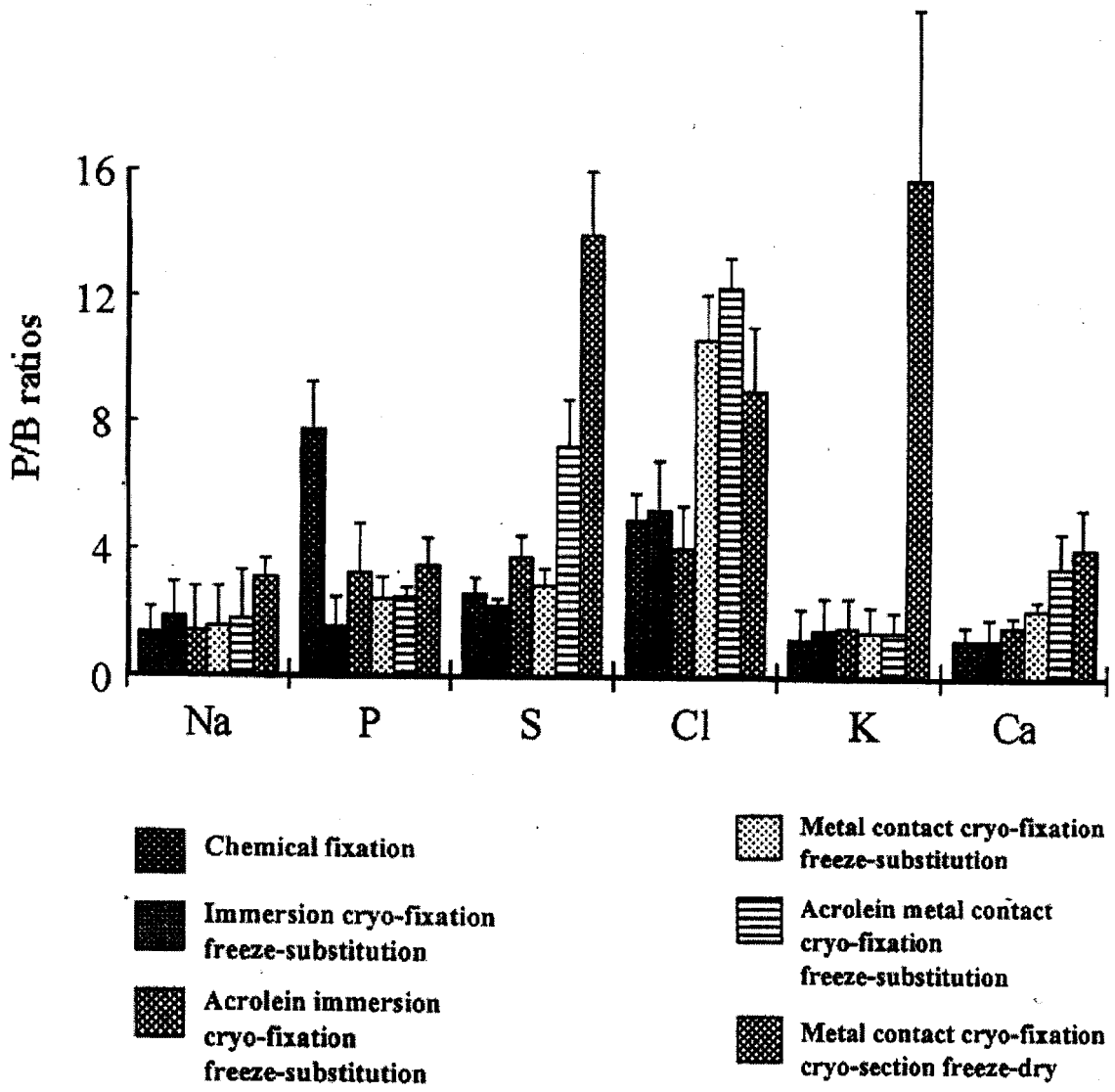

Figure 14. Histogram showing the P/B ratios of several elements obtained from mouse colonic goblet cells which were fixed by various methods of cryo-fixations as well as conventional chemical fixation and calculated from the spectra obtained respectively. From Nagata *et al.* (2000[c], Figure 14, p. 7).

was observed at 200 kV, different from the results obtained with Ag or S. Therefore, we used 200 kV for further quantification in case of Zn. Analyzing many individual mice at various ages from newborn to adult and further to senescence, fixed in glutaraldehyde, all the data expressing P/B ratio were plotted (Figure 16B). These data show that the aging changes of zinc contents in the specific granules of mouse duodenum Paneth cells as expressed by P/B ratios increased from postnatal days 2, 7 to 14 and month 2, reaching a peak at month 1, and then decreased to 2 years. The relation between the P/B ratios of Zn and the aging of animals was similar to those of S in the goblet cells.

The Macromolecular Synthesis of the Liver

The large digestive glands of mammals consist of the large salivary gland in the oral cavity, the liver and the pancreas in the abdominal cavity. We studied all these glands by means of RAG and various cytochemical reactions. The results obtained from the 3 large salivary glands, the parotid, the submandibular and the sublingual glands of ddY mice were already described in the section of the oral cavity. The other 2 large digestive

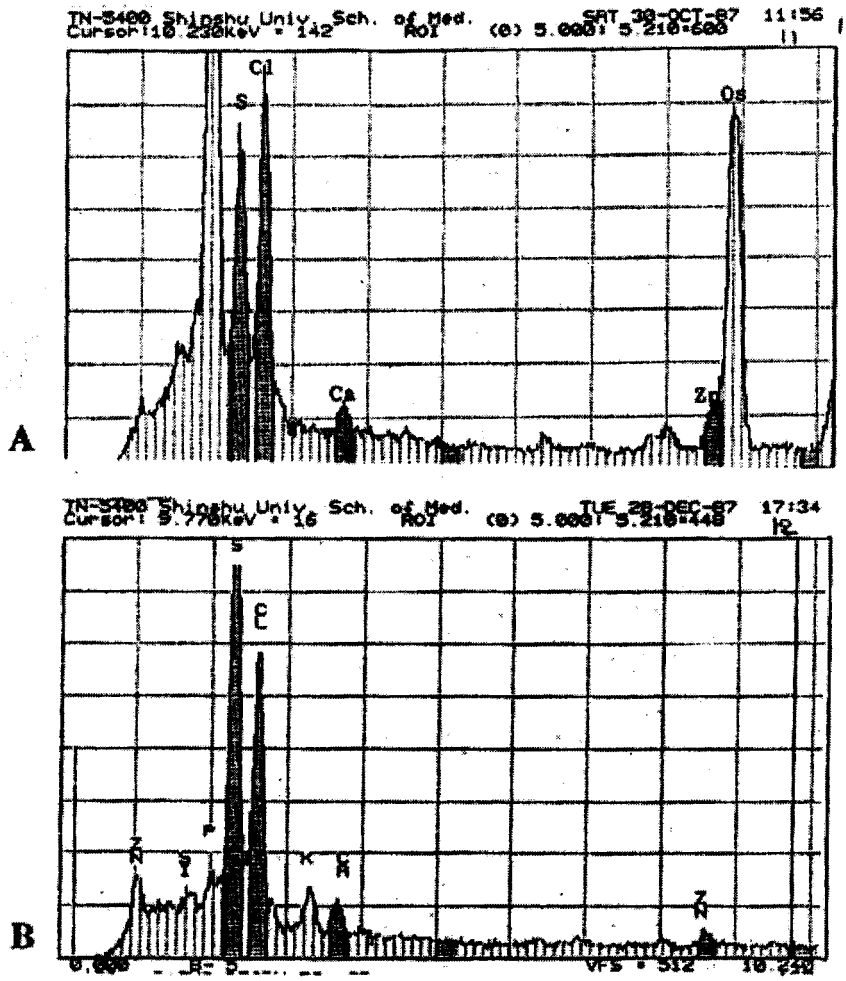

15A. X-ray spectrum obtained from the specific granules of a Paneth cell of a 1 month old mouse duodenum, fixed in buffered 2.5% glutaraldehyde and 1% osimium tetroxide. A low Zn-Kα peak can be seen with a high Os peak.

15B. X-ray spectrum obtained from the specific granule of a Paneth cell of a mouse at postnatal month 15, fixed only in buffered 2.5% glutaraldehyde, indicated with an arrow in Figure 10F. Only a low Zn-Kα can be seen without Os peak. The Cl peak is due to epoxy resin. From Nagata (2000[b], Figure 23, p. 29).

Figure 15. X-ray microanalysis of Zn in the intestines.

glands, the liver and the pancreas, should be here described separately. The liver of the mammals is a very large gland and consists of several types of cells. The hepatocyte is the main component of the liver, composing the liver parenchym which form the hepatic lobules, surrounded by the connective tissue cells, sinusoidal endothelial cells, satellite cells of Kupffer, Ito's fat-storing cells and bile epithelial cells. In the livers of perinatal animals, the liver tissues include not only the hepatocytes but also hematopoietic cells such as erythroblasts, myeloblasts and magakaryocytes. We have extensively carried out the studies on the macromolecular synthesis of the hepatocytes in the livers of aging mice by LM and EM RAG (Nagata, 1994[c], 1995[a], 1999[c]). We also studied cytochemical reactions mainly in hepatocytes of rats and mice in relation to RAG.

The DNA Synthesis of the Liver

As for the nucleic acid synthesis, we first studied the difference of DNA synthesis between mononucleate and binucleate hepatocytes of adult Wistar rats, injected with ^{3}H-thymidine (Nagata *et al.*, 1961; Nagata, 1962). The results by LMRAG showed that the frequency of labeled cells was greater in mononucleate cells than in binucleate cells. The labeled binucleate cells were classified into two types, *i.e.*, a cell whose one of the two nuclei was labeled and a cell whose two nuclei were labeled.

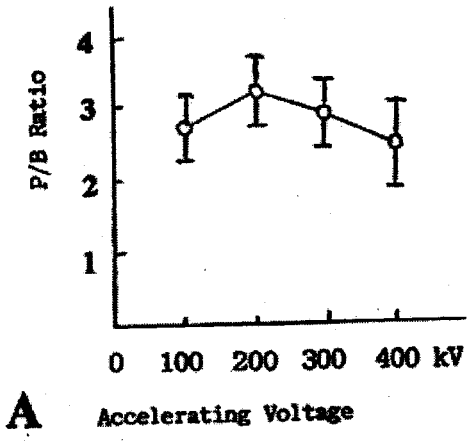

Figure 16. Relation of the P/B ratios of Zn of specific granules in the Paneth cell of a mouse by X-ray microanalysis to the accelerating voltages and aging changes.

16A. Transitional curve showing the relationship between the accelerating voltages and the P/B ratios of Zn calculated from the X-ray spectra obtained from model experiments. From Nagata (2000[b], Figure 21, p. 28).

16B. Relationship between the aging of mice and P/B ratios of Zn in the granules in Paneth cells of the duodenum at respective ages. From Nagata (2000[b], Figure 24, p. 29).

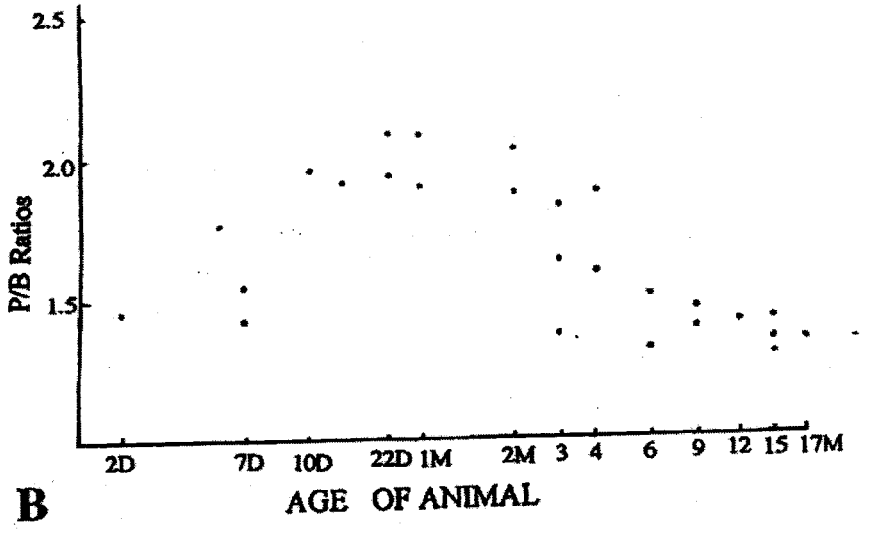

The former was more frequently observed than the latter. Grain counts revealed that the amount of DNA synthesized in the binucleate cell whose one nucleus was labeled was the same as the mononucleate cell, while the total amount of DNA synthesized in the binucleate cell whose two nuclei were labeled was almost twice as that of the mononucleate cell whose nucleus was labeled (Nagata *et al.*, 1961; Nagata 1962). We also studied the difference of DNA synthesis between the mononucleate and binucleate hepatocytes of 4 groups of ddY strain mice during the postnatal growth from newborns to aged adults, each weighing about 10, 20, 30 and 40 g, injected with ^{3}H-thymidine (Nagata *et al.*, 1966). The results by LMRAG showed that the frequency of labeled cells was greater in the mononucleate cells than in the binucleate cells. The labeled binucleate cells were classified into two types similar to rats, *i.e.*, a cell whose one of the two nuclei was labeled and a cell whose two nuclei were labeled. The former was more frequently observed than the latter. The LI of both mononucleate and binucleate hepatocytes were inversely proportional to the body weight of the animals, i.e. to the aging of animals. Grain counts revealed that the amount of DNA synthesized in the binucleate cell whose one nucleus was labeled was the same as the mononucleate cell, while the total amount of DNA synthesized in the binucleate cell whose two nuclei were labeled was almost twice as that of the mononucleate cell (Nagata *et al.*, 1966). These results were lately reconfirmed by EMRAG (Nagata &

Ma, 2002). Then, we studied incorporations of ^{3}H-thymidine into the liver cells of ddY mice in vitro by EMRAG (Nagata *et al.*, 1967[b]), in connection to soluble compounds (Nagata & Murata 1977; Nagata *et al.*, 1977). Soluble ^{3}H-thymidine, which was demonstrated by cryo-fixation, cryo-sectioning, freeze-drying and dry-mounting radioautography, was localized over the nuclei, cell organelles and cytoplasmic ground substance of hepatocytes diffusely. By conventional chemical fixation and wet-mounting by EMRAG, on the other hand, less silver grains demonstrating DNA synthesis were localized over the nuclei of the hepatocytes in S-phase only. These results revealed that soluble ^{3}H-thymidine was localized diffusely in the nuclei of S-phase hepatocytes.

We finally studied the DNA synthesis of the livers of prenatal and postnatal normal ddY mice at various ages, from fetal day 19, to postnatal days 1, 3, 9 and 14, months 1, 3, 6 and 12, labeled with ^{3}H-thymidine and observed by LM and EMRAG, which revealed that many silver grains were localized over the nuclei of various cell types consisting the liver, *i.e.*, hepatocytes (Figure 17A), sinusoidal endothelial cells (Figure 17B), Kupffer's cells, Ito's fat-storing cells, bile ductal epithelia cells, fibroblasts and hematopoietic cells (Ma, 1988; Ma & Nagata, 1990[a,b]). In hematopoietic cells, which were found in only perinatal animals from fetal day 19 to postnatal days 1, 3, 9 and 14, silver grains were observed over the nuclei of erythroblasts, myeloblasts, lymphoblasts and megekaryocytes. However, most hematopoietic cells disappeared on postnatal day 14. At fetal day 19, the liver tissues were chiefly consisted of hepatocytes and haematopoietic cells and no lobular orientation was observed. At postnatal day 1 and 3, lobular formation started and finally the hepatic lobules were formed at postnatal day 9. During the perinatal period, almost all kinds of cells were labeled with ^{3}H-thymidine. Percentage of labeled hepatocytes was the highest at fetal day 19, and rapidly decreased after birth to postnatal day 3. From postnatal day 9 to 14, percentage of labeled hepatocytes (labeling index, LI) decreased gradually and finally to the lowest at postnatal month 24 (Figure 18A). We analyzed the LI of hepatocytes in 3 hepatic acinar zones, which revealed that the indices decreased in zone 2 (intermediate zone) and zone 3 (peripheral zone) on postnatal days 3 and 9, whereas they increased in zone 1 (central) on day 9, and then they altogether decreased from day 14 to month 24 (Figure 18B). We then analyzed the size and number of cell organelles in both labeled and unlabeled hepatocytes quantitatively by image analysis using an image analyzer, Digigramer G/A (Mutoh Kogyo Co. Ltd., Tokyo, Japan). The results showed that the area size of the cytoplasm (150-200μm^2, Figure 19A), nucleus (40-50μm^2), mitochondria (40-50 μm^2, Figure 19B), endoplasmic reticulum (40-60 μm^2, Figure 19C), and the number of mitochondria in the unlabeled hepatocytes were more than the labeled cells (Ma & Nagata, 1990[a], Nagata 1995[a]). These data demonstrated that the cell organelles of the hepatocytes, which synthesized DNA, were not well developed as compared to those not synthesizing DNA during the postnatal development. In some of unlabeled hepatocytes, several silver grains were occasionally observed localizing over mitochondria and peroxisomes as was formerly reported (Nagata *et al.*, 1967; Nagata *et al.*, 1982). The mitochondrial DNA synthesis was first observed in cultured hepatocytes of chickens and mice in vitro (Nagata *et al.*, 1967). The percentages of other cell types such as sinusoidal endothelial cells also decreased from perinatal period to postnatal month 24.

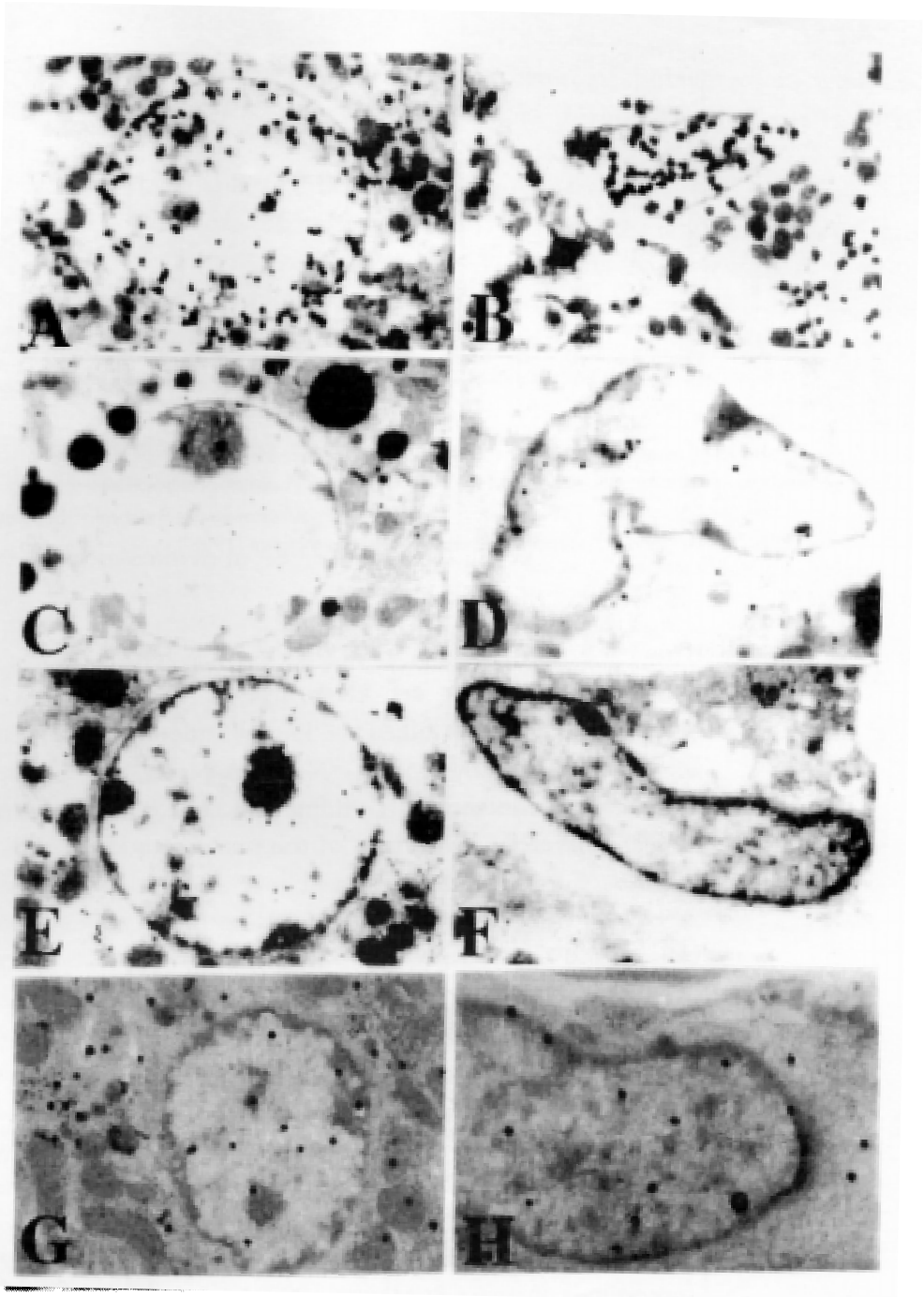

Figure 17. EMRAG of the liver of ddY mice. 17A. EMRAG of a hepatocyte of a 14 day old mouse, injected with ^{3}H-thymidine, fixed in glutaraldehyde and osmium tetroxide, and processed for wet-mounting radioautography. Many silver grains are localized over the chromatin in the nucleus, showing DNA synthesis. x12,000. From Nagata (1995[a], Figure 3, p. 25). 17B. EMRAG of a sinusoidal endothelial cell in the liver of a 14 day old mouse, injected with ^{3}H-thymidine and radioautographed. Many silver grains are localized over the chromatin in the nucleus, showing DNA synthesis. x12,000. From Nagata (1995[a], Figure 3, p. 25). 17C. EMRAG of a hepatocyte of a 14 day old mouse, injected with ^{3}H-uridine and radioautographed. Many silver grains are localized over the nucleolus and the chromatin in the nucleus, showing RNA synthesis. x5,400. From Nagata (2002, Figure 21C, p. 130). 17D. EMRAG of an Ito's fat-storing cell of a newborn mouse at postnatal day 1, injected with ^{3}H-uridine and radioautographed. Several silver grains are localized over the nucleolus and the chromatin in the nucleus, showing RNA synthesis. x8,600. From Nagata (2002, Figure 21D, p. 130). 17E. EMRAG of a hepatocyte in the liver of an adult mouse at postnatal month 1, injected with ^{3}H-leucine and radioautographed. Many silver grains are observed over the nucleus and cell organelles in cytoplasm such as endoplasmic reticulum and mitochondria, showing protein synthesis. x8,000. From Nagata (1995[a], Figure 10, p. 32). 17F. EMRAG of a sinusoidal endothelial cell of a newborn mouse at postnatal day 1, injected with ^{3}H-leucine and radioautographed. Several silver grains are observed over the nucleus and cytoplasm. From Nagata (1995[a], Figure 10, p. 32). 17G. EMRAG of a hepatocyte in the liver of an adult mouse at postnatal month 2, injected with 3H-proline and radioautographed. Many silver grains are observed over the nucleus and cell organelles in cytoplasm such as Golgi apparatus, endoplasmic reticulum, mitochondria and peroxisomes, showing collagen and protein synthesis. x5,000. From Ma & Nagata (2000, Figure 1, p. 20). 17H. EMRAG of a stellate cell of Kupffer in the liver of a newborn mouse at postnatal day 1, injected with ^{3}H-proline and radioautographed. Many silver grains are observed over the nucleus and cell organelles in cytoplasm, showing collagen and protein synthesis. x9,000. From Ma & Nagata (2000, Figure 2, p. 20).

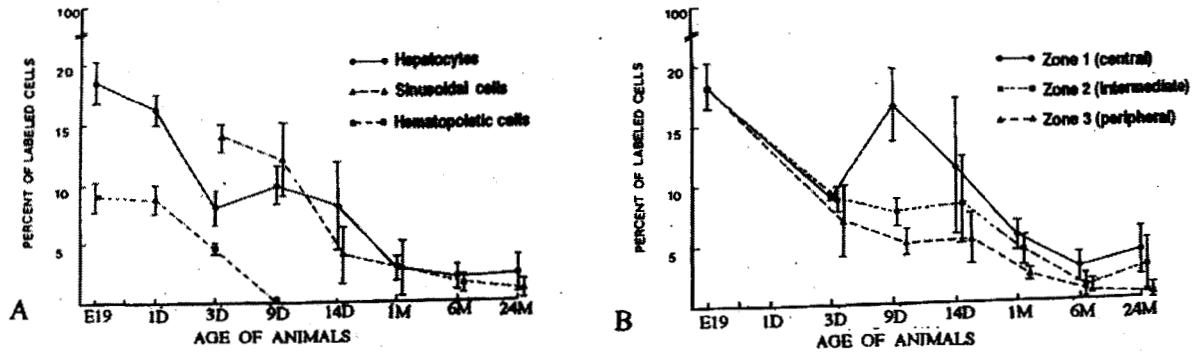

Figure 18. Transitional curves of labeling indices in the livers of aging mice after injection of ^{3}H-thymidine. 18A. Labeling indices of hepatocytes, sinusoidal endothelial cells and hematopoietic cells in respective aging groups as expressed by means ± standard deviations. 18B. Labeling indices of hepatocytes in the 3 zones of hepatic lobules in respective aging groups as expressed by means ± standard deviations. From Nagata (1995[a]).

The RNA Synthesis of the Liver

We first studied the incorporation of ^{3}H-uridine into cultured chick embryo fibroblasts in vitro by LMRAG (Nagata & Nawa, 1966[b]). Chicken fibroblasts were cultured in a medium containing ^{3}H-uridine and radioautograms were prepared. Silver grains first appeared over the chromatin of the nucleus and nucleolus of all the cells within several minutes, then silver grains spread over the cytoplasm within 30 min showing messenger RNA and ribosomal RNA. The number of silver grains was much greater in binucleate cells than mononucleate cells (Nagata & Nawa, 1966[b]). Then, the RNA synthesis of the liver cells of adult mice was studied by ^{3}H-uridine incorporation by LMRAG, in connection to binucleate cells (Nagata, 1966). ^{3}H-uridine was administered to 5 groups of adult ddY mice, each consisting of 5 liter mates, 1 h after feeding, then 5 groups of animals were sacrificed at 2, 4, 8, 24 and 28 h, respectively, after the injection. The results showed that the incorporation of ^{3}H-uridine was greater in binucleate hepatocytes than mononucleate at respective time points and the grain counts in both binucleate and mononucleate cells increased according to the time elapsed (Nagata, 1967). We further studied incorporations of ^{3}H-uridine into the liver cells of ddY mice by EMRAG, in connection to soluble compounds (Nagata & Murata 1977; Nagata *et al.*, 1977). Soluble ^{3}H-uridine, which was demonstrated by cryo-fixation, cryo-sectioning, freeze-drying and dry-mounting RAG, was localized over the nuclei, cell organelles and cytoplasmic ground substance of hepatocytes diffusely. By conventional chemical fixation and wet-mounting EMRAG, on the other hand, less silver grains demonstrating RNA synthesis were localized over the nuclei and cytoplasm of hepatocytes. These results revealed that soluble ^{3}H-uridine was localized diffusely in the nuclei and cytoplasm of hepatocytes.

We also studied aging changes of ^{3}H-uridine incorporation in the livers of aging mice at various ages from prenatal embryos to postnatal aged mice by LM and EMRAG. When aged mice were injected with ^{3}H-uridine, LM and EM RAG showed that silver grains were localized over the nucleoli, nuclear chromatin (both euchromatin and heterochromatin), mitochondria and rough surfaced endoplasmic reticulum of hepatocytes (Figure 17C) and other types of cells such as sinusoidal endothelial cells, Kupffer's cells, Ito's fat-storing cells (Figure 17D), ductal epithelial cells, fibroblasts and haematopoietic cells in the livers at various ages (Nagata, 1995[a]; Ma & Nagata, 1990[b]). By quantitative

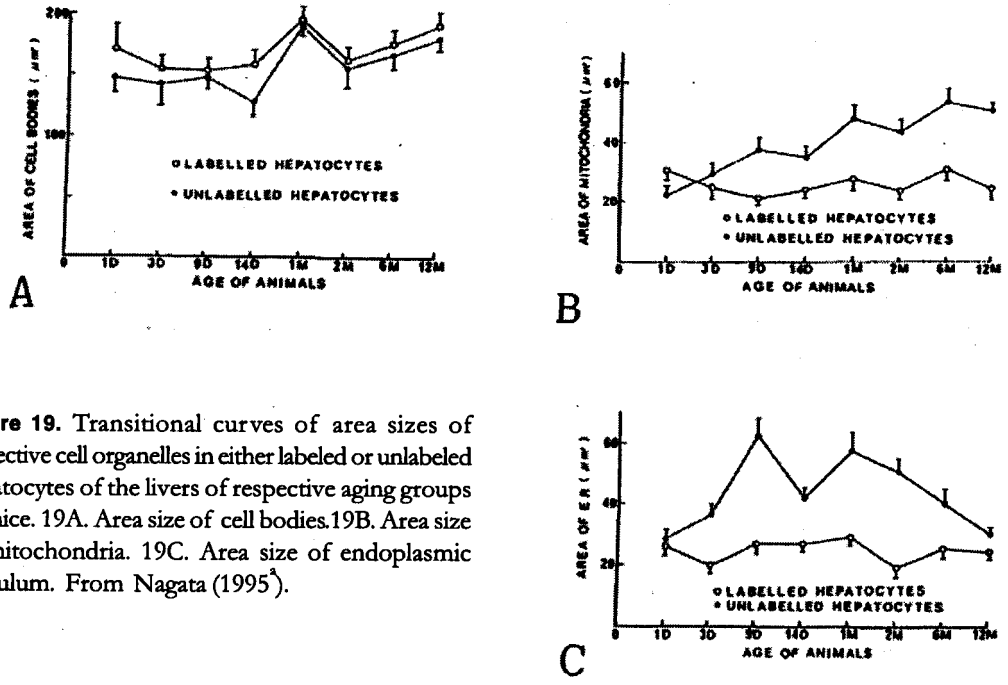

Figure 19. Transitional curves of area sizes of respective cell organelles in either labeled or unlabeled hepatocytes of the livers of respective aging groups of mice. 19A. Area size of cell bodies.19B. Area size of mitochondria. 19C. Area size of endoplasmic reticulum. From Nagata (1995[a]).

analysis, the total number of silver grains in nucleus, nucleolus and cytoplasm of each hepatocyte increased gradually from fetal day 19 to postnatal days, reached the maximum at postnatal day 14, then decreased to month 24 (Figure 20A). The number of silver grains in nucleolus, when classified into two compartments, grains over granular components and those over fibrillar components, both increased paralelly after birth, reached the maxima on postnatal day 14, then decreased to month 24 with aging (Figure 20B). However, when the ratio (%) of silver grains over euchromatin, heterochromatin of the nuclei and granular components and fibrillar components of the nucleoli were calculated, the ratio remained constant at respective aging stages (Figure 20C).

On the other hand, we studied the intracellular localization of mRNA in rat hepatocytes using cDNA probe by *situ* hybridization (Usuda *et al.*, 1992; Nagata & Usuda, 1993[a]). Acyl-CoA oxidase is a rate-limitting enzyme in the fatty acid b-oxidation system of the peroxisomes in rat hepatocytes. We used several normal adult Wistar rats, which were fed on rat-mouse chow with or without DEHP, di-ethyl-hexyl-phthalate, a peroxisome proliferator for 2 weeks. We fixed the liver tissues by perfusing with 4% paraformaldehyde/0.1M sodium phosphate and prepared cryo-sections or paraffin sections which were subjected to in situ hybridization using ^{35}S-labeled probe which was prepared by multiprime labeling system using full length acyl-CoA oxidase cDNA as a template, and both LM and EMRAG were prepared. The results showed that silver grains were localized over both nuclei and cytoplasm. The intensity of grains increased by DEHP administration. By LMRAG, the number of silver grains over the central zone of the hepatic lobules was more than that of the peripheral zone in normal rats, but the difference was not clear in the DEHP treated rats. By EMRAG, silver grains were localized mainly over cytoplasmic matrix of DEHP treated rat hepatocytes. These results suggested that acyl-CoA oxidase mRNA was localized in cytoplasmic matrix of hepatocytes treated with a peroxisome proliferator (Usuda *et al.*, 1992; Usuda & Nagata, 1992, 1995).

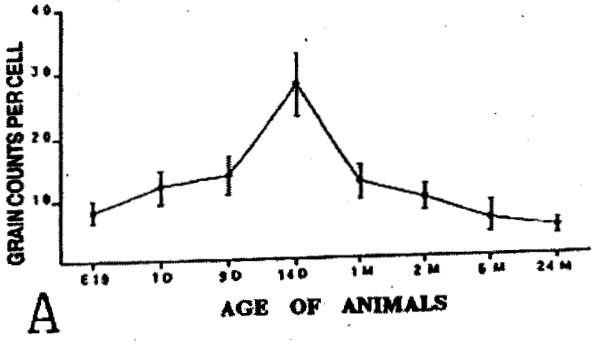

20A. Transitional curve of grain counts in hepatocytes.

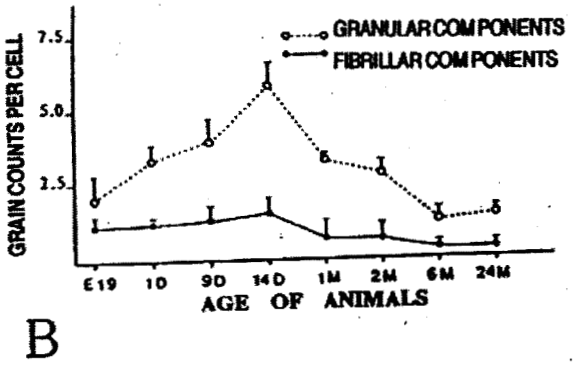

20B. Transitional curves of grain counts in granular and and fibrillar components of nucleoli of hepatocytes.

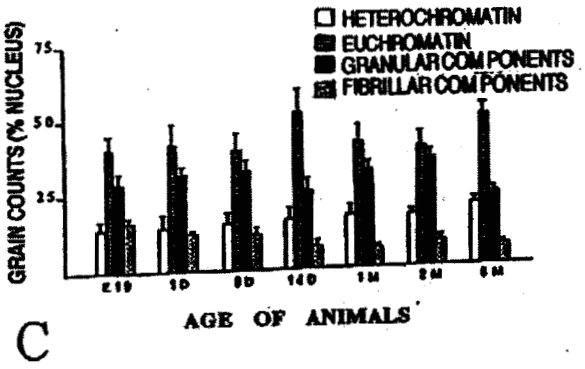

20C. Histogram showing the ratios of grain counts in heterochromatin, euchromatin of the nuclei and granular and fibrillar components of nucleoli in hepatocytes in respective aging groups. From Nagata (1995[3]).

Figure 20. Transitional curves and histograms of grain counts in hepatocytes in respective aging groups of mice after injection of ^{3}H-uridine.

The Glucide Synthesis of the Liver

Glucides or polysaccharides can be classified into simple polysaccharide and complex polysaccharide. We first studied ^{3}H-glucose incorporation into glycogen in the liver, in connection to soluble compounds (Nagata & Murata, 1977; Nagata *et al.*, 1977). Mouse liver tissues were incubated in a medium containing ^{3}H-glucose in vitro and the tissues were prepared for cryo-fixation, cryo-sectioning and dry-mounting RAG. Soluble ^{3}H-glucose was localized over the nuclei, cell organelles and cytoplasmic ground substance of hepatocytes diffusely. By conventional chemical fixation and wet-mounting RAG, on the other hand, silver grains were localized only over glycogen granules, endoplasmic reticulum and Golgi apparatus. These results revealed that soluble

^{3}H-glucose was localized diffusely in the nuclei and cytoplasm of hepatocytes. However, the relation of glycogen synthesis in hepatocytes to aging has not yet been clarified.

The Protein Synthesis of the Liver

We first studied the difference of the protein synthesis in mononucleate and binucleate hepatocytes of 3 groups of adult ddY mice by incorporations of 3H-leucine and ^{3}H-tryptophane before and after feeding by LMRAG (Nagata, 1967). The results showed that the incorporations of both amino acids were greater in binucleate hepatocytes than mononucleate in respective groups (Nagata, 1967). Then, we studied incorporations of ^{3}H-glycine into the liver cells of ddY mice by EMRAG, in connection to soluble compounds (Nagata & Murata 1977; Nagata *et al.*, 1977). Soluble ^{3}H-glycine, which was demonstrated by cryo-fixation, cryo-sectioning, freeze-drying and dry-mounting RAG, was localized over the nuclei, cell organelles and cytoplasmic ground substance of hepatocytes diffusely. By conventional chemical fixation and wet-mounting EMRAG, on the other hand, less silver grains demonstrating protein synthesis were localized over the nuclei and cell organelles of hepatocytes. These results revealed that soluble ^{3}H-glycine was localized diffusely in the nuclei and cytoplasm.

On the other hand, we studied the incorporation of ^{3}H-leucine into the livers of several groups of ddY litter mice at various ages. On LM and EMRAG, silver grains were observed over all cell types of the liver, *i.e.* hepatocytes (Figure 17E), sinusoidal endothelial cells (Figure 17F), ductal epithelial cells, Kupffer's cells, Ito's fat storing cells, fibroblasts and haematopoietic cells (Ma *et al.*, 1991). In hepatocytes, number of silver grains in cytoplasm and karyoplasm increased from perinatal animals to postnatal 1 month adult animals and decreased with aging to month 24 (Figure 21A). Number of silver grains observed by grain counting over respective cell organelles, *i.e.* the Golgi apparatus, mitochondria, endoplasmic reticulum, changed with aging, reaching the maxima at 1 month but the ratio remained constant at each point (Figure 21B).

We also injected ^{3}H-proline into several groups of ddY mice at various ages from prenatal embryos to postnatal senescence and studied the quantitative changes of collagen and protein synthesis in the livers by EMRAG. Silver grains were localized over the nuclei, cytoplasmic matrix, endoplasmic reticulum, Golgi apparatus, mitochondria and peroxisomes of almost all the cells at various ages (Figure 13F). The number of silver grains in the nuclei and cytoplasmic matrix (Figure 22A), as well as over respective cell organelles such as endoplasmic reticulum, mitochondria, Golgi apparatus and peroxisomes of hepatocytes gradually increased from embryo, reached the maxima at postnatal month 1 and 6, and decreased with aging until month 24 (Figure 22B). The number of silver grains localized over the extracellular collagen fibrils and matrices was not so many in respective aging groups and did not show any remarkable changes with aging. From the results, it was concluded that ^{3}H-proline was incorporated not only into collagen but also into the structural proteins of hepatocytes under normal aging conditions (Ma & Nagata, 2000).

The Lipid Synthesis of the Liver

Lipids are esters of glycerol and fatty acids, which can be classified into simple lipids and compound lipids. Therefore, we can localize the sites of lipid synthesis by labeling cells with either ^{3}H-glycerol or ^{3}H-fatty acids. We first observed lipid synthesis in the liver tissues of adult Wistar rats using ^{3}H-glycerol

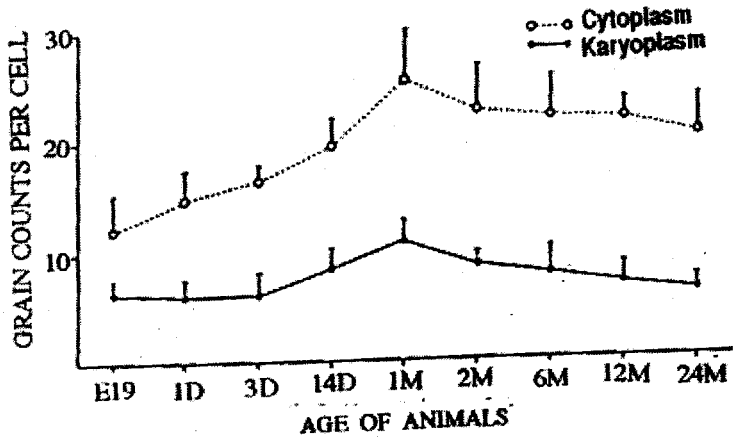

A

21A. Transitional curves of grain counts in the nucleus and the cell body of each hepatocyte of the liver in respective aging groups.

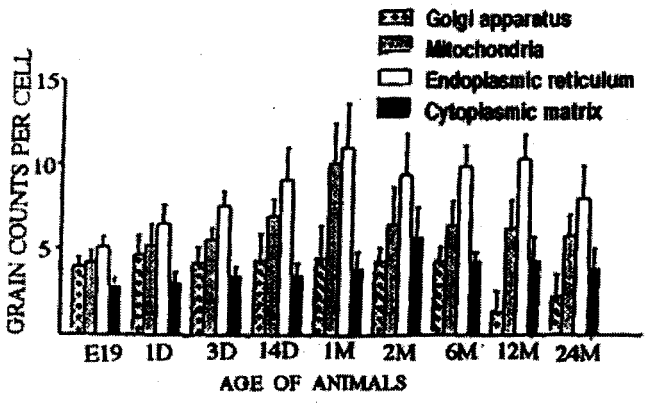

B

21B. Histogram showing grain counts over the Golgi apparatus, mitochondria, endoplasmic reticulum and cytoplasmic ground substance of each hepatocyte in the livers of respective aging groups. From Nagata (1995[a]).

Figure 21. Transitions of grain counts in cell compartments of hepatocytes in aging mice after injection of ^{3}H-leucine.

in connection to soluble compounds (Nagata & Murata 1977; Nagata *et al.*, 1977; Nagata 1994[b]). We labeled adult mouse liver tissues in a medium containing ^{3}H-glycerol in vitro and the tissues were cryo-fixed at -196 °C, freeze-substituted embedded in epoxy resin, dry-sectioned, and prepared for dry-mounting EMRAG. On EMRAG many silver grains appeared over the nuclei and cytoplasm including cell organelles diffusely. However, when the same liver tissues were fixed chemically in buffered glutaraldehyde and osmium tetroxide and radioautographed by conventional wet-mounting procedures, very few silver grains were observed only over the endoplasmic reticulum and lipid droplets, which demonstrated macromolecular lipid synthesis. Thus, it was shown that soluble ^{3}H-glycerol was localized over the nuclei and cytoplasm of hepatocytes diffusely. However, the aging change of the lipid synthesis in the liver has not yet been clarified.

We also studied the intracellular localization of bezafibrate, a hypolipidemic agent that is also a peroxisome proliferator in rat hepatocytes, by LM and EMRAG. We cultured adult rat hepatocytes in primary culture and added ^{14}C-labeled bezafibrate in the medium and processed for LM and EMRAG (Momose & Nagata 1993; Momose *et al.*, 1993, 1995). As the results, about 90% of all the silver grains were localized over the cytoplasm of hepatocytes on LMRAG. On EMRAG of whole mount cultured cells, silver grains were localized on cytoplasmic matrix especially over the endoplasmic reticulum. The results

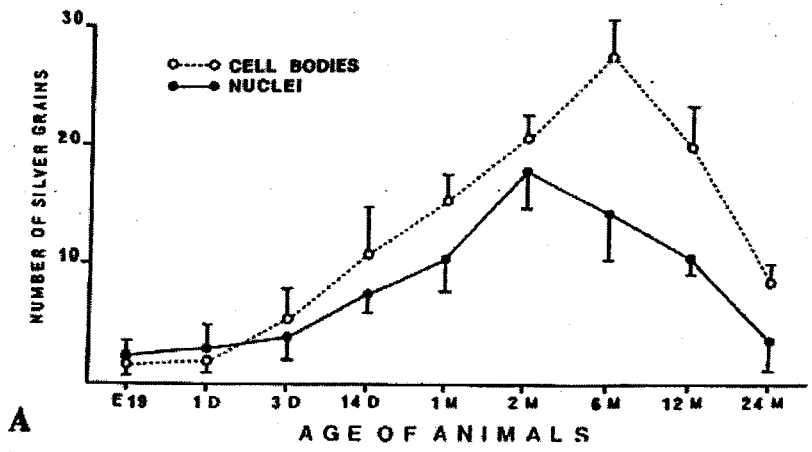

A

22A. Transitional curves of grain counts in cell bodies and nuclei of labeled hepatocytes in the livers of mice.

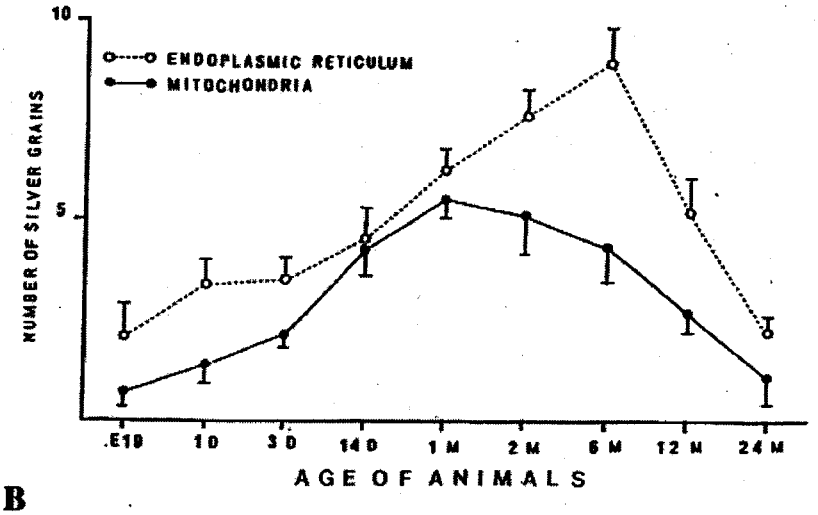

B

22B. Transitional curves of grain counts in endoplasmic reticulum and mitochondria of labeled hepatocytes in the livers of mice. From Ma & Nagata (2000).

Figure 22. Transitional curves of grain counts in cell compartments of hepatocytes in aging mice after injection of ^{3}H-proline.

showed that the receptor of the hypolipidemic factor was associated with the endoplasmic reticulum (Momose *et al.*, 1995).

Macromolecular Synthesis of the Pancreas

The pancreas of mammals is an exocrine and endocrine organ and it consists of both exocrine portion and endocrine portion. The exocrine portion is composed of ductal epithelial cells, centro-acinar cells, acinar cells and connective tissue cells, while the endocrine portion, the islet of Langerhans, is composed of 3 types of endocrine cells, A, B and C cells as well as connective tissue cells. We studied the macromolecular synthesis, DNA, RNA, proteins, glucides, glycoproteins and lipids, of the pancreatic tissues of ddY mice at several aging stages.

The DNA Synthesis of the Pancreas

We first studied the difference of DNA synthesis between mononucleate and binucleate pancreatic acinar cells of 4 groups of ddY strain mice during the postnatal growth from newborns to aged adults, each weighing about 10, 20, 30 and 40 g, injected with ^{3}H-thymidine and processed for LMRAG

(Nagata *et al.*, 1966). The results showed that the frequency of labeled cells was greater in mononucleate cells than in binucleate cells. The labeled binucleate cells were classified into two types similar to hepatocytes, *i.e.*, a cell whose one of the two nuclei was labeled and a cell whose two nuclei were labeled. The former was more frequently observed than the latter. The relationship of LI of both mononucleate and binucleate cells to the postnatal growth of animals, which was shown to be inversely proportional to the body weight of the animals in case of hepatocytes was not clear in the pancreatic acinar cells. Grain counts revealed that the amount of DNA synthesized in the binucleate cell whose one nucleus was labeled was the same as the mononucleate cell whose nucleus was labeled, while the total amount of DNA synthesized in the binucleate cell whose two nuclei were labeled was almost twice as that of the mononucleate cell similar to hepatocytes (Nagata *et al.*, 1966). Then, we studied incorporations of ^{3}H-thymidine into the pancreatic acinar cells of ddY mice by EMRAG, in connection to soluble compounds (Nagata & Murata 1977; Nagata *et al.*, 1977). Soluble ^{3}H-thymidine, which was demonstrated by cryo-fixation, cryo-sectioning, freeze-drying and dry-mounting radioautography, was localized over the nuclei, cell organelles and cytoplasmic ground substance of pancreatic acinar cells diffusely. By conventional chemical fixation and wet-mounting EMRAG, on the other hand, silver grains demonstrating DNA synthesis were localized over the nuclei of pancreatic acinar cells (Figure 23A), centro-acinar cells (Figure 23B), ductal epithelial cells and endocrine cells. We studied LM and EMRAG of the pancreatic cells in 5 groups of aging mice, fetal day 15, postnatal days 1, 20, 60 and 700 (2 years) and analyzed the labeling indices of respective cell types (Nagata *et al.*, 1984). The LI of these cells reached the maxima at postnatal day 1 and decreased gradually to month 24 (Figure 24). The maximum in the pancreatic acinar cells proceeded to the ductal and centro-acinar cells (Nagata *et al.*, 1984; Nagata & Usuda, 1986). From these results, it was concluded that the acinar cells completed their development earlier than the ductal cells and centro-acinar cells.

The RNA Synthesis of the Pancreas

Concerning the RNA synthesis of the pancreas, we first studied the localization of ^{3}H-uridine in the pancreatic acinar cells of ddY adult mice by cryo-fixation, cryo-sectioning, freeze-drying and dry-mounting EMRAG (Nagata & Murata 1977; Nagata *et al.*, 1977; Nagata 1994[b]). Soluble ^{3}H-uridine, which was demonstrated by dry-mounting RAG, was localized over the nuclei, cell organelles and cytoplasmic ground substance of pancreatic acinar cells diffusely. By conventional chemical fixation and wet-mounting EMRAG, on the other hand, silver grains demonstrating RNA synthesis were localized over the nuclei and a few cell organelles such as endoplasmic reticulum, ribosomes and mitochondria of pancreatic acinar cells. Then, we studied the aging changes of RNA synthesis by LM and EMRAG in the pancreases of ddY mice in several groups at various ages, from fetal day 19 to postnatal days 1, 3, 7, 14 and months 1, 2, 6, 12, injected with ^{3}H-uridine. We observed the incorporations into all types of cells in both the exocrine portion and the endocrine portion. The number of silver grains was more in the exocrine portion than in the endocrine portion, and more in the pancreatic acinar cells than in ductal or centro-acinar cells in the exocrine portion (Nagata *et al.*, 1984, 1986; Nagata & Usuda, 1985; Nagata, 1991, 1993). Among the acinar cells, the number of silver grains increased after birth (Figure

23C) to postnatal day 14 (Figure 23D) and then decreased with aging (Nagata *et al.*, 1984, 1986). Quantitative analysis of silver grains in the nucleoli, chromatin, and cell body were carried out by X-ray microanalysis (Nagata *et al.*, 1986), which verified the results obtained by visual grain counting (Nagata, 2000[d]). In EMRAG obtained from the pancreases of fetal day 19 embryos, newborn day 1 (Figure 23C) and newborn day 14 mice (Figure 23D) labeled with ^{3}H-uridine, demonstrating RNA synthesis, the number of silver grains in the nucleoli, nuclear chromatin and cytoplasm increased (Nagata & Usuda, 1985; Nagata, 1991, 1993). In order to quantify the silver contents of grains observed over the nucleoli, nuclei and cytoplasm, X-ray spectra were recorded by energy dispersive X-ray microanalysis (JEM-4000EX TN5400), demonstrating Ag-Kα peaks at higher energies (Figure 24). Thus, P/B ratios expressing relative silver contents were determined and compared between the two age groups. Table 1 shows the results obtained by X-ray microanalysis (XMA counts) in different cell compartments in postnatal day 1 and 14 animal groups. The results obtained by visual grain counting in different cell compartments in day 1 and 14 animals are also listed. The number of silver grains was calculated to express the counts per unit area to be compared with the XMA counts. These two results, the silver content analyzed by X-ray microanalysis and the results obtaining from visual grain counting were in good accordance with each other (Table 1). In the literature, Hodges and Muir (1975) were the first to quantify silver contents on EMRAG obtained from cultured cells labeled with 3H-thymidine by observation with a scanning electron microscope (SEM). Our report (Nagata & Usuda, 1985; Nagata, 1991, 1993) was the first to quantify the silver grains by the TEM mode. This procedure should be useful in calculating and recording the data with an on-line.

The Glucide Synthesis of the Pancreas

As for the glucide synthesis, we first studied 3H-glucose incorporation into the pancreases of ddY mice, in connection to soluble compounds (Nagata & Murata, 1977; Nagata *et al.*, 1977). Soluble ^{3}H-glucose, which was demonstrated by cryo-fixation and dry-mounting EMRAG, was localized over the nucleus, cell organelles and cytoplasmic ground substance of pancreatic acinar cells diffusely. By conventional chemical fixation and wet-mounting EMRAG, on the other hand, silver grains were localized only over glycogen granules, endoplasmic reticulum and Golgi apparatus. We also studied incorporation of ^{3}H-glucosamine into the pancreas of several groups of aging mice at various ages by LM and EM RAG (Nagata *et al.*, 1992). When perinatal baby mice received ^{3}H-glucosamine injection and the pancreatic tissues were radioautographed, silver grains were observed over exocrine and endocrine pancreatic cells. However, the number of silver grains was not so many (Figure 23G). When juvenile mice at the age of postnatal day 14 were examined, many silver grains appeared over the exocrine pancreatic acinar cells (Figure 23H). Less silver grains were observed over endocrine pancreatic cells and ductal epithelial cells. The grains in the exocrine pancreatic acinar cells were localized over the nucleus, endoplasmic reticulum, Golgi apparatus and secretory granules, demonstrating glycoprotein synthesis. Adult mice at the ages of postnatal month 1 and 6 or senile mice at the ages of postnatal month 12 or 24 showed very few silver grains on RAG. Thus, the glucide synthesis of ^{3}H-glucosamine incorporation in the pancreas of mice revealed quantitative changes, an increase and a decrease, with aging (Nagata *et al.*, 1992).

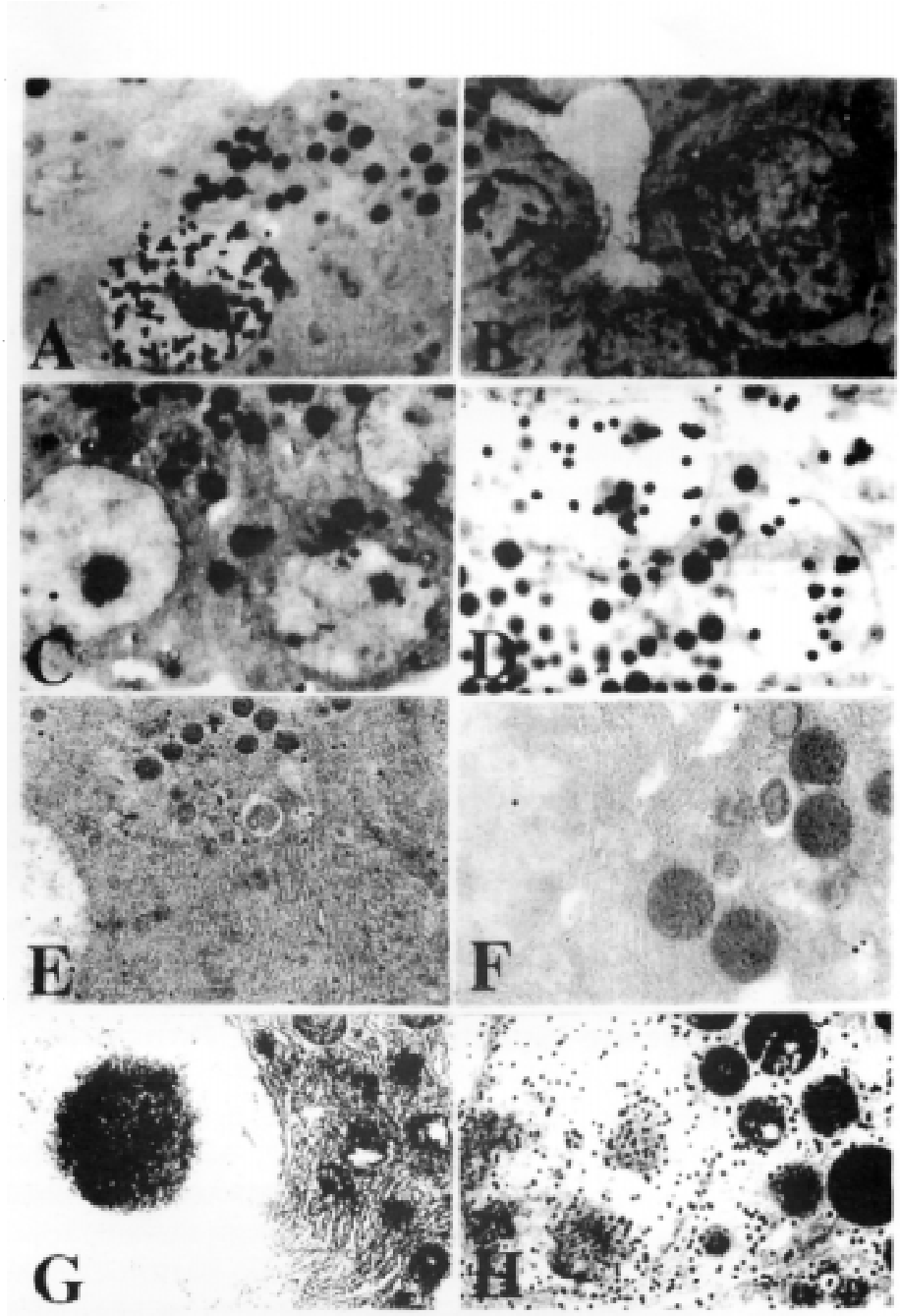

Figure 23. EMRAG of the pancreas. 23A. EMRAG of 2 pancreatic acinar cells of a young mouse at postnatal day 14, injected with ^{3}H-thymidine and radioautographed. Many silver grains are localized over the chromatin in the nucleus of a cell at center, showing DNA synthesis. x10,000. From Nagata (1995[a], Figure 6, p. 28). 23B. EMRAG of 2 pancreatic centro-acinar cells of a young mouse at postnatal day 14, injected with ^{3}H-thymidine and radioautographed. Many silver grains are localized over the chromatin in the nuclei of 2 cells at left and right, showing DNA synthesis. x10,000. From Nagata (1995[a], Figure 9, p. 31). 23C. EMRAG of 3 pancreatic acinar cells of a newborn mouse at postnatal day 1, injected with ^{3}H-uridine and radioautographed. Only a few silver grains are localized over the chromatin in the 2 nuclei of 2 cells at lower right and left, showing RNA synthesis. x12,000. From Nagata (1995[a], Figure 9, p. 31). 23D. EMRAG of 3 pancreatic acinar cells of a 14 day old mouse, injected with ^{3}H-uridine and radioautographed. Many silver grains are localized over the nucleolus and the chromatin in the nucleus at upper left, as well as several silver grains over the 2 nuclei at upper and lower right, showing RNA synthesis. x10,000. From Nagata (1995[a], Figure 9, p. 31). 23E. EMRAG of the pancreas of an adult mature mouse at postnatal day 30, injected with ^{3}H-leucine and radioautographed. Many silver grains are observed over the secretory granules at the apical portions of the cytoplasm, showing protein synthesis. x6,000. From Nagata (2000[c], Figure 16, 19). 17F. EMRAG of the pancreas of a senescent mouse at postnatal month 12, injected with ^{3}H-leucine and radioautographed. Only a few silver grains are observed over the cytoplasmic matrix, showing protein synthesis. x6,000. From Nagata (2000[c], Figure 20, p. 23). 23G. EMRAG of a pancreatic acinar cell of a newborn mouse at postnatal day 1, injected with ^{3}H-glucosamine and radioautographed. Only a few silver grains are observed over the nucleus, nucleolus and cell organelles in cytoplasm such as endoplasmic reticulum, mitochondria and cytoplasmic ground substance, showing less glucide synthesis. x6,000. From Nagata (1995[a], Figure 12, p. 34). 23H. EMRAG of a pancreatic acinar cell of a 14 day old mouse, injected with ^{3}H-glucosamine and radioautographed. Many silver grains are observed over the nucleus, nucleolus and cell organelles in cytoplasm such as endoplasmic reticulum, Golgi apparatus, secretory granules and cytoplasmic ground substance, showing much glucide synthesis than Figure 23G. x6,000. From Nagata (1995[a], Figure 12, p. 34).

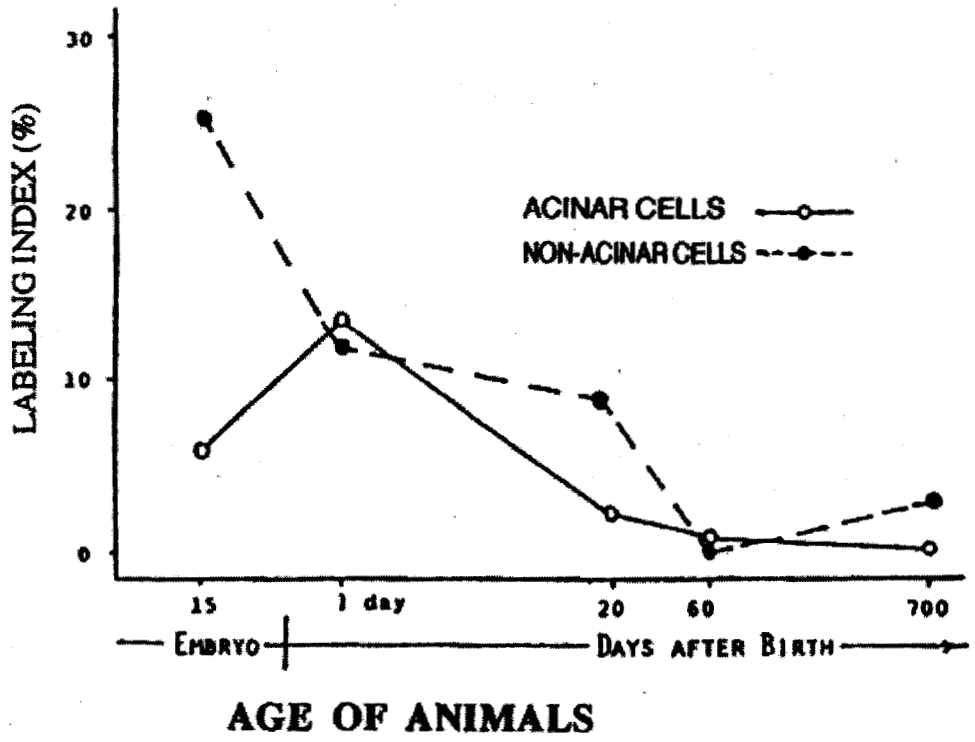

Figure 24. Transitional curves of the labeling indices of respective cells in the pancreas of aging mice labeled with ^{3}H-thymidine at various ages. From Nagata (1995[a]).

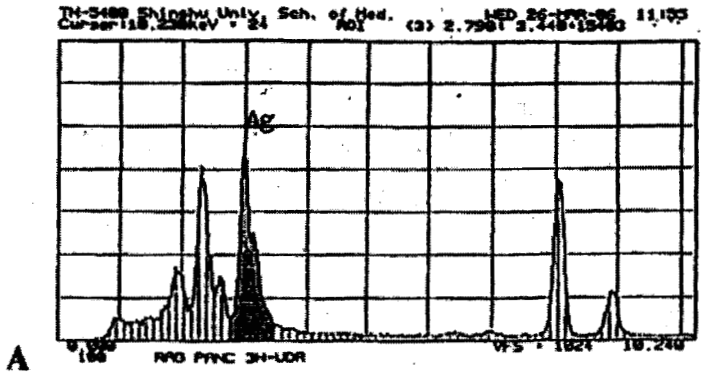

25A. X-ray spectrum from EMRAG of the pancreas of a newborn mouse at postnatal day 1 as in Figure 23C.

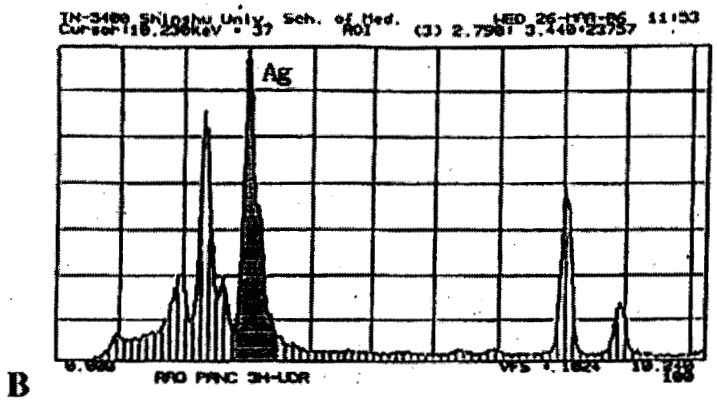

25B. X-ray spectrum from EMRAG of the pancreas of a young mouse at postnatal day 14 as in Figure 23D. From Nagata (1993[a]).

Figure 25. X-ray spectra of Ag-Kα obtained from the silver grains in EM radioautograms of pancreatic acinar cells labeled with ^{3}H-uridine.

Table 1. Comparison between visual grain counting and X-ray microanalysis in electron microscopic radioautograms corrected grain counts by Visual Grain Counting ($CNT/cm^2 \times 10^{-8}$).

Corrected Grain Counts by Visual Grain Counting ($CNT/cm^2 \times 10^{-8}$)		
	Age of animals	
Cell compartment	1 day old	14 day old
Nucleolus	2.60	5.35
Nucleus	0.29	0.88
Cytoplasm	0.15	0.21
Corrected Silver Contents by X-ray Microanalysis ($CNT/cm^2 \times 10^{-8}$)		
	Age of animals	
Cell Compartment	1 day old	14 day old
Nucleolus	4130.1	21068.1
Nucleus	61.6	176.8
Cytoplasm	15.5	51.7

The Protein Synthesis of the Pancreas

With regards the protein synthesis in the pancreas, ^{3}H-leucine incorporation into endoplasmic reticulum, Golgi apparatus and secretory granules of pancreatic acinar cells was first demonstrated by Jamieson and Palade (1967) using EMRAG. We first studied ^{3}H-glycine incorporation into these cell organelles of mouse pancreatic acinar cells in connection with soluble compounds (Nagata & Murata, 1977; Nagata *et al.*, 1977[a]). Soluble ^{3}H-glycine, which was demonstrated by cryo-fixation and dry-mounting EMRAG, was localized over the nuclei, cell organelles and cytoplasmic ground substance of pancreatic acinar cells diffusely. By conventional chemical fixation and wet-mounting radioautography, on the other hand, silver grains were localized only over endoplasmic reticulum, Golgi apparatus and secretory granules. Then, the quantitative analysis of protein synthesis concerning the aging from prenatal to postnatal stages, from fetal day 19, to postnatal days 1, 3, 7, 14 and months 1, 2, 5 and 12, using ^{3}H-leucine, were also carried out (Nagata, 2000[c]; Nagata & Usuda, 1993), resulting in an increase of silver grain counts labeled with ^{3}H-leucine after birth , reaching a peak from postnatal week 2 to month 1 (Figure 23E), and decreasing from month 2 to 1 year (Figure 23F). These results revealed aging changes of protein synthesis in pancreatic acinar cells.

On the other hand, experimental studies to clarify the pathogenesis of experimental pancreatitis were carried out by means of LM and EMRAG (Yoshizawa *et al.*, 1974). Several male Wistar rats were treated with daily DL-ethionine injections for 2 days or for 1 month to cause the acute and chronic experimental ethionine pancreatitis. Then, both normal and experimental pancreatitis animals were injected with ^{3}H-ethionine and the pancreatic tissues after 5 and 10 min were fixed and processed for LM and EMRAG. Ethionine is the ethyl homologue of methionine, an essential amino acid, and should be incorporated into proteins. As the results, much more silver grains were observed over the secretory granules and the lumen of the exocrine pancreatic tissues of pancreatitis animals than the normal animals, suggesting the pathogenesis of the ethionine induced pancreatitis

to have the rapid intracellular transport of ethionine (Yoshizawa *et al.*, 1974).

Furthermore, another group of several male Wistar rats were fed with 20% ethanol for 3 months to cause alcoholic pancreatitis. Both the normal and experimental pancreatitis animals were then injected with ^{3}H-leucine and the pancreatic tissues after 5 to 60 min of injection were fixed and processed for LM and EMRAG (Yoshizawa *et al.*, 1977). As the results, less silver grains were observed over the secretory granules and the lumen of the exocrine pancreatic tissues of pancreatitis animals than the normal animals, suggesting the lower protein synthetic activity in the alcohol induced pancreatitis animals (Yoshizawa *et al.*, 1977). These results revealed pathologic changes of protein synthesis of pancreatic acinar cells under abnormal conditions.

The Lipid Synthesis of the Pancreas

The lipids can be demonstrated by LM and EMRAG with the incorporations of either ^{3}H-glycerol or ^{3}H-fatty acids. We first studied the localization of ^{3}H-glycerol in mouse pancreatic cells by cryo-fixation, cryo-sectioning, dry-mounting EMRAG to demonstrate soluble ^{3}H-glycerol (Nagata & Murata, 1977; Nagata *et al.*, 1977). Soluble ^{3}H-glycerol, which was demonstrated by dry-mounting EMRAG, was localized over the nuclei, cell organelles and cytoplasmic ground substance of pancreatic acinar cells diffusely. However, by conventional chemical fixation and wet-mounting RAG, few silver grains were localized only over nuclei and such cell organelles as endoplasmic reticulum, Golgi apparatus, mitochondria and lipid droplets. The results demonstrated that soluble ^{3}H-glycerol was localized over nuclei and cytoplasm of pancreatic acinar cells diffusely.

Then, we studied the aging changes of macromolecular synthesis by injecting several litters of ddY mice aged from fetal day 19 to postnatal days 1, 3, 7, 14, and months 1, 2, 6 up to 12, with ^{3}H-glycerol and the pancreases were prepared for LM and EMRAG. On LMRAG. Silver grains were observed in both exocrine and endocrine cells of respective ages (Nagata *et al.*, 1988[b]; Nagata *et al.*, 1990). In perinatal animals from fetal day 19 to postnatal days 1, 3, and 7, cell organelles were not well developed in exocrine and endocrine cells and number of silver grains was very few (Nagata *et al.*, 1988[b]). In postnatal day 14 juvenile animals, cell organelles such as endoplasmic reticulum, Golgi apparatus, mitochondria and secretory granules were well developed and many silver grains were observed over these organelles and nuclei in both exocrine and endocrine cells. The number of silver grains was more in exocrine cells than endocrine cells. In postnatal months 1, 2, 6 adult animals, number of silver grains remained constant. In 12 month old senile animals, silver grains were fewer than younger animals. The number of silver grains expressed the quantity of lipids synthesis, which increased from perinatal period to adult and decreased to senescence (Nagata *et al.*, 1990). These data indicated that lipid synthesis in pancreatic acinar cells resulted in a peak at the adult stage followed by a decrease at the senile stage due to aging.

Conclusions

The methods we have developed in our laboratory to demonstrate both soluble and insoluble radioactive compounds by either wet-mounting or dry-mounting radioautography at both light and electron microscopic levels and to quantify macromolecular synthesis or small molecular precursors, preparing many radioautograms at once, were briefly described. The results from these methods applied to macromolecular syntheses, DNA, RNA, glucides, proteins, glycoproteins and lipids in digestive organs,

as well as the results from the X-ray microanalysis were summarized and reviewed in connection with the aging of animals.

The results obtained in our laboratory include not only 3-dimensional structures of the organs but also the 4-dimensional features taking the time dimension into account by labeling cells and localizing the sites of incorporation and synthesis in connection with the time lapse and aging of animals (Nagata, 1995[c], 1997[b], 1999[a], 2001[a,b]). The technologies that were developed recently and the results obtained from the applications to various organs should be systematized as a new filed of science designated as histochemistry of the organs (Nagata, 1995[b], 1999[b], 2001[c]) or special radioautographology (Nagata, 1996[c], 1998[b], 1999[e], 2000[e], 2002). From the results obtained, it is demonstrated that these radioactive precursors were incorporated into various cell types in various organs at various aging groups from perinatal to juvenile, mature and senescent stages showing organ specific patterns of macromolecular synthesis.

Acknowledgements

The author thanks Dr. Kiyokazu Kametani, Technical Official, Research Center for Instrumental Analysis, Shinshu University, for his technical assistance. The author is also grateful to many collaborators during the course of these studies, mainly Japanese and several foreign graduate students from Asian countries as well as Brazil, supported by the scholarships for foreign graduate students from the Ministry of Education, Science, Sports and Culture of Japan Government during their visits to Japan, whose names are listed as co-authored references at the end of this paper.

References

Bando Y. Microstructure analysis of advanced ceramics by high-resolution analytical transmission electron microscopy. J Electron Microsc 1995;44: 115-23.

Bando Y, Matsui Y, Uemura Y. The usefulness of a 400 kV high-resolution analytical electron microscope. Ultramicroscopy 1985;18:117-24.

Chandler J A. X-ray microanalysis in the electron microscope. In: Glauert A M (ed.). Practical Methods in Electron Microscopy. North-Holland Publishing Company: Asmsterdam, New York, Oxford, 1976;319-547.

Chen S, Gao F, Kotani A, Nagata T. Age-related changes of male mouse submandibular gland: A morphometric and radioautographic study. Cell Mol Biol 1995;41:117-24.

Cheng H. Origin, differentiation and renewal of the four main epithelial cell types in the mouse small intestine. II. Mucous cells. Amer J Anat 1974[a];141:481-502.

Cheng H. Origin, differentiation and renewal of the four main epithelial cell types in the mouse small intestine. IV. Paneth cells. Amer J Anat 1974[b];141:521-36.

Cheng H, Leblond CP. Origin, differentiation and renewal of the four main epithelial cell types in the mouse small intestine. I. Columnar cells. Amer J Anat 1974[a];141:461-80.

Cheng H, Leblond CP. Origin, differentiation and renewal of the four main epithelial cell types in the mouse small intestine. III. Entero-endocrine cells. Amer J Anat 1974[b];141:503-20.

Cui H. Light microscopic radioautographic study on DNA synthesis of nerve cells in the cerebella of aging mice. Cell Mol Biol 1995;41:1139-54.

Cui H, Gao F, Nagata T. Light microscopic radioautographic study on protein synthesis in perinatal mice corneas. Acta Histochem Cytochem 2000;33:31-7.

Duan H, Gao F, Li S, Hayashi K, Nagata T. Aging changes and fine structure and DNA synthesis of esophageal epithelium in neonatal, adult and old mice. J Clin Electron

Microsc 1992;25:452-53.
Duan H, Gao F, Li S, Nagata T. Postnatal development of esophageal epithelium in mouse: a light and electron microscopic radioautographic study. Cell Mol Biol 1993;39:309-16.
Gao F. Study on the macromolecular synthesis in aging mouse seminiferous tubules by light and electron microscopic radioautography. Cell Mol Biol 1993;39:659-72.
Gao F, Toriyama K, Nagata T. Light microscopic radioautographic study on the DNA synthesis of prenatal and postnatal aging mouse retina after labeled thymidine injection. Cell Mol Biol 1992[a];38:661-68.
Gao F, Li S, Duan H, Ma H, Nagata T. Electron microscopic radioautography on the DNA synthesis of prenatal and postnatal mice retina after labeled thymidine injection. J Clin Electron Microsc 1992[b];25:721-2.
Gao F, Toriyama K, Ma H, Nagata T. Light microscopic radioautographic study on DNA synthesis in aging mice corneas. Cell Mol Biol 1993;39:435-41.
Gao F, Ma H, Sun L, Jin C, Nagata T. Electron microscopic radioautographic study on the nucleic acids and protein synthesis in the aging mouse testis. Med Electron Microsc 1994;27:360-2.
Gao F, Chen S, Sun L, Kang W, Wang Z, Nagata T. Radioautographic study of the macromolecular synthesis of Leydig cells in aging mice testis. Cell Mol Biol 1995[a];41:145-50.
Gao F, Jin C, Ma H, Sun L, Nagata T. Ultrastructural and radioautographic studies on DNA synthesis in Leydig cells of aging mouse testis. Cell Mol Biol 1995[b];41:151-60.
Gunarso W, Gao F, Cui H, Ma H, Nagata T. A light and electron microscopic radioautographic study on RNA synthesis in the retina of chick embryo. Acta Histochem 1996;98:309-22.
Gunarso W, Ga, F, Nagata T. Development and DNA synthesis in the retina of chick embryo observed by light and electron microscopic radioautography. Cell Mol Biol 1997;43:189-201.
Hanai T. Light microscopic radioautographic study of DNA synthesis in the kidneys of aging mice. Cell Mol Biol 1993;39:81-91.
Hanai T, Nagata T. Study on the nucleic acid synthesis in the aging mouse kidney by light and electron microscopic radioautography. In: Nagata T (ed.). Radioautography in Medicine. Matsumoto: Shinshu University Press, 1994[a];209-14.
Hanai T, Nagata T. Electron microscopic study on nucleic acid synthesis in perinatal mouse kidney tissue. Med Electron Microsc 1994[b];27:355-7.
Hanai T, Usuda N, Morita T, Shimizu T, Nagata T. Proliferative activity in the kidneys of aging mice evaluated by PCNA/cyclin immunohistochemistry. Cell Mol Biol 1993;39:181-91.
Hayashi K, Gao F, Nagata T. Radioautographic study on ^{3}H-thymidine incorporation at different stages of muscle development in aging mice. Cell Mol Biol 1993;39:553-60.
Hodges GM, Muir MD. Quantitative evaluation of autoradiographs in X-ray spectroscopy. J Microsc 1975;104:173-8.
Ichikawa R, Hayashi K, Nagata T. X-ray microanalysis of the secretory granules in the intestinal goblet cells of aging mice. Med Electron Microsc 1994;27:337-9.
Ito M. The radioautographic studies on aging change of DNA synthesis and the ultrastructural development of mouse adrenal gland. Cell Mol Biol 1996;42:279-92.
Ito M, Nagata T. Electron microscopic radioautographic studies on DNA synthesis and ultrastructure of aging mouse adrenal gland. Med Electron Microsc 1996;29:145-52.
Jamieson J D, Palade G E. Intracellular transport of secretory proteins in the pancreatic

exocrine cells. J Cell Biol 1967;34:577-615.
Jin C. Study on DNA synthesis of aging mouse colon by light and electron microscopic radioautography. Cell Mol Biol 1996;42:255-68.
Jin C, Nagata T. Light microscopic radioautographic study on DNA synthesis in cecal epithelial cells of aging mice. J Histochem Cytochem 1995[a];43:1223-8.
Jin C, Nagata T. Electron microscopic radioautographic study on DNA synthesis in cecal epithelial cells of aging mice. Med Electron Microsc 1995[b];28:71-5.
Johkura K. The aging changes of glycoconjugate synthesis in mouse kidney studied by ^{3}H-glucosamine radioautography. Acta Histochem Cytochem 1996;29:57-63.
Johkura K, Usuda N, Nagata T. Quantitative study on the aging change of glycoconjugates synthesis in aging mouse kidney. Proc Xth Internat Cong Histochem Cytochem, Kyoto, Acta Histochem Cytochem 1996;29(Suppl):507-8.
Kametani K, Ichikawa R, Nagata T. X-ray microanalysis of the secretory granules in goblet cells of mouse intestinal tracts: changes with age. Med Electron Microsc 1998;31:107-14.
Komiyama K, Iida F, Furihara R, Murata F, Nagata T. Electron microscopic radioautographic study on ^{125}I-albumin in rat gastric mucosal epithelia. J Clin Electron Microsc 1978;11:428-9.
Kong Y. Electron microscopic radioautographic study on DNA synthesis in perinatal mouse retina. Cell Mol Biol 1993;39:55-64.
Kong Y, Nagata T. Electron microscopic radioautographic study on nucleic acid synthesis of perinatal mouse retina. Med Electron Microsc 1994;27:366-8.
Kong Y, Usuda N, Nagata T. Radioautographic study on DNA synthesis of the retina and retinal pigment epithelium of developing mouse embryo. Cell Mol Biol 1992[a];38:263-72.
Kong,Y, Usuda N, Morita T, Hanai T, Nagata T. Study on RNA synthesis in the retina and retinal pigment epithelium of mice by light microscopic radioautography. Cell Mol Biol 1992[b];38:669-78.
Leblond CP. The life history of cells in renewing systems. Amer J Anat 1981;160:113-58.
Leblond CP, Messier B. Renewal of chief cells and goblet cells in the small intestine as shown by radioautography after injection of thymidine-^{3}H into mice. Anat Rec 1958;132:247-59.
Lee ER. Dynamic histology of the antral epithelim in the mouse stomach: I. Architecture of antral unit. Amer J Anat 1985[a];172:187-204.
Lee ER. Dynamic histology of the antral epithelim in the mouse stomach: III. Ultrastucture and renewal of pit cells. Amer J Anat 1985[b];172:225-40.
Lee ER, Leblond CP. Dynamic histology of the antral epithelium in the mouse stomach: II. Ultrastructura and renewal of isthmal cells. Amer J Anat 1985[a];172:205-24.
Lee ER, Leblond CP. Dynamic histology of the antral epithelium in the mouse stomach: IV. Ultrastructura and renewal of gland cells. Amer J Anat 1985[b];172:241-59.
Li S. Relationship between cellular DNA synthesis, PCNA expression and sex steroid hormone receptor status in the developing mouse ovary, uterus and oviduct. Histochemistry 1994;102:405-13.
Li S, Nagata T. Nucleic acid synthesis in the developing mouse ovary, uterus and oviduct studied by light and electron microscopic radioautography. Cell Mol Biol 1995;41:185-95.
Li S, Gao F, Duan H, Nagata T. Radioautographic study on the uptake of $^{35}SO_4$ in mouse ovary during the estrus cycle. J Clin Electron Microsc 1992;25:709-10.
Liang Y. Light microscopic radioautographic study on RNA synthesis in the adrenal glands

of aging mice. Acta Histochem Cytochem 1998;31:203-10.
Liang Y, Ito M, Nagata T. Light and electron microscopic radioautographic studies on RNA synthesis in aging mouse adrenal gland. Acta Anat Nippon 1999;74:291-300
Ma H. Light microscopic radioautographic study on DNA synthesis of the livers in aging mice. Acta Anat Nippon 1988;63:137-47.
Ma H, Nagata T. Electron microscopic radioautographic study on DNA synthesis of the livers in aging mice.J Clin Electron Microsc 1988[a];21:335-43.
Ma H, Nagata T. Studies on DNA synthesis of aging mice by means of electron microscopic radioautography. J Clin Electron Microsc 1988[b];21:715-16.
Ma H, Nagata T. Electron microscopic radioautographic studies on DNA synthesis in the hepatocytes of aging mice as observed by image analysis. Cell Mol Biol 1990[a];36:73-84.
Ma H, Nagata T. Study on RNA synthesis in the livers of aging mice by means of electron microscopic radioautography. Cell Mol Biol 1990[b];36:589-600.
Ma H, Nagata T. Collagen and protein synthesis in the livers of aging mice as studied by electron microscopic radioautography. Ann Microsc 2000;1:13-22.
Ma H, Gao F, Olea MT, Nagata T. Protein synthesis in the livers of aging mice studied by electron microscopic radioautography. Cell Mol Biol 1991;37:607-15.
Maruyama M, Nagata T. X-ray microanalysis with a high voltage electron microscope quantifying sulfur in colonic goblet cells of aging mice. J Clin Electron Microsc 1987;20:678-9.
Matsumura H, Kobayashi Y, Kobayashi K, Nagata T. Light microscopic radioautographic study of DNA synthesis in the lung of aging salamander, Hynobius nebulosus. J Histochem Cytochem 1994;42:1004-04.
Momose Y, Nagata T. Radioautographic study on the intracellular localization of a hypolipidemic agent, bezafibrate, a peroxisome proliferator, in cultured rat hepatocytes. Cell Mol Biol 1993;39:773-81.
Momose Y, Shibata N, Kiyosawa I, Naito J, Watanabe T, Horie S, Yamada J, Suga T, Nagata T. Morphometric evaluation of species differences in the effects of bezafibrate, a hypolipidemic agent, on hepatic peroxisomes and mitochondria. J Toxicol Pathol 1993;6:33-45.
Momose Y, Naito J, Suzawa H, Kanzawa M, Nagata T. Radioautographic study on the intracellular localization of bezafibrate in cultured rat hepatoctyes. Acta Histochem. Cytochem 1995;28:61-6.
Morita T. Radioautographic study on the aging change of ^{3}H-glucosamine uptake in mouse ileum. Cell Mol Biol 1993;39:875-84.
Morita T , Usuda N, Hanai T, Nagata T. Changes of colon epithelium proliferation due to individual aging with PCNA/cyclin immunostaining comparing with ^{3}H-thymidine radioautography. Histochemistry 1994[a];101:13-20.
Morita T, Usuda N, Hanai T, Kong Y, Nagata T. Lectin histochemistry of the developing and aging mice colons. Acta Histochem Cytochem 1994[b],24:527-27.
Murata F, Momose Y, Yoshida K, Nagata T. Incorporation of ^{3}H-thymidine into the nucleus of mast cells in adult rat peritoneum. Shinshu Med J 1977[a];25:72-7.
Murata F, Momose Y, Yoshida K, Ohno S, Nagata T. Nucleic acid and mucosubstance metabolism of mastocytoma cells by means of electron microscopic radioautography. Acta Pharmacol Toxicol 1977[b];41:58-9.
Murata F, Yoshida K, Ohno S, Nagata T. Ultrastructural and electron microscopic radioautographic studies on the mastocytoma cells and mast cells. J Clin Electron Microsc 1978;11:561-2.

Murata F, Yoshida K, Ohno S, Nagata T. Mucosubstances of rabbit granulocytes studied by means of electron microscopic radioautography and X-ray microanalysis. Histochemistry 1979;61:139-50.

Nagata T. A radioautographic study of the DNA synthesis in rat liver, with special reference to binucleate cells. Med J Shinshu Univ 1962;7:17-25.

Nagata T. A quantitative study on the ganglion cells in the small intestine of the dog. Med J Shinshu Univ 1965;10:1-11.

Nagata T. A radioautographic study on the RNA synthesis in the hepatic and the intestinal epithelial cells of mice after feeding with special reference to binuclearity. Med J Shinshu Univ 1966;11:49-61.

Nagata T. A radioautographic study on the protein synthesis in the hepatic and the intestinal epithelial cells of mice, with special reference to binucleate cells. Med J Shinshu Univ 1967;12:247-57.

Nagata T. Application of microspectrophotometry to various substances. Chapter 3. In: Isaka S, Nagata T, Inui N (Eds). Introduction to Microspectrophotometry. Tokyo: Olympus Co., 1972[a];49-155.

Nagata T. Simple method for mass production of radioautographs. The Cell (Saibo, Tokyo). 1982;14:40-50.

Nagata, T. Principles and techniques of radioautography. In: Histo- and Cyto-chemistry (ed.). Japan Society of Histochemistry and Cytochemistry. Tokyo: Gakusai Kikaku Co, 1985;207-26.

Nagata T. Electron microscopic radioautography and analytical electron microscopy. J Clin Electron Microsc 1991;24:441-2.

Nagata T. Radiolabeling of soluble and insoluble compounds as demonstrated by light and electron microscopy. In: Wegmann RJ, Wegmann MA (Eds). Recent Advances in Cellular and Molecular Biology. Vol. 6. Molecular Biology of Pyridines, DNA, Peroxisomes, Organelles and Cell Movements. Leuven: Peeters Press, 1992;9-21.

Nagata T. Quantitative analysis of histochemical reactions: Image analysis of light and electron microscopic radioautograms. Acta Histochem Cytochem 1993[a];26:281-91.

Nagata T. Quantitative light and electron microscopic radioautographic studies on macromolecular synthesis in several organs of prenatal and postnatal aging mice. Chinese J Histochem Cytochem 1993[b];2:106-08.

Nagata T. Electron microscopic radioautography with cryo-fixation and dry-mounting procedure. Acta Histochem Cytochem 1994[a];27:471-89.

Nagata T. Application of electron microscopic radioautography to clinical electron microscopy. Med Electron Microsc 1994[b];27:191-212.

Nagata T. Radioautography in Medicine. Matsumoto: Shinshu University Press, 1994[c].

Nagata T. Light and electron microscopic radioautographic study on macromolecular synthesis in digestive organs of aging mice. Cell Mol Biol 1995[a];41:21-38.

Nagata T. Histochemistry of the organs; Application of histochemistry to anatomy. Acta Anat Nippon 1995[b];70:448-71.

Nagata T. Three-dimensional observation of whole mount cultured cells stained with histochemical reactions by ultrahigh voltage electron microscopy. Cell Mol Biol 1995[c];41:783-92.

Nagata T. Morphometry in anatomy: image analysis on fine structure and histochemical reactions with special reference to radioautography. Ital J Anat 1995[d];100(Suppl 1):591-605.

Nagata T. Technique and application of electron microscopic radioautography. J Electron Microsc 1996[a];45:258-74.

Nagata T. Techniques of light and electron microscopic radioautography. In, Histochemistry

and Cytochemistry 1996. Proc. X[th] Internat Congr Histochem Cytochem. Kyoto: Acta Histochem Cytochem 1996[b];29(suppl):343-4.

Nagata T. Introductory Remarks: Radioautographology, general and special. Cell Mol Biol 1996[c];42(suppl):11-12.

Nagata T. Techniques and applications of microscopic radioautography. Histol Histopathol 1997[a];12:1091-124.

Nagata T. Three-dimensional observation on whole mount cultured cells and thick sections stained with histochemical reactions by high voltage electron microscopy. In: Motta P (ed.). Recent Advances in Microscopy of Cells, Tissues and Organs. Roma: Antonio Delfino Editore, 1997[b];37-44.

Nagata T. Radioautographic study on collagen synthesis in the ocular tissues. J Kaken Eye Res 1997[c];15:1-9.

Nagata T. Techniques of radioautography for medical and biological research. Braz J Biol Med Res 1998[a];31:185-95.

Nagata T. Radioautographology, the advocacy of a new concept. Braz J Biol Med Res 1998[b];31:201-41.

Nagata T. Radioautographic studies on DNA synthesis of the bone and skin of aging salamander. Bull Nagano Women´s Jr College 1998[c];6:1-14.

Nagata T. 3D observation of cell organelles by high voltage electron microscopy. Microscopy and Analysis, Asia Pacific Edition 1999[a];9:29-32.

Nagata T. Application of histochemistry to anatomy: Histochemistry of the organs, a novel concept. Proc XV[th] Congress of the International Federation of Associations of Anatomists, Ital. J Anat Embryo 1999[b];104(suppl 1):486-86.

Nagata T. Aging changes of macromolecular synthesis in various organ systems as observed by microscopic radioautography after incorporation of radiolabeled precursors. Methods Find Exp Clin Pharmacol 1999[c];21:683-706.

Nagata T. Radioautographic study on protein synthesis in mouse cornea. J Kaken Eye Res 1999[d];8:8-14.

Nagata T. Radioautographology, general and special: a novel concept. Ital J Anat Embryol 1999[e];104(suppl 1):487-87.

Nagata T. Three-dimensional observations on thick biological specimens by high voltage electron microscopy. Image Analysis Stereolog 2000[a];19:51-6.

Nagata T. Biological microanalysis of radiolabeled and unlabeled compounds by radioautography and X-ray microanalysis. Scanning Microscopy International 2000[b];14:on line.

Nagata T. Electron microscopic radioautographic study on protein synthesis in pancreatic cells of perinatal and aging mice. Bull Nagano Women´s Jr College 2000[c];8:1-22.

Nagata T. Light microscopic radioautographic study on radiosulfate incorporation into the tracheal cartilage in aging mice. Acta Histochem Cytochem 2000[d];32:377-83.

Nagata T. Introductory remarks: Special radioautographology. Cell Mol Biol 2000[e];46(suppl):161-61.

Nagata T. Special radioautographology: the eye. J Kaken Eye Res 2000[f];18:1-13.

Nagata T. Three-dimensional high voltage electron microscopy of thick biological specimens. Micron 2001[a];32:387-404.

Nagata T. Three-dimensional and four-dimensional observation of histochemical and cytochemical specimens by high voltage electron microscopy. Acta Histochem Cytochem 2001[b];34:153-69.

Nagata T. Special cytochemistry in cell biology. In: Jeon KW (ed.). Internat Rev Cytol Vol. 211, Chapter 2. New York: Academic Press, 2001[c];33-154.

Nagata T. Aging changes of macromolecular synthesis in the respiratory organs as revealed by microscopic radioautography. ARBS 2001[d];3:127-55.
Nagata T. Radioautographology, General and Special. In: Graumann W (ed.). Prog Histochem Cytochem, Vol. 37, No. 2. Germany: Urban & Fischer 2002;57-228.
Nagata T, Cui H, Gao F. Radioautographic study on glycoprotein synthesis in the ocular tissues. J Kaken Eye Res 1995;13:11-18.
Nagata T, Cui H, Kong Y. The localization of TGF-b1 and its mRNA in the spinal cords of prenatal and postnatal aging mice demonstrated with immunohistochemical and in situ hybridization techniques. Bull Nagano Women´s Jr College 1999[b];7:75-88.
Nagata T, Hirano I, Shibata O. A radioautographic study on the DNA synthesis in the hepatic and the pancreatic acinar cells of mice during the postnatal growth, with special reference to binuclearity. Med J Shinshu Univ 1966;11:35-42.
Nagata T, Ito M, Chen S. Aging changes of DNA synthesis in the submandibular glands of mice as observed by light and electron microscopic radioautography. Ann Microsc 2000[a];1:4-12.
Nagata T, Ito M, Liang Y. Study of the effects of aging on macromolecular synthesis in mouse steroid secreting cells using microscopic radioautography. Methods Find Exp Clin Pharmacol 2000[b];22:5-18.
Nagata T, Kametani K, Maruyama M. X-ray microanalysis of sulfur in cryo-fixed colonic goblet cells by high voltage electron microscopy. Scanning Microsc Internat 2000[c];14:on line.
Nagata T, Kawahara I. Radioautographic study of the synthesis of sulfomucin in digestive organs of mice. J Trace Microprobe Analysis 1999;17:339-55.
Nagata T, Kawahara I, Usuda N, Maruyama M, Ma H. Radioautographic studies on the glycoconjugate synthesis in the gastrointestinal mucosa of the mouse. In: Ohyama M, Muramatsu T, (eds). Glycoconjugate in Medicine. Tokyo: Professional Postgrad Service, 1988[a];251-6.
Nagata T, Kong Y. Distribution and localization of TGFb1 and bFGF, and their mRNAs in aging mouse eye. Bull Nagano Women´s Junior College 1998;6:87-105.
Nagata T, Ma H. Electron Microscopic Radioautographic Study On the Macromolecular Synthesis in Binucleate Hepatocytes Of Aging Mouse. Ann Microsc 2002;3: in press.
Nagata T, Morita T, Kawahara I. Radioautographic studies on radiosulfate incorporation in the digestive organs of mice. Histol Histopathol 1999[a];14:1-8.
Nagata T, Murata F. Electron microscopic dry-mounting radioautography for diffusible compounds by means of ultracryotomy. Histochemistry 1977;54:75-82.
Nagata T, Nawa T. A modification of dry-mounting technique for radioautography of water-soluble compounds. Histochemie 1966[a];7:370-1.
Nagata T, Nawa T. A radioautographic study on the nucleic acids synthesis of binucleate cells in cultivated fibroblasts of chick embryos. Med J Shinshu Univ 1966[b];11:1-5.
Nagata T, Nawa T, Yokota S. A new technique for electron microscopic dry-mounting radioautography of soluble compounds. Histochemie 1969;18:241-9.
Nagata T, Ohno S, Murata F. Electron microscopic dry-mounting radioautography for soluble compounds. Acta Phamacol Toxicol 1977;41:62-3.
Nagata T, Olea M T. Electron microscopic radioautographic study on the protein synthesis in aging mouse spleen. Bull Nagano Women's Jr College 1999;7:1-9.
Nagata T, Shibata O, Nawa T. Incorporation of tritiated thymidine into mitochondrial DNA of the liver and kidney cells of chickens and mice in tissue culture. Histochemie 1967;10:305-8.
Nagata T, Shibata O, Omochi S. A new method for radioautographic observation on

isolated cells. Histochemie 1961;2:255-9

Nagata T, Toriyama K, Kong Y, Jin C, Gao F. Radioautographic study on DNA synthesis in the ciliary bodies of aging mice. J Kaken Eye Res 1994;12:1-11.

Nagata T, Usuda N. Image processing of electron microscopic radioautograms in clinical electron microscopy. J Clin Electron Microsc 1985;18:451-2.

Nagata T, Usuda N. Studies on the nucleic acid synthesis in pancreatic acinar cells of aging mice by means of electron microscopic radioautography. J Clin Electron Microsc 1986;19:486-7.

Nagata T, Usuda N. Electron microscopic radioautography of protein synthesis in pancreatic acinar cells of aging mice. Acta Histochem Cytochem 1993[a];26:481-81.

Nagata T, Usuda N. In situ hybridization by electron microscopy using radioactive probes. J Histochem Cytochem 1993[b];41:1119-19.

Nagata T, Usuda N, Ma H. Electron microscopic radioautography of nucleic acid synthesis in pancreatic acinar cells of prenatal and postnatal aging mice. Proc XI[th] Intern Cong Electron Microsc 1984;3:2281-2.

Nagata T, Usuda N, Ma H. Studies on the nucleic acid synthesis in pancreatic acinar cells of aging mice by means of electron microscopic radioautography. J Clin Electron Microsc 1986;19:486-7.

Nagata T, Usuda N, Ma H. Electron microscopic radioautography of lipid synthesis in pancreatic cells of aging mice. J Clin Electron Microsc 1990;23:841-2.

Nagata T, Usuda N, Maruyama M, Ma H. Electron microscopic radioautographic study on lipid synthesis in perinatal mouse pancreas. J Clin Electron Microsc 1988[b];21:756-7.

Nagata T, Usuda N, Suzawa H, Kanzawa M. Incorporation of 3H-glucosamine into the pancreatic cells of aging mice as demonstrated by electron microscopic radioautography. J Clin Electron Microsc 1992;25:646-7.

Olea MT, Nagata T. Simultaneous localization of 3H-thymidine incorporation and acid phosphatase activity in mouse spleen: EM radioautography and cytochemistry. Cell Mol Biol 1992[a];38:115-22.

Olea M T, Nagata T. A radioautographic study on RNA synthesis in aging mouse spleen after 3H-uridine labeling in vitro. Cell Mol Biol 1992[b];38:399-405.

Oliveira SF, Nagata T, Abrahamsohn PA, Zorn TMT. Electron microscopic radioautographic study on the incorporation of 3H-proline by mouse decidual cells. Cell Mol Biol 1991;37:315-23.

Oliveira SF, Abrahamsohn PA, Nagata T, Zorn TMT. Incorporation of 3H-amino acids by endometrial stromal cells during decidualization in the mouse. A radioautographical study. Cell Mol Biol 1995;41:107-16.

Sato A. Quantitative electron microscopic studies on the kinetics of secretory granules in G-cells. Cell Tissue Res 1978;187:45-59.

Sato A, Iida F, Furihara R, Nagata T. Electron microscopic raioautography of rat stomach G-cells by means of 3H-amino acids. J Clin Electron Microsc 1977;10:358-9.

Sun L. Age related changes of RNA synthesis in the lungs of aging mice by light and electron microscopic radioautography. Cell Mol Biol 1995;41:1061-72.

Sun L, Gao F, Duan H, Nagata T. Light microscopic radioautography of DNA synthesis in pulmonary cells in aging mice. In: Nagata T. (ed.). Radioautography in Medicine. Matsumoto: Shinshu University Press, 1994;201-05.

Sun L, Gao F, Nagata T. Study on the DNA synthesis of pulmonary cells in aging mice by light microscopic radioautography. Cell Mol Biol 1995[a];41:851-9.

Sun L, Gao F, Jin C, Duan H, Nagata T. An electron microscopic radioautographic study

on the DNA synthesis of pulmonary tissue cells in aging mice. Med Electron Microsc 1995[b];28:129-31.

Sun L, Gao F, Jin C, Nagata T. DNA synthesis in the tracheae of aging mice by means of light and electron microscopic radioautography. Acta Histochem Cytochem 1997[a];30:211-20.

Sun L, Gao F, Nagata T. A Light Microscopic Radioautographic Study on Protein Synthesis in Pulmonary Cells of Aging Mice. Acta Histochem Cytochem 1997[b];30:463-70.

Terauchi A, Mori T, Kanda H, Tsukada M, Nagata T. Radioautographic study of 3H-taurine uptake in mouse skeletal muscle cells. J Clin Electron Microsc 1988;21:627-8.

Terauchi, A., Nagata, T. Observation on incorporation of 3H-taurine in mouse skeletal muscle cells by light and electron microscopic radioautography. Cell Mol Biol 1993; 39: 397-404.

Terauchi A, Nagata T. In corporation of 3H-taurine into the blood capillary cells of mouse skeletal muscle. In: Nagata T. (ed.). Radioautography in Medicine. Matsumoto: Shinshu University Press, 1994;155-9.

Toriyama K. Study on the aging changes of DNA and protein synthesis of bipolar and photo-receptor cells of mouse retina by light and electron microscopic radioautography. Cell Mol Biol 1995;41:593-601.

Usuda N, Nagata T. Electron microscopic radioautography of acyl-CoA mRNA by *in situ* hybridization. J Clin Electron Microsc 1992;25:332-3.

Usuda N, Nagata T. The immunohistochemical and in situ hybridization studies on hepatic peroxisomes. Acta Histochem Cytochem 1995;28:169-72.

Usuda N, Hanai T, Morita T, Nagata T. Radioautographic demonstration of peroxisomal acyl-CoA oxidase mRNA by in situ hybridization. In: Wegmann R J, Wegmann M. (Eds). Recent Advances in Cellular and Molecular Biology. Leuven: Peeters Press. Vol. 6. Molecular biology of nucleus, peroxisomes, organelles and cell movement, 1992;181-4. .

Watanabe I, Makiyama MCK, Nagata T. Electron microscopic radioautographic observation of the submandibular salivary gland of aging mouse. Acta Microscopica 1997;6:130-1.

Watanabe I, Nagata T. Changes of glucide synthesis in the submandibular glands of aging mice as observed by light and electron microscopic radioautoagraphy. Ann Microsc 2001;2:4-15.

Yamada AT. Timely and topologically defined protein synthesis in the periimplanting mouse endometrium revealed by light and electron microscopic radioautography. Cell Mol Biol 1993;39:1-12.

Yamada A, Nagata T. Ribonucleic acid and protein synthesis in the uterus of pregnant mouse during activation of implantation window. Med Electron Microsc 1992[a];27:363-5.

Yamada A., Nagata T. Light and electron microscopic raioautography of DNA synthesis in the endometria of pregnant-ovariectomized mice during activation of implantation window. Cell Mol Biol 1992[b];38:763-74.

Yamada A, Nagata T. Light and electron microscopic raioautography of RNA synthesis of peri-implanting pregnant mouse during activation of receptivity for blastocyst implantation. Cell Mol Biol 1993;38:211-33.

Yoshizawa S, Nagata A, Honma T, Oda M, Murata F, Nagata T. Study of ethionine pancreatitis by means of electron microscopic radioautography. J Clin Electron Microsc 1974;7:349-50.

Yoshizawa S, Nagata A, Honma T, Oda M, Murata F, Nagata T. Radioautographic study of protein synthesis in pancreatic exocrine cells of alcoholic rats. J Clin Electron Microsc 1977;10:372-3.